

The Dynamic Adsorption of Charged Amphiphiles Characterized Using Maximum Bubble  
Pressure Tensiometry

By

Camila Alexandra Uribe Ortiz

B.S. Universidad Nacional de Colombia, 2015

THESIS

Submitted as partial fulfillment of the requirements for the degree of Master of Science in  
Chemical Engineering in the Graduate College of the University of Illinois at Chicago, 2017

Chicago, Illinois

Committee:

Vivek Sharma, Chair and Advisor

Sangil Kim, Chemical Engineering UIC

Ludwig Nitsche, Chemical Engineering UIC

This thesis is dedicated to my parents (Jose Uribe and Doris Ortiz), friends and my turtle without whom it would never have been accomplished.

## ACKNOWLEDGEMENTS

I would like to thank my professor/advisor Vivek Sharma for his continuous support, patience, motivation, and guidance throughout this research. I would also like also to thank the members of the committee: Sangil Kim and Ludwig Nitsche for taking the time to read my thesis and for their useful feedback.

I would also like to thank Norman Moreno for his assistance in conducting experimental tests on the experiment set-up, also for sharing his knowledge of related topics with me. I want to thank my research group in special all of those people who gave me a useful advice on my research and on my writing.

Thanks to my colleges from other groups, who advise, encourage and support me through all of this process of learning, without them this could have been no fun and thrilled.

I am grateful for having excellent professors who tried to teach as much as they could in order to have the basic knowledge to face real problems in the chemical engineering field.

# TABLE OF CONTENTS

CHAPTER		PAGE
1	INTRODUCTION .....	1
	1.1 Surfactants Active Agents.....	1
	1.2 Maximum Bubble Pressure Technique.....	4
	1.3 Adsorption of amphiphiles.....	7
	1.4 Motivation.....	8
2	BACKGROUND THEORIES .....	11
	2.1 Dynamic adsorption of surfactants .....	11
	2.1.1 Dynamic Surface Tension.....	16
	2.1.2 Equilibrium Surface Tension .....	18
	2.2 Additional Parameters.....	22
	2.2.1 Diffusivity.....	22
	2.2.2 Energy of adsorption.....	23
	2.2.3 Gibbs elasticity.....	24
	2.2.4 Area per adsorbed molecule.....	25
3	MATERIALS AND METHOD .....	26
	3.1 Materials .....	26
	3.2 Experimental Procedure.....	27
	3.3 Validation.....	32
4	RESULTS AND DISCUSSION .....	34
	4.1 Hexadecyltrimethylammonium Bromide (CTAB).....	34
	4.1.1 Dynamic surface tension.....	34
	4.1.2 Universal surface age.....	44
	4.1.3 Quasi-equilibrium surface tension .....	46
	4.1.4 Adsorption Isotherms and surface tension data .....	51
	4.1.5 CTAB summary .....	59
	4.2 Bile Salts .....	61

	4.2.1	Dynamic Surface Tension.....	62
	4.2.2	Equilibrium surface tension .....	71
5		CONCLUSIONS.....	81
	5.1	Summary.....	81
	5.2	Recommendations for future work .....	82
6		REFERENCE LIST .....	83
8		APPENDICES .....	89
	8.1	Appendix A.....	89
9		VITA.....	92

## LIST OF TABLES

TABLE	PAGE
Table I. Diffusion coefficients of bile salts and CTAB .....	22
Table II. Properties of surfactant molecules provided by Sigma-Aldrich .....	26
Table III. Parameters of van der Waals and Frumkin isotherms. ....	53
Table IV. Maximum surface concentration from the Gibbs equation and CMC values for bile salts and CTAB. ....	74
Table V. The parameters of Frumkin for CTAB and bile salts. ....	76

## LIST OF FIGURES

Figure 1. Chemical structure of CTAB molecule. .... 3

Figure 2. Schematic structure of the bile salts and the chemical structure of the studied bile salts.  
..... 3

Figure 3. Dynamic surface tension: Techniques and Timescale (15, 16). .... 5

Figure 4. Schematic showing the dynamic adsorption of surfactants..... 11

Figure 5. Schematic showing interfacial adsorption area of ionic surfactant solution. Ionic surfactant dissociates in aqueous solution into surfactant ions and counterions. .... 13

Figure 6 Dynamic surface tension data corresponding to the dynamic adsorption sketched in Figure 4..... 17

Figure 7. Schematic of Maximum Bubble Pressure Tensiometer. .... 29

Figure 8. Pressure evolution over time as a function of bubble radius..... 31

Figure 9. Pressure evolution with time as a function of flow rate for a concentration of 0.5mM CTAB in water..... 32

Figure 10. Maximum pressure and surface tension variation with flow rate for deionized water.  
..... 33

Figure 11. The plot of maximum pressure vs flow rate for CTAB solutions with concentrations of 0.4 mM, 0.58 mM, and 0.92 mM..... 35

Figure 12. Dynamic surface tension versus apparent surface age for CTAB solutions with concentrations of 0.4 mM, 0.5 mM, and 0.92 mM. .... 36

Figure 13. Dynamic surface tension vs apparent surface age plotted on a semilog scale in for CTAB solutions with a range of concentration from 0.23 - 50 mM. .... 38

Figure 14. Dynamic surface tension data for aqueous CTAB solutions (below CMC) is plotted as a function of $t_{app}^{-1/2}$ .	39
Figure 15. $S_\gamma$ vs concentration for aqueous solutions of CTAB obtained by analyzing dynamic surface tension data.	40
Figure 16. Dynamic surface tension data of aqueous CTAB solutions are shown with symbols and the lines represent the behavior captured by the asymptotic result (equation 8).	41
Figure 17. Plot of $(\gamma - \gamma_{eq,c}) / S_{\gamma,c}$ vs apparent surface age ( $t_{app}$ ).	42
Figure 18. Dynamic surface tension vs adsorption time of CTAB of different tensiometers.	43
Figure 19. Apparatus constant versus CTAB concentration.	44
Figure 20. Variation of dynamic surface tension with universal surface age.	45
Figure 21. The dynamic surface tension of CTAB from MBPM with universal surface age for concentration ranging from 0.23 mM to 0.92 mM.	46
Figure 22. The plot of dynamic surface tension vs apparent surface age for solutions of CTAB with concentrations from 0.23 mM – 50 mM.	48
Figure 23. Quasi-equilibrium surface tension as a function of bulk surfactant concentration for CTAB.	50
Figure 24. The variation in surface pressure with concentration for aqueous CTAB solutions is shown together with Frumkin and van der Waals isotherm.	52
Figure 25. The plot of surface potential as a function of CTAB bulk concentration, using Frumkin and van der Waals isotherm models.	54
Figure 26. Occupancy of the Stern layer $\left(\frac{\Gamma_2}{\Gamma_1}\right)$ as a function of CTAB concentration in the bulk, evaluated using Frumkin and van der Waals isotherms.	55

Figure 27. Plots of dimensionless adsorption of surfactant ion ( $\Gamma_1/\Gamma_\infty$ ) vs concentration of CTAB. Surface concentration and the maximum surface concentration were obtained from the best fitting of experimental data (Figure 24)..... 56

Figure 28. Gibbs elasticity as a function of CTAB concentration in bulk solution..... 57

Figure 29. Gibbs elasticity as a function of CTAB concentration in bulk solution. The empty symbols in the figure represent data taken by Stubenrauch (63). ..... 59

Figure 30. The plot of dynamic surface tension as a function of apparent surface age and concentration for CTAB (a) and Sodium Glycodeoxycholate (b). ..... 64

Figure 31. The plot of dynamic surface tension vs universal surface age for Sodium Glycodeoxycholate solutions with a range of concentration from 0.1 - 20 mM..... 65

Figure 32. The plot of dynamic surface tension vs apparent surface age of Sodium Glycodeoxycholate from reported data by Valderrama et al. (2) and experimental data obtained in this report. .... 66

Figure 33. The plot of dynamic surface tension vs universal surface age for Sodium Cholate solutions in a range of solution concentrations from 1 - 40 mM. .... 67

Figure 34. The plot of dynamic surface tension vs universal surface age for Sodium Deoxycholate solutions with a range of concentration of 0.5 - 30 mM..... 68

Figure 35. The plot of dynamic surface tension vs universal surface age for sodium taurocholate solutions with a range of concentration from 0.1 mM to 20mM . .... 70

Figure 36. The dynamic surface tension of sodium taurocholate, data is closed symbols show values reported by Valderrama et al.(2) and the open symbols show valued of MBP measurements obtained in this study. .... 71

Figure 37. Equilibrium surface tension of Sodium taurocholate, Sodium Cholate, Sodium Glycodeoxycholate, Sodium Deoxycholate, and CTAB. ....	72
Figure 38 Equilibrium Surface Tension Sodium Cholate (NaC), Sodium Deoxycholate, Sodium Glycodeoxycholate, Sodium taurocholate and CTAB.....	73
Figure 39. Occupancy of the Stern layer of counterion ( $G_2/G_1$ ) vs concentration of surfactant in the bulk solution.....	77
Figure 40. Dimensionless adsorption ( $\Gamma_1/\Gamma_\infty$ ) for Bile salts vs concentration in the bulk solution. ....	78
Figure 41. The surface potential of biles salts as a function of concentration.....	80
Figure 42. Surface pressure vs Concentration .....	89
Figure 43. Potential vs Concentration.....	90
Figure 44. Dimensionless Adsorption.....	91
Figure 45. Occupancy in the Stern Layer .....	91

## LIST OF ABBREVIATIONS

CMC	Critical Micelle Concentration
MBPM	Maximum Bubble Pressure Method
DST	Dynamic Surface Tension
EST	Equilibrium Surface Tension
MBPT	Maximum Bubble Pressure Tensiometry
BS	Bile Salts
NaC	Sodium Cholate
NaDC	Sodium Deoxycholate
NaTC	Sodium Taurocholate
NaGDC	Sodium Glycodeoxycholate

## SUMMARY

Mass transfer of surfactant molecules from the bulk to the fluid interface determines time-dependent variation in surface tension known as dynamic surface tension. Many biological and industrial processes that involve the formation of drops or bubbles or free surface flows are influenced by dynamic surface tension. In particular foamability, printability and foam/emulsion stability are affected by the dynamic adsorption of surfactant molecules. In addition to bulk diffusion and adsorption-desorption fluxes that control the rate of mass transfer for non-ionic surfactants, the effects of the electrostatic potential created by adsorbed surfactants must be accounted for the mass transfer of ionic surfactants. In this study, the dynamic surface tension (DST) and dynamic adsorption of ionic surfactant cetyltrimethylammonium bromide (CTAB) and four bile salts are characterized and analyzed using maximum bubble pressure (MBP) tensiometry. The interfacial adsorption of CTAB and bile salts is a relatively fast process, and surface tension variation timescales (<50 ms) inaccessible in measurements with Du nouy ring, Wilhelmy plate, and pendant drop methods. A home-built MBP tensiometer is utilized for obtaining dynamic and quasi-equilibrium surface tension data. The time evolution of surface tension is analyzed using a full transient model for mass transfer of ionic surfactants that accounts for non-stationary interface, charge, and diffusion, and the quasi-equilibrium surface tension data are analyzed by using Frumkin and van der Waals isotherms. Surface concentration, surface potential, Gibbs elasticity, critical micelle concentration is obtained for CTAB and four bile salts. In addition, the CTAB data are analyzed to determine an apparatus constant that allows computation of the universal surface age, that corrects for the influence of non-stationary interface as bubble surface is younger than nominal surface age obtained from MBP method. The dynamic adsorption data for bile surfactants shows a more rapid adsorption to the interface, and the quasi-equilibrium datasets indicate that

even though bile micelles are highly surface active, the effectiveness as surfactants for reducing surface tension values is quite limited.

# 1 INTRODUCTION

## 1.1 Surfactants Active Agents

Amphiphilic molecules like lipids and soaps that contain both hydrophilic and hydrophobic groups, spontaneously adsorb at water-air interfaces. The adsorption of such surface active agents leads to a change in interfacial properties including surface tension. Due to their surface activity, surfactants play an important role in many industrial applications (1) and biological processes (2) as self-assembled micelles, cell membranes and vesicles, as foam and emulsion stabilizers, as soaps and detergents for solubilizing dirt and oils (3), as denaturing agents, as frothing agents in food and beverage industry as well as in mining operations, among others. Adsorption times of amphiphiles and their influence on interfacial properties, depends on physicochemical properties of the surfactant, including chemical structure, size, and type of hydrophilic tail, charge (if present), etc. Surfactant molecules are typically categorized according to their charge and the shape of the surfactant molecule.

Surfactants can be classified as ionic, amphoteric or nonionic, depending on presence or absence of charge. The presence of charge influences functionality and properties of surfactants in processes where interaction with other charged molecules is involved. In the context of foams, emulsions or biological membranes, adsorbed ionic surfactant molecules create an electrical potential that affects the mass transport and adsorption of other charged species (proteins, surfactants or drug molecules) to the interface. Ionic surfactants also contribute electrostatic forces that influence the drainage and stability of thin films, influencing stability and properties of foams and emulsions (3).

Many surfactants that are used as soaps and detergents comprise of a charged, hydrophilic head and hydrophobic tail. A typical example of such surfactant is cetyltrimethylammonium bromide, known as CTAB (Figure 1). In this study, we investigate properties of CTAB and contrast their behavior with the bile salts. Unlike CTAB which is a cationic surfactant, bile salts are anionic, and as their chemical structure contains steroid ring system, bile salts have a rigid, flat and slightly curved structure (2) (Figure 2). CTAB dissociates into Cetyltrimethylammonium (CTA<sup>+</sup>) and counterion bromide (Br<sup>-</sup>) when added to water, and it is used in industry to isolate DNA from tissues (4, 5), as a medium for self-assembly nanoparticles (6) and production of gold or silver nanorods (7). On the other hand, bile salts are bio-surfactants present in digestion and they participate in processes such as nutrient absorption, transport of food residues, solubilization and transport of insoluble fats and nutrients in the small intestine, and digestion of lipids (2). The nearly flat shape and rigid structure of bile influence their self-assembly as well interfacial properties including their packing and local interactions as well as dynamic of adsorption and desorption. Human bile contains a mixture of bile salts that are produced by the liver for digestion of lipids. Due to the difference in the number, position and stereochemistry of conjugated amino acids (taurine or glycine) and hydroxyl ions, the surface activity and self-assembly of each bile salt needs to be evaluated separately. Furthermore, bile salts not only play a critical role in physiological processes, bile salts are also fast emerging as valuable biosurfactants with applications in healthcare and pharmaceuticals. For instance the design of healthier foods to avoid obesity (2), the combination of drugs with bile salts for the creation of specific drugs to act in the liver (8), the control of lipid digestion to reduce levels of cholesterol and saturated fats (9), and extraction of DNA for later analysis as vehicles for gene delivery and gene transfection (5). Understanding and

quantifying interfacial properties including DST of bile salts is an important step towards addressing challenges in the field of medicine and pharmaceuticals.

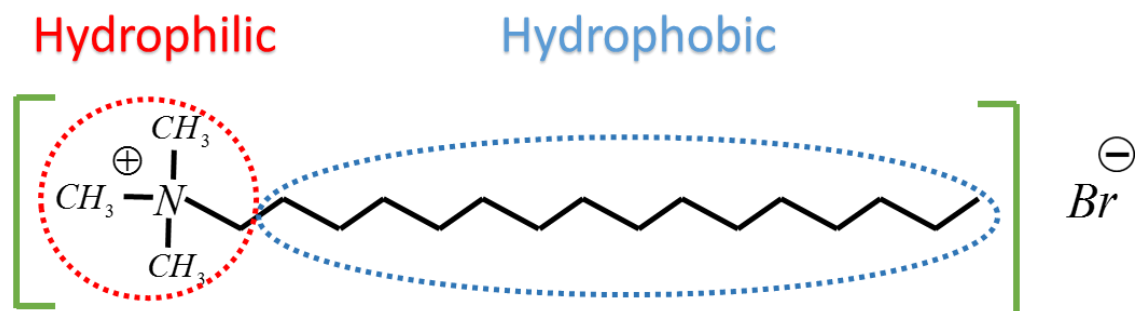


**Figure 1. Chemical structure of CTAB molecule.**  
CTAB is a cationic surfactant molecule

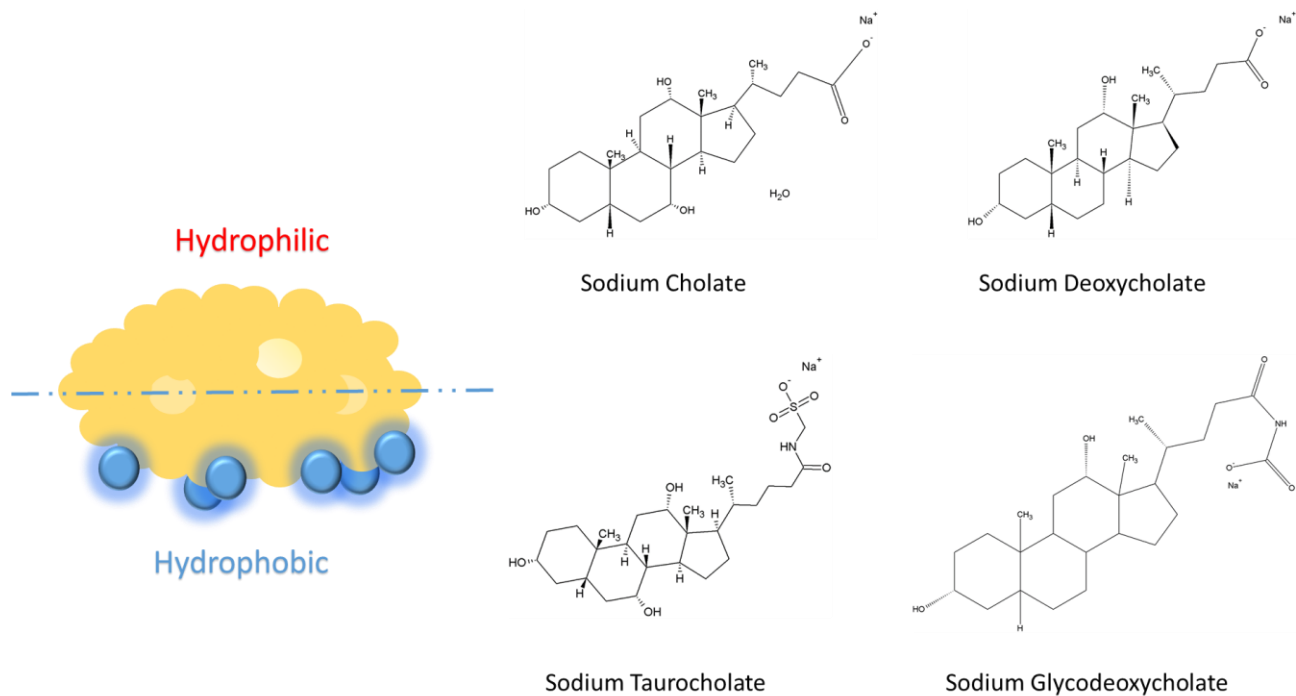


**Figure 2. Schematic structure of the bile salts and the chemical structure of the studied bile salts.**

The hydrophobic side is convex and hydrophilic side is concave and contains hydroxyl groups and amino groups that can be conjugated (2).

Surfactants like CTAB and bile salts spontaneously adsorb at the air-water interface, and the measurement of surface tension and other interfacial properties can be used for determining the hydrodynamic and thermodynamic properties of such amphiphilic molecules. Mass transfer of surfactant molecules from the bulk to a freshly created fluid interface occurs over a finite time and the time-dependent variation in surface tension known as dynamic surface tension. Dynamic adsorption itself depends on the transport mechanism (role of diffusion, adsorption-desorption, and migration or transport of charged species in the response to an electric field). The measurement of dynamic surface tension, allows a comparison between the adsorption time of surfactants, in fast processes like drop or bubble formation or generation of foams or emulsion and in the rapid and precise transfer of fluids as in printing technologies. Therefore, dynamic surface tension affects foamability, foam stability and emulsion stability (10, 11) and printing(12). In this study, we describe the measurement of DST using maximum bubble pressure technique, as discussed next.

## **1.2 Maximum Bubble Pressure Technique**

Dynamic surface tension can be measured by different techniques typically used for making equilibrium surface tension measurements such as shape analysis methods (sessile drop and pendant drop tensiometry), force-based method (Wilhelmy plate, du Noüy ring) and Laplace pressure measurement (as in maximum bubble pressure (MBP) tensiometry). Each method has a range of measurable time scales, limiting the shortest and longest time for which surface tension variations can be evaluated (Figure 3). Macromolecules or proteins take longer times to populate the interface, thus they require techniques with longer time scales. Shape analysis methods like

pendant drop tensiometry as well as force-based techniques such as Wilhelmy plate and Du Noüy ring are well studied for such an application. On the other hand, for small surfactant molecules, adsorption times are shorter, and the conventional techniques are of limited value. However, maximum bubble pressure method can measure dynamic surface tension significantly fast adsorption kinetics and for adsorption of milliseconds to minutes (13). Maximum bubble pressure is a technique that consists in producing fresh interface by creating a solution at a constant flow rate through a capillary that is submerged into it. The pressure inside the bubble is measured, and surface tension is evaluated by means of Laplace equation (14).

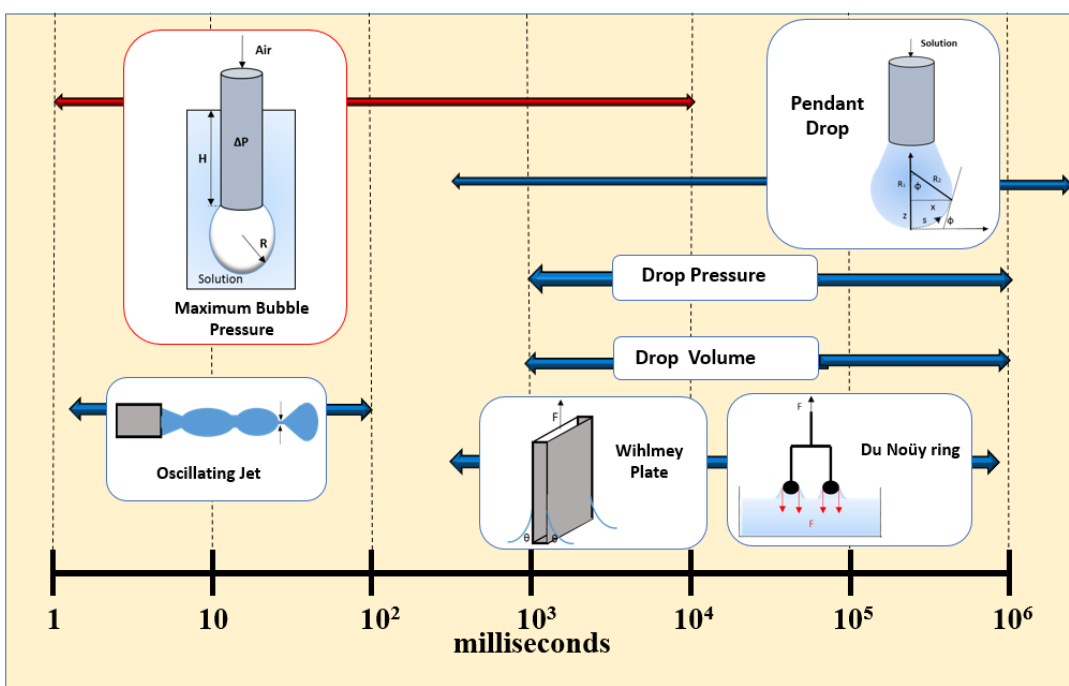


**Figure 3. Dynamic surface tension: Techniques and Timescale (15, 16).**

Techniques as Oscillating Jet and Maximum Bubble Pressure can measure surface tension at short time scales. While Pendant Drop and du Noüy ring are suitable for measuring the effectiveness of molecules which take longer times to reach interfaces such as polyelectrolytes, proteins, and large molecules.

Maximum bubble pressure tensiometry is particularly suitable for analysis of dynamic surface tension effects associated with fast events and fast diffusion process. Short times make this technique attractive among the other techniques in the market although this method has its limitations. For example, dynamic surface tension data measured using different MBP apparatuses differ among themselves, because adsorption occurs at a moving interface [see next section for detailed discussing] and the presence of convective mass transport makes quantitative comparisons harder.

Due to the differences between measurements made with different MBP tensiometers and between MBP and other tensiometry techniques, several authors including Christov *et al.* (13) and Frainerman *et al.* (17) developed theoretical arguments and analysis protocols to standardize the measurements made with MBP method. Christov *et al.* (13) determines an apparatus constant that accounts for contributions by convective transport to the nonstationary interface and the apparatus constant is used for calculating a corrected universal surface age. Fainerman *et al.* (18) evaluated a critical pressure and a critical flow rate for bubbling to jetting transition and developed that a formula based on these values to define an effective adsorption time that they call a surface lifetime. The surface lifetime computed in this protocol allows measurement of sub-millisecond adsorption processes; but as aperiodic and chaotic bubbling can occur even before jetting sets-in, the accuracy of their measurement at short time-scales is questionable. In this study, the approach described by Christov *et al.* (13) is followed for its appears to more theoretically robust. Furthermore, Christov *et al.* (13) describe the transport model that can be used for capturing variation in surface tension, as is discussed next.

### 1.3 Adsorption of amphiphiles

For non-ionic surfactants, the transport of surfactant molecules to the static interface depends on two transport mechanisms: diffusion (from bulk to subsurface) and adsorption-desorption (subsurface-interface). Ward and Tordai (19) developed the first comprehensive model for the describing transport of surfactants from bulk phase to an interface. When diffusion times are longer than the adsorption-desorption times, diffusion is said to be the transport-limiting step and a local equilibrium is assumed between the subsurface and the surface. However when the adsorption-desorption times are longer, an adsorption barrier is said to exist between the subsurface and surface, and the adsorption-desorption is modeled by a kinetic model (20).

In the case of ionic surfactants, the mass transfer to the interface is affected by the potential generated due to the charge density produced at the interface due to the adsorption of surfactants. Three different approaches have been proposed to model the mass transfer of ionic surfactants to the air-water interface (21) that is considered energetically homogeneous. The first model accounts for the effect of electrical potential on bulk transport, involves the solution of Nernst-Planck equation to account for both diffusion and migration (in response to electric field), and either assumes an equilibrium between the subsurface and surface, or account for sorption-desorption using an equilibrium or kinetic model (22, 23). The second model, called quasi-equilibrium model, neglects the effect of the electrical potential of the diffusion process, and the adsorption-desorption of the surfactant between subsurface and surface can be assumed in equilibrium or kinetic model (21, 23). Finally, the third approach uses a free-energy formulation, wherein the electrochemical potential is used and effect of entropy at the interface and in the bulk are all accounted for in a non-equilibrium formulation (24).

In this study, we will follow the formulation and the analytical solution (for long-time asymptotics) developed by Danov *et al.* (22) and utilized by Christov *et al.* (13) for analyzing dynamic surface tension data, because it takes into account the interfacial expansion that is present in the maximum bubble pressure method, and additionally also account for the influence of electrostatic potential on the mass transfer process (first approach). The analytical solution obtained in this model makes it attractive compared to other solutions proposed to evaluate the electrodiffusion model (23). For example, MacLeod and Radke (23) presented a numerical solution to for their model for mass transfer of ionic surfactants, but as convection term is not included, the laborious numerical is less insightful than the model from Danov and coworkers (22). The thermodynamics of adsorption will be evaluated following the approach described in Kralchevsky *et al.* (25), where the quasi-equilibrium surface tension data from MBP measurements are compared to the isotherm models, to determine the value of surface potential and surface excess for counterion and surfactant.

## 1.4 Motivation

The dynamic surface tension (DST) and dynamic adsorption of ionic surfactant cetyltrimethylammonium bromide (CTAB) and four bile salts are characterized and analyzed using maximum bubble pressure (MBP) tensiometry in this study. Due to the relevance of bile salts in physiological processes including digestion, a large number of studies (from the physical chemistry perspective) have focussed on the solubilization of fats by micelles (26-29) and were carried out using a mixture of bile salts to emulate the conditions within the human body (8). Only a countable few studies examine the dynamic adsorption of bile salts. The dynamic surface tension measurements have been reported only for a few concentrations of sodium taurocholate and

sodium glycodeoxycholate (2, 30), and to the best of our knowledge, have not dynamic surface tension measurements have not been reported for sodium cholate and sodium deoxycholate. The lack of data is possibly due to the fact that fast rate of interfacial adsorption requires the use of maximum bubble pressure tensiometry as more readily available techniques (like pendant drop tensiometry or Wilhelmy plate methods) lack the time resolution necessary for carrying out the necessary measurements. In the case of thermodynamic of adsorption, maximum surfaces excesses have only been reported for sodium deoxycholate (29) and sodium cholate (29, 31, 32), these data have been determined by Gibbs equation or have been obtained by assuming that these charged molecules follow models developed for non-ion surfactants (31). The present study is motivated by the need for more extensive data on dynamic surface tension and analysis of dynamic adsorption of bile salts with theoretical model that accounts for charge on the surfactant as well as counterion binding in the adsorption layer, similar to the approach described by Kralchevsky *et al.*(25) for surfactants like sodium dodecyl sulfate (SDS) typically used as soaps and detergents (25).

In the present study, we focus on the dynamic adsorption of four bile salts. We first optimize the experimental procedure and analysis framework by examining the adsorption kinetics of CTAB using maximum bubble pressure tensiometer. The time evolution of surface tension is analyzed using a full transient model for mass transfer of ionic surfactants that accounts for non-stationary interface, charge, and diffusion, and the quasi-equilibrium surface tension data are analyzed by using Frumkin and van der Waals isotherms. The dimensionless apparatus constant for our MBP apparatus is evaluated by using dynamic surface tension data and equilibrium surface tension data, and this allows an estimation of universal surface age. The analysis of quasi-equilibrium surface tension data includes consideration of both counterion binding and electrical double layer (EDL) and finally, additional parameters such as Gibbs elasticity, the energy of adsorption, and area per

molecule are determined. The analysis protocols are then repeated for the four bile salts. The present thesis includes extensive data sets acquired for dynamic adsorption of bile salts and a thorough analysis of fluxes that contribute to mass transfer and thermodynamic effects that affect adsorption behavior.

## 2 BACKGROUND THEORIES

### 2.1 Dynamic adsorption of surfactants

In aqueous solutions, amphiphilic molecules like CTAB and bile salts spontaneously adsorb at the liquid-gas interface. The transfer of these amphiphiles molecules from the bulk to the fluid interface is driven by a chemical potential gradient, which eventually leads to an equilibrium concentration at the interface (24). As the concentration of adsorbed surfactant increases at the interface, surface tension decreases (Figure 4) over time.

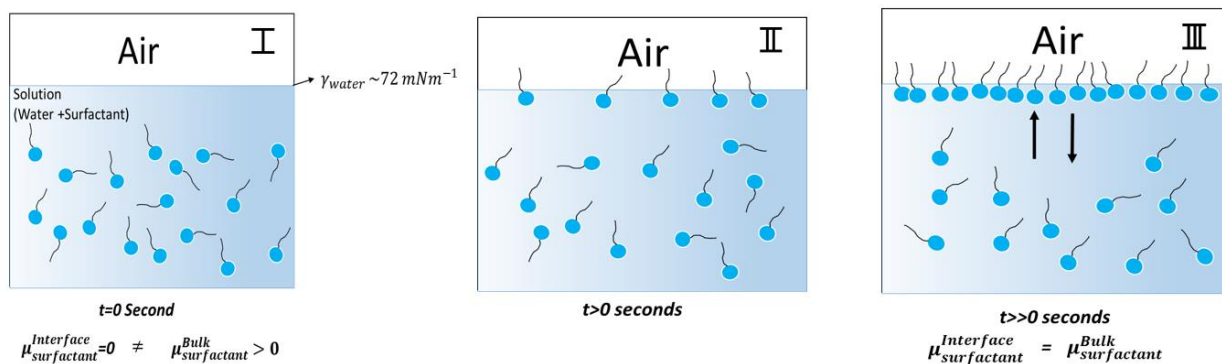


**Figure 4. Schematic showing the dynamic adsorption of surfactants**

When a surfactant is added into the water at time zero, surfactant chemical potential is zero at the interface while in the solution it is greater than zero. Therefore, a chemical potential gradient induces the transport of surfactant molecules to the interface until equilibrium is reached.

For non-ionic species, mass transfer from the bulk to the interface is controlled by two dynamic processes: diffusion and adsorption (21). Surfactant molecules are transported from the bulk to a subsurface by diffusion (gradient of concentration) and then from the subsurface to the interface by adsorption (also known as a jump to the interface). When the adsorption is faster than diffusion, the transport of the surfactant is controlled by diffusion and a local equilibrium between the subsurface and the interface can be assumed, which can be modeled by an isotherm. For a freshly created interface, diffusion is usually the rate limiting step (see Step 1 in Figure 4). In the late stage, adsorption is the rate-controlling process, and a kinetic relation is needed (33). The latter case occurs due to the formation of an adsorption barrier due to the configuration and orientation of adsorbed molecules, an increase of surface pressure at the interface, or due to fewer sites of adsorption. Though the dynamic adsorption of ionic surfactants involves additional effects due to the presence of charge on surfactant and counterions, as well as at the interface, flux contributions by diffusion and adsorption-desorption are also present. Surface tension against  $t^{-1/2}$  plot helps to determine whether it is diffusion-controlled or adsorption controlled. If surface tension shows a linear dependence with  $t^{-1/2}$  for a long time, the process is diffusion-controlled, otherwise, an adsorption barrier is said to exist (31). In this work, it is assumed and verified that for the case of CTAB, the process is diffusion-controlled at long times. Unlike non-ionic surfactants that display diffusion-limited kinetics at short time scales, the ionic surfactants are deterred initially by the presence of a barrier, and even with maximum bubble pressure tensiometry, the resistance of adsorption at an early stage of dynamic adsorption is often not captured, as discussed later in the thesis. For ionic surfactants, an electrostatic diffuse layer (see Figure 5) appears near to the surface due to the charged interface, which affects the mass transfer of the molecule surfactant. The complete analysis of mass transfer to the interface turns out to be a singular perturbation problem,

and since a detailed analysis can be found in Danov *et al.*(22), only highlights of the underlying physics and final asymptotic solution, with relevant assumptions, are summarized in the following pages.

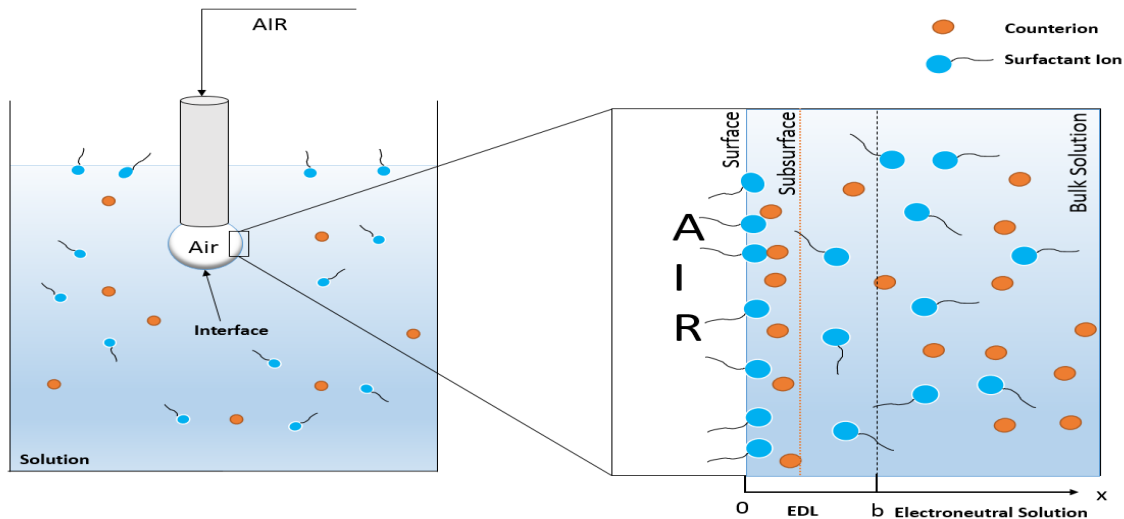


**Figure 5. Schematic showing interfacial adsorption area of ionic surfactant solution. Ionic surfactant dissociates in aqueous solution into surfactant ions and counterions.**

Surfactant ions adsorb at the interface while counterions adsorb at the Stern plane. Charged surface generates a diffuse electrical double layer (EDL). From the end of the EDL to further the solution is electroneutral. Surfactant molecules diffuse until the subsurface and from the latter, they adsorb to the interface.

The surfactant transport from the bulk to the interface is defined by the conservation equation, which considers convection, diffusion, migration (34).

$$\frac{DC_i}{Dt} = \left[ D_i \nabla^2 C_i + D_i \frac{z_i F}{RT} \nabla \psi (C_i \nabla \psi) \right] \quad (1)$$

Here  $C_i$  is a concentration of the ion  $i$ ;  $D_i$  is the diffusion coefficient the ion  $i$ ;  $\psi$  is the electrostatic potential;  $F$  is the Faraday constant and  $z_i$  is the charge of the ion. For ionic surfactants and mobile interfaces, the migration and convection terms need to be considered respectively. Here we follow the notation and framework described by Danov *et al.* (22). The conservation equation for a system with continuously expanding interface can be rewritten as:

$$\frac{\partial C_i}{\partial t} = D_i \frac{\partial}{\partial x} \left( \frac{\partial C_i}{\partial x} + C_i \frac{\partial \phi}{\partial x} \right) + \dot{\alpha} x \frac{\partial C_i}{\partial x} \quad (2)$$

Here  $\phi$  is the dimensionless electrostatic potential and  $\dot{\alpha}$  represents the interfacial expansion rate as convection contribution defined by Danov *et al.* (22). The first term represents contribution by diffusional and migration fluxes respectively.

When the diffusion layer is smaller than curvature radius, the bubble surface can be modeled as a planar interface (applied for curvature radius larger than or equal to 100–150  $\mu\text{m}$ ). In our MBP set-up the minimum curvature radius (capillary radius  $\approx 130\mu\text{m}$ ) is large enough, (assumption is thus valid), therefore it is reasonable to consider it as a planar surface (22).

The potential is related to charge distribution by using a Poisson-Boltzmann equation that combines the Poisson's formula for potential distribution with the statistical ion density that follows Boltzmann distribution:

$$\frac{\partial^2 \psi}{\partial x^2} = -\frac{F}{\varepsilon} \sum_i z_i C_i \quad (3)$$

The  $\varepsilon$  parameter is the permittivity of the solution. Out of the EDL, the solution is considered as electroneutral. Therefore:

$$\sum_i z_i C_{i\infty} = 0 \quad (4)$$

The concentration of ion  $i$  at  $x \rightarrow \infty$  is the parameter  $C_{i\infty}$ . The first boundary condition is given by the mass balance between amount adsorbed and the amount of surfactant in diffuse layer.

$$\frac{d\Gamma_i}{dt} + \dot{\alpha} \Gamma_i = D_i \left( \frac{\partial C_i}{\partial x} + C_i \frac{\partial \phi}{\partial x} \right)_{x=0} \quad (5)$$

The surface concentration of the ion  $i$  is the parameter  $\Gamma_i$ . The second boundary condition is obtained from electric field intensity is,

$$\left(\frac{\partial\phi}{\partial x}\right)_{x=0} = -\frac{\kappa^2}{2C_{2\infty}}(\Gamma_2 - \Gamma_1) \quad (6)$$

$\kappa$  is the Debye length that is the same thickness of the EDL.

Finally, using Gibbs adsorption equation, in order to connect surface tension with surface concentration, and replacing terms, leads to the following expression which is an asymptotic approximation for long times derived by Danov *et al.* (22):

$$\gamma = \gamma_{eq} + \frac{S_\gamma}{(t_{age})^{1/2}} \quad (7)$$

$$S_\gamma = \frac{kT\Gamma_{1,eq}^2 \lambda}{(\pi D_{eff})^{1/2}} \left( \frac{1}{C_{1\infty}} + \frac{1}{C_{2\infty}} \right) \quad (8)$$

Where  $\lambda$  is a constant for each MBPM apparatus that rely on the surface expansion rate of the bubble (13), and allows comparing dynamic surface tension data among tensiometers. The universal surface age is defined as the ratio of surface age (experimental one) by  $\lambda^2$ .

$$t_u = \frac{t_{age}}{\lambda^2} \quad (9)$$

This apparatus constant  $\lambda$  can be calculated either from shape analysis of the bubble growth (measuring rate area change per time) or can be calculated directly by fitting dynamic surface tension data obtained from a tensiometer with immobile interface and contrasting it with data from a tensiometer with mobile, nonstationary interface (for example using MPB measurements) (13).

The first fitting (non-mobile interface) can also be evaluated from the fitting of equilibrium surface tension curves with an equation of state.

From shape analysis of the bubble, a function of the change of interfacial area with time can be determined. The apparatus constant can be evaluated using the following equation.

$$\lambda = \int_0^{\tau_1} \frac{1}{(\tau_1 - \tau_d)} \frac{d}{dt_d} [\tilde{A}(t_d)] dt_d \quad (10)$$

Here  $\tau_d$  and  $\tilde{A}$  are dimensionless time and area respectively;  $\tau_1$  and  $\tau_d$  are integrals of the dimensionless area with the time that goes from 0 to 1 for the first one and from 0 to  $t_d$  for the latter one. From fittings of dynamic surface tension and equilibrium surface tension curves,  $S_\gamma$  and  $S_{\gamma,0}$  can be calculated respectively, and  $\lambda$  can be evaluated as follows.

$$\lambda = S_\gamma / S_{\gamma,0} \quad (11)$$

The  $S_\gamma$  is a constant obtained from the slope surface tension versus  $t^{-1/2}$  for long times and  $S_{\gamma,0}$  is determined by the following expression:

$$S_{\gamma,0} = \frac{kT\Gamma_{1,eq}^2}{(\pi D)^{1/2} \gamma \pm C_\infty} \quad (12)$$

$\Gamma_{1,eq}$  is equilibrium surface concentration of the surfactant ion;  $\gamma$  is the activity coefficient.

### 2.1.1 Dynamic Surface Tension

Dynamic surface tension refers to the change of surface tension with time. For the pure solvent, there is no change in surface tension with time because the interfacial composition and intermolecular interactions do not change with time. In the case of solutions, the change of surface

tension could be positive (salt) or negative (surfactant), depending on the interactions between the surfactant molecules, solvent-solvent molecules, and surfactant-air molecules (or second phase). Dynamic surface tension graph indicates the decrease in surface tension with a surfactant as well as the rate with surfactant populates the interface (Figure 6). At time zero, the surface tension is equal to the solvent surface tension because surfactant molecules have not reached the interface. When the slope of the curve of dynamic surface tension is almost zero, surface tension is equal to the equilibrium surface tension. In maximum bubble pressure tensiometry, often quasi-equilibrium values are measured (as shown in the example below).

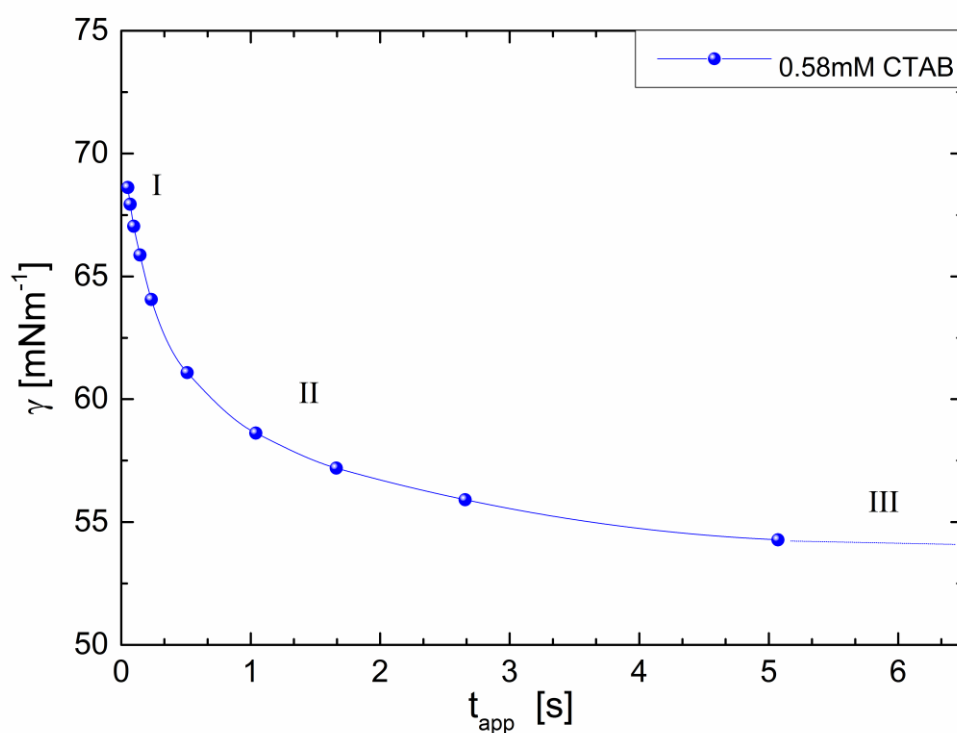


**Figure 6 Dynamic surface tension data corresponding to the dynamic adsorption sketched in Figure 4.**

Apparent surface age ( $t_{app}$ ) is the adsorption time measured using MBP tensiometer without applying a correction for expanding interface. Stage I shows that nearly clean interface when the surface tension values are similar to the value for a pure solvent. Stage II shows the decrease of surface tension value as the surfactant concentration increase in the interface. Stage III shows that a quasi-equilibrium has been reached.

Dynamic surface tension measurements by tensiometers where surface area is fixed during the adsorption period differ from the ones where surface area is expanding constantly while surfactants are adsorbing at the interface. In the case of maximum bubble pressure, convection will influence the transport of surfactants to the interface (13). The raw data obtained from maximum bubble pressure tensiometer needs to be rescaled using apparatus constant as discussed earlier.

### **2.1.2 Equilibrium Surface Tension**

The equilibrium surface tension refers to the surface tension reached when the gradient of chemical potential between the bulk solution and the interface becomes zero for all active surface agents present in the solution (24). Dynamic surface tension shows the change in surface tension with time, which is correlated with change in concentration and conformation/packing of surfactants at the interface. Surface tension eventually attains constant time invariant value. At this stage, the system has attained the equilibrium and the surface tension at that point is equilibrium surface tension (ST). Values for the equilibrium surface tension should be taken at intermediate times in order to avoid the effect of impurities which lower the ST due to high surface activity (35). Equilibrium surface tension decreases with increase in the concentration of the surfactant. A rapid change or sharp transition in the slope of equilibrium surface tension curve with concentration is observed. The concentration at the end of the sharp transition is the critical micelle concentration (CMC). Beyond CMC, surfactants in the bulk self-assemble to form agglomerates called micelles, and the shape and size of micelles depends on the concentration of surfactants as well as the

geometric shape and interactions. Above CMC, surfactant exists in a dynamic equilibrium between aggregated state, adsorbed to the interface and as monomers.

From equilibrium surface tension data, the isotherm that relates the surface concentration with the subsurface concentration can be determined, following the algorithm established by Kralchevsky *et al.* (25). In this approach, an equation of state that accounts for the counterion binding and the effect of the electrostatic double layer (EDL) is used for fitting the equilibrium surface tension data.

The algorithm works as follows. Firstly, the subsurface concentration is calculated using Boltzmann's distribution and dimensionless surface potential value  $\phi_s$  is assumed as initial value of the posterior iteration.

$$a_{is} = a_{i\infty}(-z_i\phi_s) \quad (13)$$

Where  $a_{is} = \pm\gamma C_{is}$ ,  $z_i = \frac{z_i}{z_1}$  and  $\phi_s = \frac{z_i e\psi_s}{kT}$ .  $C_{is}$  is the concentration in the subsurface and the activity coefficient ( $\pm\gamma$ ) is considered as 1. Then an estimated surfactant surface concentration ( $\Gamma_1$ ) is calculated from Frumkin and Van der Waals isotherm, by assuming values for the constants  $\beta$ ,  $\Gamma_\infty$ ,  $K_1$  and  $K_2$ , as discussed next.

Frumkin isotherm

$$Ka_{is} = \frac{\Gamma_1}{\Gamma_\infty - \Gamma_1} \exp\left(-\frac{2\beta\Gamma_1}{kT}\right) \quad (14)$$

van der Waals isotherm

$$Ka_{1s} = \frac{\Gamma_1}{\Gamma_\infty - \Gamma_1} \exp\left(\frac{\Gamma_1}{\Gamma_\infty - \Gamma_1} - \frac{2\beta\Gamma_1}{kT}\right) \quad (15)$$

Frumkin model refers to localized adsorption while van der Waals model refers to non-localized adsorption (36). Here the parameter  $\beta$  reflects the interaction of the molecules that are adsorbed to the interface. For air-water interface, the value of  $\beta > 0$  and this parameter characterizes the attraction between hydrocarbon tails. In the case of the oil phase,  $\beta = 0$ . The maximum surface excess  $\Gamma_\infty$  is reached when surfactant molecules are closed packed at the interface (37). In the case of Frumkin isotherm  $1/\Gamma_\infty$  express the area per adsorption site, and  $\Gamma_\infty$  is a scale parameter, whereas in the case of van der Waals isotherm (see equation 15),  $1/\Gamma_\infty$  refers to the excluded area per molecule (37, 38).

The parameter  $K$  is related to the activity of the surfactant and to the free energy of adsorption i.e energy gained from bringing a surfactant molecule to the interface (38).

$$K = K_1 + \sum_{i=2,4,6..} K_i a_{is} \quad (16)$$

Where  $K_i$  is the contribution from counterions to the constant of the adsorption model. After calculating the surface concentration of the surfactant the counterion adsorption can be evaluated using an isotherm for the counterion that meets the Euler's condition.

$$\frac{\Gamma_i}{\Gamma_1} = \frac{K_i a_{is}}{K_1 + \sum_{i=2,4,6..} K_i a_{is}} \quad (17)$$

Additionally, Gouy's equation relates the surface concentration of surfactant ion and counterion with the surface potential. The surface potential value is then obtained by an iterative procedure such that the following equation is satisfied [18].

$$\Gamma_1 - \Gamma_2 = 4 / k_c \sqrt{a_{2\infty}} \sinh\left(\frac{\phi_s}{2}\right) \quad (18)$$

Finally, by using the surface tension isotherm that includes the effects of the electrical double layer and counterion binding, surface tension is evaluated for each concentration by minimizing the error between the calculated surface tension and the experimental data and surface potential and the other mentioned constants are then calculated. The surface tension isotherm follows by considering the Gibbs adsorption model for ionic surfactants, and it relates the total adsorption ( $\tilde{\Gamma}_i$ ) (which is the produced surface concentration of surfactant by the Stern layer ( $\Gamma_i$ ) and the electrical double layer) corresponding to the bulk concentration ( $C_{i,\infty}$ ) with a surface tension value ( $\gamma$ ). Also, the expression is derived by assuming an equilibrium between the subsurface and the surface with the equilibrium isotherm ( $a_{is} = \pm \gamma C_{is} = f(\Gamma_i)$ ) and the concentration in the bulk is related to in the subsurface concentration by using the Boltzmann's equation  $C_{is} = f(C_{i\infty}, \phi_s)$  in conjunction with the Poisson equation. The total surface tension thus includes two contributions, as discussed below.

$$\gamma = \gamma_o - kT(J + 2F) \quad (19a)$$

Here  $J$  is the contribution from the adsorbed molecules, and it is obtained from the adsorption isotherms ( $a_{1s} = f(\Gamma_1)$ ), as follows.

$$J = \int_0^{\Gamma_1} \Gamma_1 \frac{d \ln C_1}{d \Gamma_1} d \Gamma_1 \quad (19b)$$

The parameter  $F$  represents the contribution from the electrical double layer, and is evaluated using the following expression:

$$F = \frac{1}{\kappa} \int_0^{\phi_s} \left\{ \sum_{j=1}^N a_{i\infty} [\exp(-z_i \Phi) - 1] \right\}^{1/2} d \Phi \quad (19c)$$

## 2.2 Additional Parameters

There are additional parameters that are needed for analyzing the dynamic and static surface tension data, or can be deduced or computed using the datasets obtained. We next list these parameters and describe their role in leading to a better understanding dynamic adsorption of any surfactant.

### 2.2.1 Diffusivity

The diffusion coefficient can be calculated by using Stokes Einstein's equation (39):

$$D_{AB} = \frac{kT}{6\pi R_A \mu_B} \quad (20)$$

Here  $D_{AB}$  represents diffusivity of the solute (A) in the solvent (B),  $R_A$  is the radius of the solute and  $\mu_B$  is the solvent viscosity. The literature values for Stokes' radii and diffusion coefficient for different species (40-43) are included in the following table, along with diffusion coefficients calculated using equation [20].

#### **Table I. Diffusion coefficients of bile salts and CTAB**

The reported values for Sodium Taurocholate and Sodium Glycodeoxycholae Oh(40), Sodium Cholate (44), Sodium Deoxycholate (45), CTAB (46).

	Literature values Diffusion coefficients ( $\text{cm}^2\text{s}^{-1}$ )	Stokes Radii (nm)	Diffusion Coefficients ( $\text{cm}^2\text{s}^{-1}$ ) Stokes Einstein Equation
Sodium Taurocholate	$1.57 \times 10^{-6}$	2.09	$1.17 \times 10^{-6}$
Sodium Glycodeoxycholate	$1.50 \times 10^{-6}$	2.19	$1.12 \times 10^{-6}$
Sodium Cholate	$0.46 \times 10^{-6}$ - $0.68 \times 10^{-6}$	-	-
Sodium Deoxycholate	$0.45 \times 10^{-5}$ - $0.72 \times 10^{-5}$	-	-
CTAB	$4.5 \times 10^{-6}$	-	-

Once the data is fitted, the following parameters can be calculated.

### 2.2.2 Energy of adsorption

The standard free energy of adsorption of an ion  $i$  can be calculated using the following relationship (25).

$$K_1 = \frac{\delta_1}{\Gamma_\infty} \exp\left(\frac{\Delta\mu_1^{(0)}}{kT}\right) \quad (21)$$

Here  $\Delta\mu_1^{(0)}$  is the standard free energy of adsorption and  $\delta_1$  is the thickness of the adsorption layer created by the packing of surfactant molecules. The thickness  $\delta_1$  can be assumed as the characteristic dimension of the respective molecule (36).

Similarly, the free energy of the adsorption of the counterion binding can be calculated by the following expression.

$$\frac{K_2}{K_1} = \frac{\delta_2}{\Gamma_\infty} \exp\left(\frac{\Delta\mu_2^{(0)}}{kT}\right) \quad (22)$$

$\delta_2$  is the thickness of the Stern layer, which is formed by counterion adsorbed on the adsorption layer.

### 2.2.3 Gibbs elasticity

The Gibbs elasticity ( $E_G$ ) measures the mobility of the surfactant at the interface (38). At high values of  $E_G$  the interface is considered as an immobile interface (or rigid interface) (38). For low concentration, “Marangoni effect” that is the flow caused by the gradient of surface tension, affects the hydrodynamic regimes at the interface (38). The elasticity of the adsorbed monolayer can be calculated by the following equations (38).

$$E_G = -\Gamma_1 \frac{\partial \sigma}{\partial \Gamma_1} \quad (23)$$

This Gibbs equation returns the following expressions for Frumkin and van der Waals adsorption isotherms (38).

Frumkin

$$E_G = kTG_1 \left( \frac{G_\infty}{G_\infty - G_1} - \frac{2bG_1}{kT} \right) \quad (24)$$

van der Waals

$$E_G = kTG_1 \left( \frac{G_\infty^2}{(G_\infty - G_1)^2} - \frac{2bG_1}{kT} \right) \quad (25)$$

## 2.2.4 Area per adsorbed molecule

The area per adsorbed surfactant molecule is defined as:

$$\alpha \equiv 1/\Gamma_\infty \quad (26)$$

Area per adsorbed molecule can be obtained from surface tension data and can also be calculated theoretically from the following expression (assuming circular cross section).

$$\alpha = \pi r^2 \quad (27)$$

where  $r$  is the ion radius, in the case of the  $C_nTAB$  ( $n = 12, 14, 16$ ) in the literature (38) the area calculated from molecular size is  $37.8 \text{ \AA}^2$  and from reported surface tension fits is  $36.5 - 39.5 \text{ \AA}^2$  (46).

### 3 MATERIALS AND METHOD

#### 3.1 Materials

Cetyltrimethylammonium bromide (CTAB) is a cationic surfactant that dissociates into cetyltrimethylammonium and bromide in an aqueous solution (47). In this study, CTAB is studied as a representative example of common surfactants that typically contain a hydrophobic tail and hydrophilic head.

Bile salts found in the human body are normally conjugated, mostly with glycine (75%) and on smaller percentage with taurine (25%) (8, 48). For this reason, four conjugated bile salts were selected for this study: sodium taurocholate (NaTC) and sodium glycodeoxycholate (NaGDC), and their simpler structural forms, sodium cholate (NaC), and sodium deoxycholate (NaDC), which differ due to their hydroxyl groups. All surfactants used in this study were purchased from Sigma-Aldrich and were used without further purification. The following table lists the properties for chosen surfactants (provided by the seller):

**Table II. Properties of surfactant molecules provided by Sigma-Aldrich**

Surfactant	Purity	CMC	Solubility Water
Sodium Taurocholate Hydrate	≥97% (TLC)	-	50 mg/ml
Sodium Glycodeoxycholate	≥97% (TLC)	-	0.1 M
Sodium Deoxycholate	≥97% (titration)	2-6 mM (20-25°C)	-
Sodium Cholate Hydrate	≥99%	9-15 mM (20-25°C)	1 M

Hexadecyltrimethylammonium Bromide	≥98%	-	-
---------------------------------------	------	---	---

The aqueous solutions were prepared with deionized water purified by a Milli-Q. The water was taken with a resistivity of 18 MΩ-cm.

### 3.2 Experimental Procedure

Aqueous solutions of CTAB were prepared in a concentration range  $C = 0.23\text{ mM} - 40\text{ mM}$ . The prepared solutions precipitated due to the low temperatures in the lab and crystals appear in some of the solutions as the Krafft temperature, for CTAB in water ranges between 20 °C – 25 °C (49). Before performing the experiments, the surfactants were solubilized by heating slightly and then cooling down to a temperature moderately higher than the room temperature ( $\sim 27\text{ °C}$ ).

Solutions of Sodium Cholate [NaC] with water were prepared in a range of concentrations of 1 mM - 40 mM. Solutions of Sodium Deoxycholate [NaDC] with water were prepared in a range of concentrations of 0.5 mM - 30 mM; Solutions of Sodium Glycodeoxycholate [NaGDC] with water were prepared in a range of concentrations of 0.1 mM - 20 mM and solutions of Sodium Taurocholate [NaTC] with water were prepared in a range of concentrations of 0.1 mM - 20 mM. The range of concentrations selected is both below and above CMC.

Surface tension was measured by the maximum bubble pressure method (MBPM) using a home-build set-up showed schematically using Figure 7. The experimental set-up consists of a capillary submerged in a beaker filled with the sample solution (or pure solvent). Air is pumped into the

solution to produce bubbles at a predetermined volumetric flow rate, or bubbling rate, set by using 20 ml BD syringe affixed to a syringe pump (Harvard Apparatus PHD 2000 infusion). The BD syringe is connected to a three-way valve, with its the two other outlets connected to the capillary, and the pressure sensor respectively. For the measurements involving CTAB solutions, a hydrophilic capillary with an inner radius of 0.13 mm was used, and the capillary exit was immersed at depth of 1.65 cm within the surfactant solution. For measurements involving solutions of four bile salts, hydrophobic capillary, with an inner radius 0.139 mm was used and. The hydrophobic capillary was immersed 0.5 cm into the solution samples. The pressure transducer used for procured for OmegaDyne INC. Data is recorded using a PC using 800 scans per second. The pressure sensor has a range 0-1psi (+/- 0.08%).

Surface tension measurements are performed with sample volumes of 100 ml. Before each set of measurements, the capillary and tubes are purged by pumping gas through it. After purging, the system is left at rest for 5 minutes, and the system pressure is measured without submerging the needle (correction factor see eq. [29]). After purging and measuring system pressure, a calibration check is made with deionized water to ensure validity to our results. Gas flow rates in the ranges 0.1 ml/s - 6ml/s are used to obtain maximum pressure measurements for a range of adsorption times, and the resulting data is used for obtaining dynamic surface tension data [as explained next].

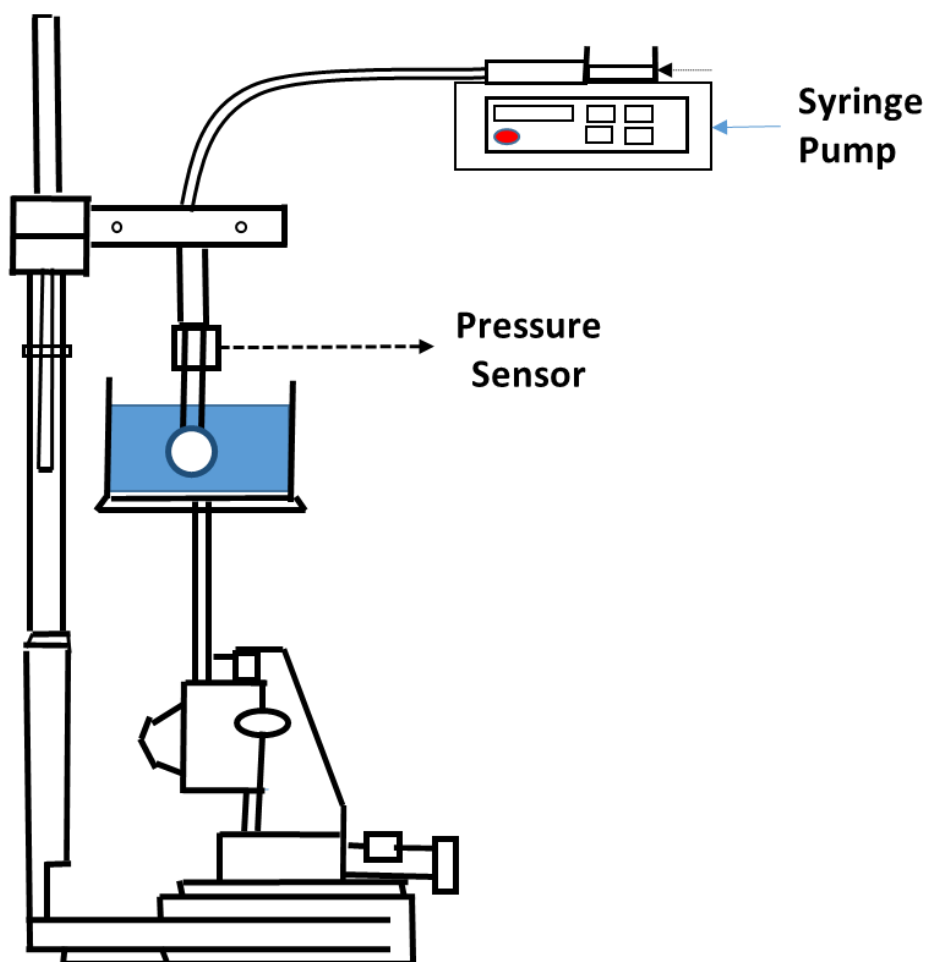


**Figure 7. Schematic of Maximum Bubble Pressure Tensiometer.**

A syringe pump sets the bubbling rate, and a pressure sensor measures the pressure variation within the bubble as it forms, grows and pinches-off.

In the maximum bubble pressure method (MBPM), the fresh interface is generated with each bubble blown into the solution. The bubbling rate is set by using a syringe pump to control the constant volumetric flow rate at which air is pumped through the capillary submerged in a sample solution or pure solvent. The pressure sensor measures the variation in pressure inside each growing bubble. The measured pressure includes contributions from the hydrostatic pressure that depends on the depth of the bubble and the capillary pressure that depend on the curvature radius

according to the Young-Laplace equation. The Young-Laplace equation relates surface tension with the pressure differential across a curved surface (14, 50).

$$\Delta P = \sigma \left( \frac{1}{R_1} + \frac{1}{R_2} \right) \quad (28)$$

In the case of a spherical bubble immersed into a fluid, the two radii of curvature are equal  $R_1 = R_2 = R$  and the pressure change is, therefore  $\Delta P = \sigma \frac{2}{R}$ . However, as other forces are being exerted on the bubble in the case of maximum bubble pressure method, the expression for the pressure is (14).

$$P = \frac{2S}{r} - rgh - C \quad (29)$$

The correction factor  $C$  corrects for system pressure and sensor calibration. Since pressure values are inversely proportional to the radius of curvature, initially, the radius of curvature is large [I] as shown schematically in Figure 8, and as the bubble grows, the radius of curvature decreases with the pressure value rising up till it reaches its maximum value when the radius of curvature is minimum. The maximum pressure value is obtained for bubble radius equal to capillary radius [II]. After stage [II], the pressure decreases dramatically as the bubble shows abrupt growth. A new cycle begins right after a bubble detaches from the capillary [III].

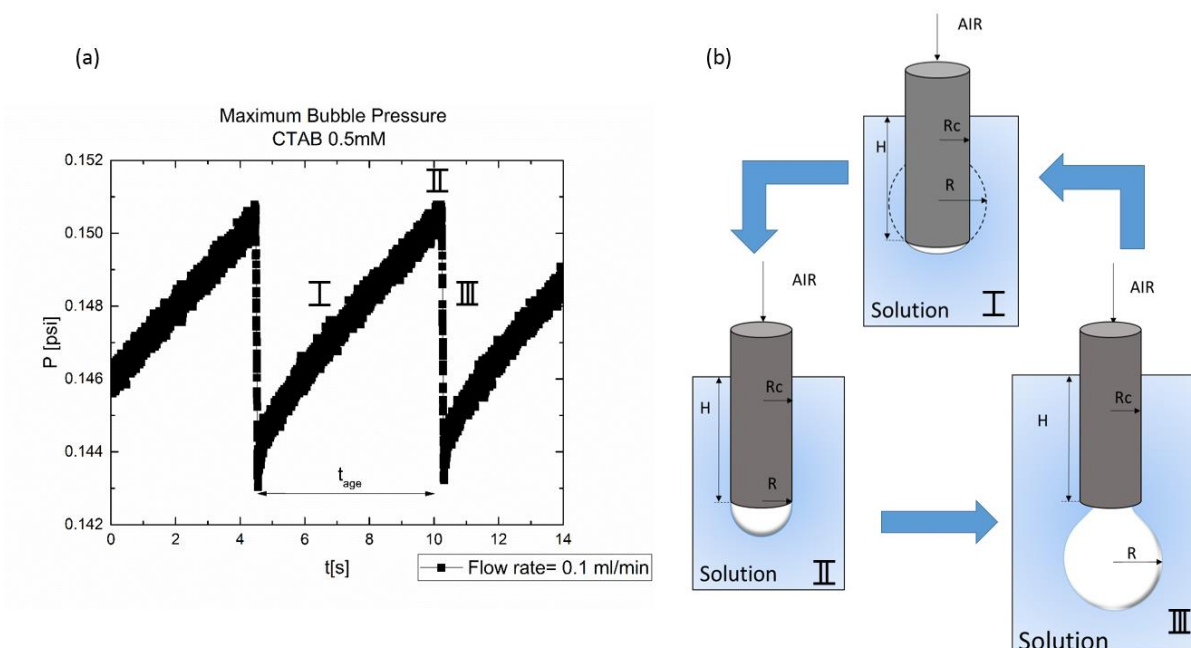


**Figure 8. Pressure evolution over time as a function of bubble radius**

(a) Pressure evolution data for bubble formation in a solution of 0.5mM of CTAB with a flow rate of 0.1ml/min. (b) The schematic shows the corresponding stages in bubble growth.

When a new bubble emerges, curvature radius is large [I]. The radius decreases as the bubble grows and achieves a minimum radius value when bubble radius is equal to the radius of the capillary [II]. Maximum pressure is measured for this radius. The last stage involves an increase in radius with growth in a bubble, culminating in its detachment [III], accompanied by a decrease in pressure in each cycle.

The time available for surfactants to populate the interface increases if the bubbling rate is reduced and higher surfactant concentration results in a lower value of measured  $P_{max}$ , as shown in Figure

9.

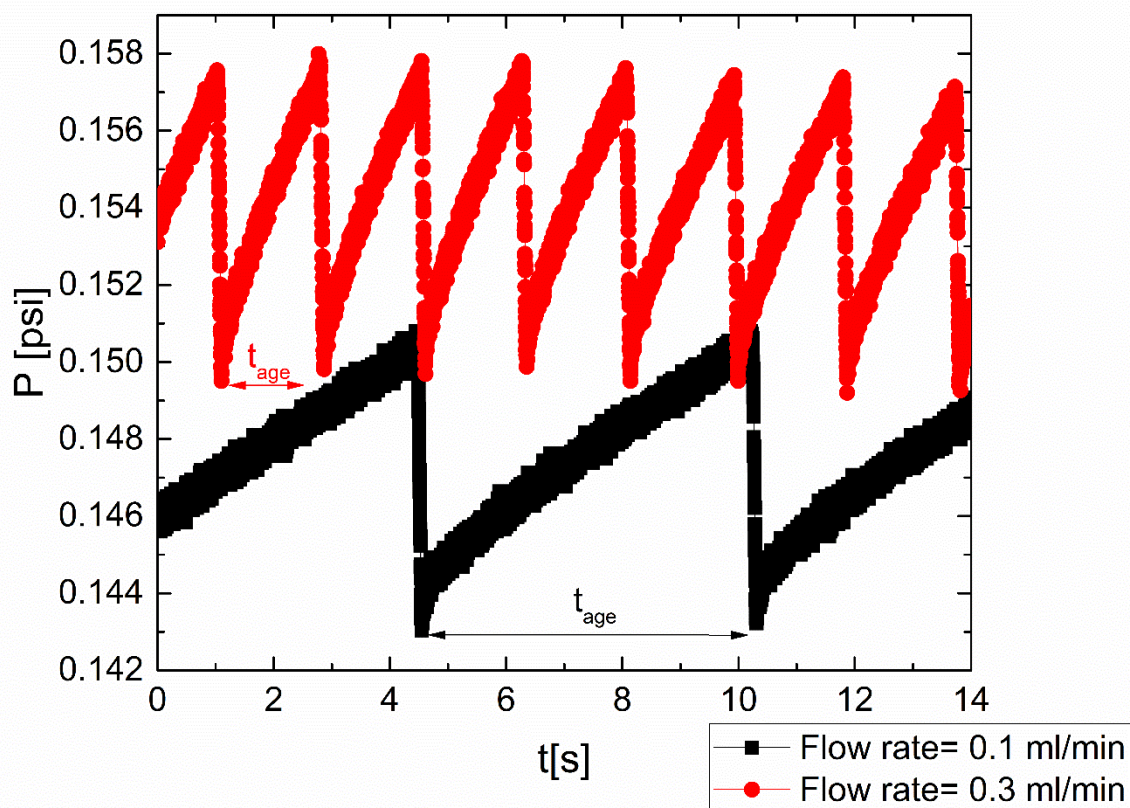


**Figure 9. Pressure evolution with time as a function of flow rate for a concentration of 0.5mM CTAB in water.**

At larger flow rates, surface age decreases and the maximum pressure measured increases for surfactant solutions.

### 3.3 Validation

We first measure  $P_{\max}$  as a function of flow rate or bubbling rate using water. As water contains no added surface active agents, the maximum pressure, and resulting  $\gamma$  values are expected to remain constant at all flow rates (unless inertial effects become relevant (14, 18)). In order to achieve shorter times, flow rates need to be increased (Figure 9). However, a bubbling-to-jetting transition occurs (17) at higher flow rates, resulting in a lower bound to how short timescales can we resolve using the set-up described. The critical flow rate that causes the transition can be

determined by measuring the surface tension of water at a different flow rate, and simultaneously visualizing the bubble formation. The measured  $P_{\max}$  and surface tension of water are found to be constant for flow rate between 0.1 ml/s - 7 ml/s as can be seen in Figure 8. Such validation runs are made frequently to ensure everything is in good working order.

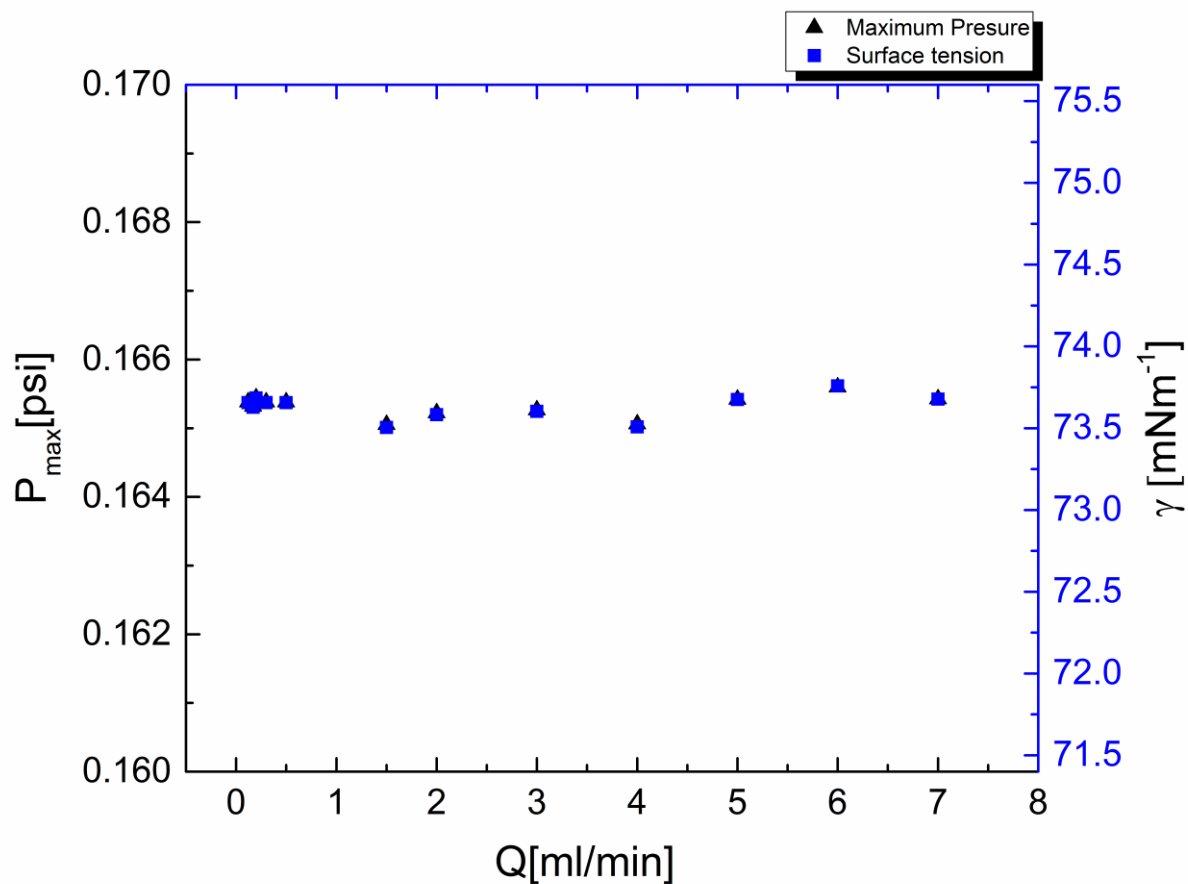


**Figure 10. Maximum pressure and surface tension variation with flow rate for deionized water.**

For a pure solvent like, surface tension shows no change with bubbling rate.

## 4 RESULTS AND DISCUSSION

### 4.1 Hexadecyltrimethylammonium Bromide (CTAB)

The dynamic and quasi-equilibrium surface tension data for CTAB solutions are reported and fitted to the models proposed by Kralchevsky *et al.* (25) and Danov *et al.* (22) respectively (see the theoretical background, section 2 for details). The parameter  $S_\gamma$  is determined from fits to dynamic surface tension data and  $\Gamma_1$  is determined from first to the quasi-equilibrium surface tension data, along with another parameter as maximum surface concentration, surface potential, beta, counterion binding.  $S_\gamma$  and  $\Gamma_1$  are used to determine the apparatus constant of the Maximum Bubble Pressure (MBP) tensiometer, and consequently, obtain universal surface age. The universal surface age or real adsorption time for MBP tensiometry will allow comparing dynamic surface tension (DST) data from our measurements with other methods that do not involve interfacial expansion during the measurements (as Wilhelmy method). The dynamic surface tension measurements for four bile salts and CTAB surfactants are presented next and the dynamic adsorption of these ionic surfactants is analyzed in detail.

#### 4.1.1 Dynamic surface tension

In the maximum bubble pressure tensiometer, the adsorption time is controlled by adjusting the bubbling rate. At lower flow rate, longer adsorption times are obtained. As the adsorption time increases, the surface concentration of surface active agents increases, which produce a decrease in the capillary forces (as surface tension decrease) and the maximum pressure decreases, as observed in the data shown in in Figure 11. Furthermore, at higher concentration, the maximum

pressure decreases as more surfactant gets absorbed at the interface, leading to a lower value of surface tension. At higher flow rates, the maximum pressure is higher because the formation of the bubble is faster, thus the total amount of surfactant adsorbed is less at the interface.

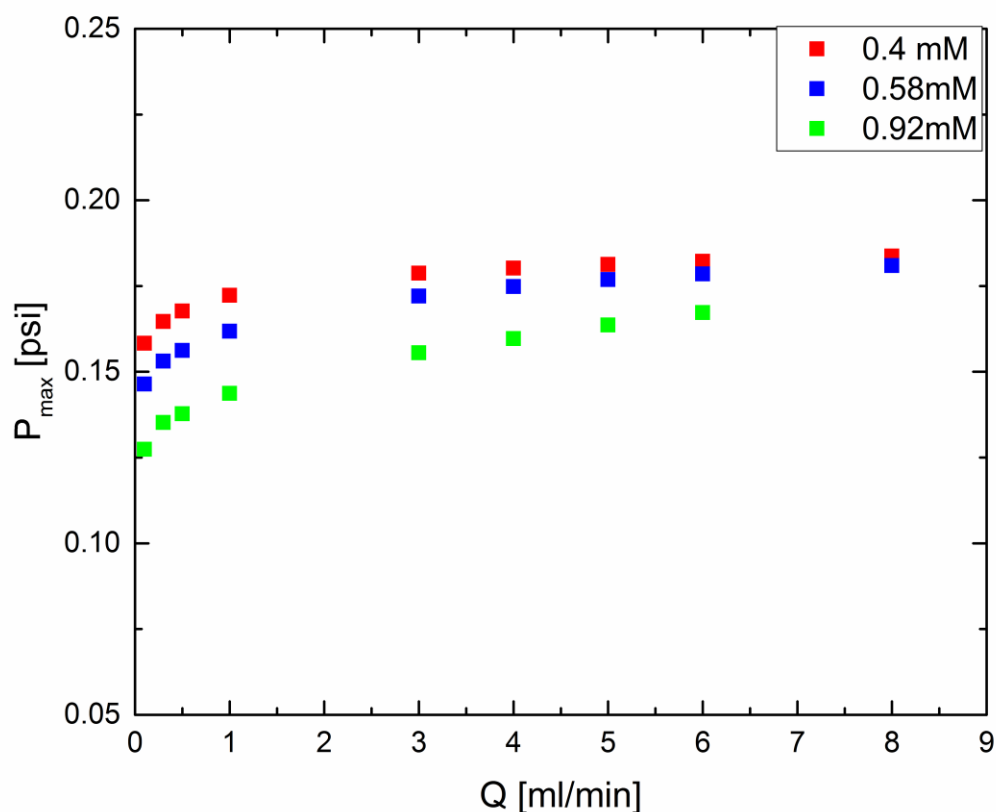


**Figure 11.** The plot of maximum pressure vs flow rate for CTAB solutions with concentrations of 0.4 mM, 0.58 mM, and 0.92 mM.

Each surface tension value shown in Figure 12 is computed using the pressure value plotted in Figure 11, and as flow rate,  $Q$  sets the bubbling rate and surface age, the higher  $Q$  values correspond to short surface age. The adsorption time determined from the pressure vs. time diagram (Figure 9) for each flow rate is shown in Figure 12 as  $t_{app}$  "apparent surface age", since

the convection effects due to the expansion of the interface contribute to adsorption, and a correction factor are needed to make datasets comparable with measurements obtained with technique that relies on a stationary interface.

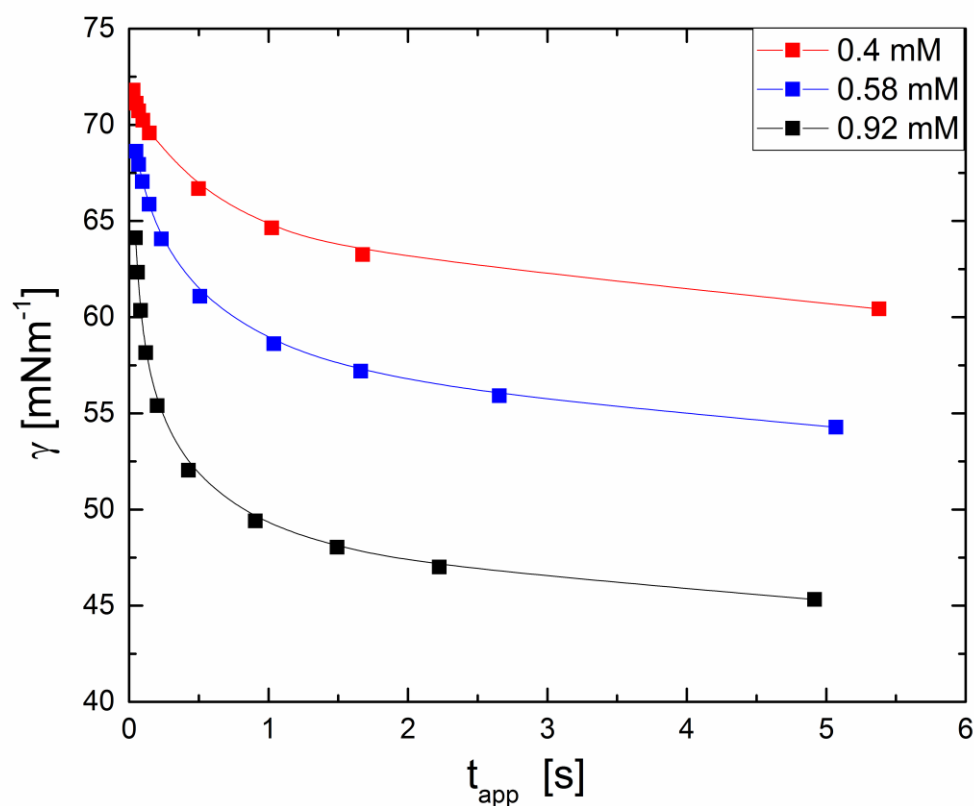


**Figure 12. Dynamic surface tension versus apparent surface age for CTAB solutions with concentrations of 0.4 mM, 0.5 mM, and 0.92 mM.**

Surface tension decrease with time and with concentration, as an increase in the surface concentration of the surfactant, leads to a decrease in measured surface tension.

The dynamic surface tension data shows the affinity of the surfactants to the interface, this is due because if the surfactant affinity is higher, the surfactant will reach faster the interface, then the surface tension faster will reach an equilibrium value (where surface tension does not change). So

surfactant which reaches an interface faster will be able to create thin films more stable in the case of foams because it will decrease the drainage of the thin film (3). The affinity of surfactant to the interface also will be important in the case where there is competitiveness of different surfactant molecules, so in order to know which surface active agent reach faster the interface and act on it, dynamic surface tension curves of the surfactant will give the information of the adsorption time at certain solution concentration.

Surface tension values decrease with adsorption times ("apparent surface age"), reaching a quasi-equilibrium value where the surface tension variation is nearly negligible. This quasi-equilibrium value is reached faster at higher concentrations, and the comparison is shown for eight concentrations in Figure 13. For the solutions with the lowest concentration of added surfactant, the surface tension values at short surface age are quite close to that of the pure solvent (water). As the concentration of the solution is increased, the  $\gamma$  value measured at the shortest surface age resolved is much lower than the surface tension of the solvent, indicating significant adsorption has taken place within a few milliseconds. Due to aperiodic bubbling and bubbling-to-jet transition at higher bubbling rates, short time scales are not accessible and the dynamic effects leading to the initial decrease in surface tension are not resolved. The change in surface tension for short apparent surface age can be observed more clearly by using a logarithmic scale (see Figure 13) for the abscissa. In Figure 13, the minimum apparent surface age is nearly 50 ms.

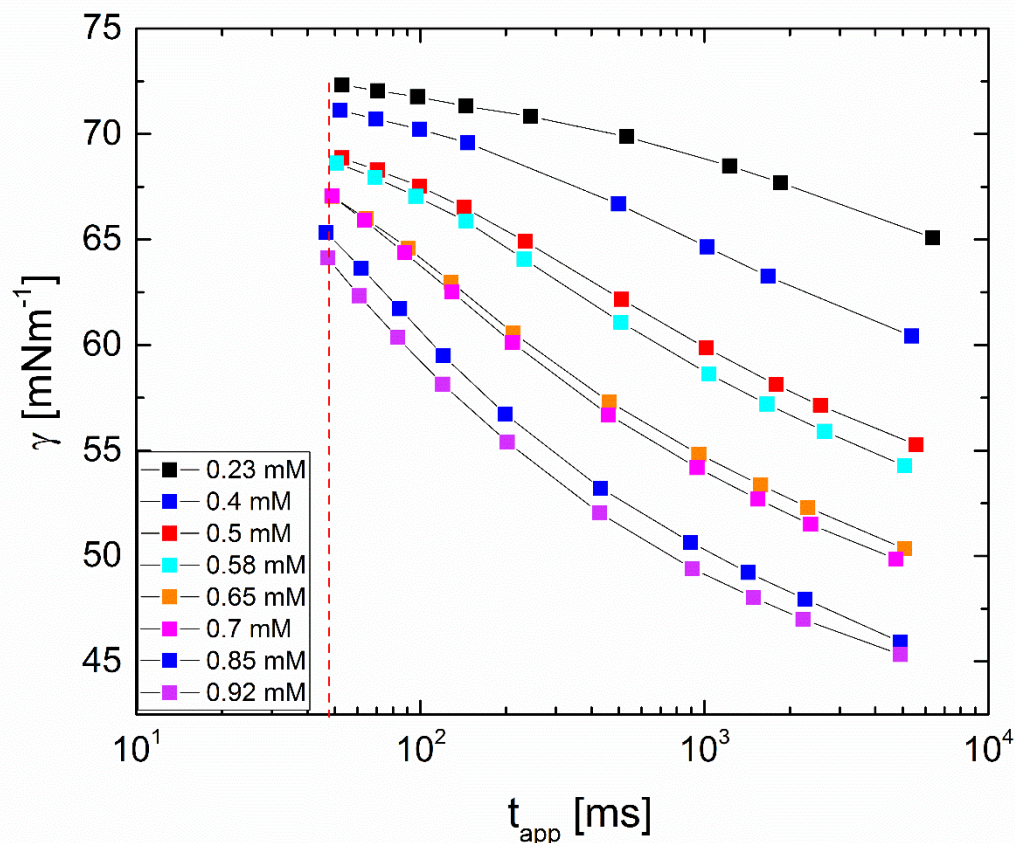


**Figure 13. Dynamic surface tension vs apparent surface age plotted on a semilog scale in for CTAB solutions with a range of concentration from 0.23 - 50 mM.**

Surface tension is measured for relatively short apparent surface age.

The DST data is analyzed next by following the adsorption kinetics model for ionic surfactants based on a theory by Danov *et al.* (22) discussed in the previous section. Bleys *et al.* (31) suggested that the plot of dynamic surface tension vs  $t^{-1/2}$  provides insight into whether diffusion or adsorption is the controlling steps. Dynamic surface tension data is plotted as a function of  $t_{app}^{-1/2}$  in Figure 14. As the longer surface age corresponds to the data near the left axis corner, a long time or asymptotic behavior of surface tension is described reasonably well by  $g \mu t_{app}^{-1/2}$

relationship. In Figure 14, a linear region near the origin indicates that for CTAB solutions in a concentration range from 0.23 mM to 0.92 mM, diffusion is the rate-controlling step.

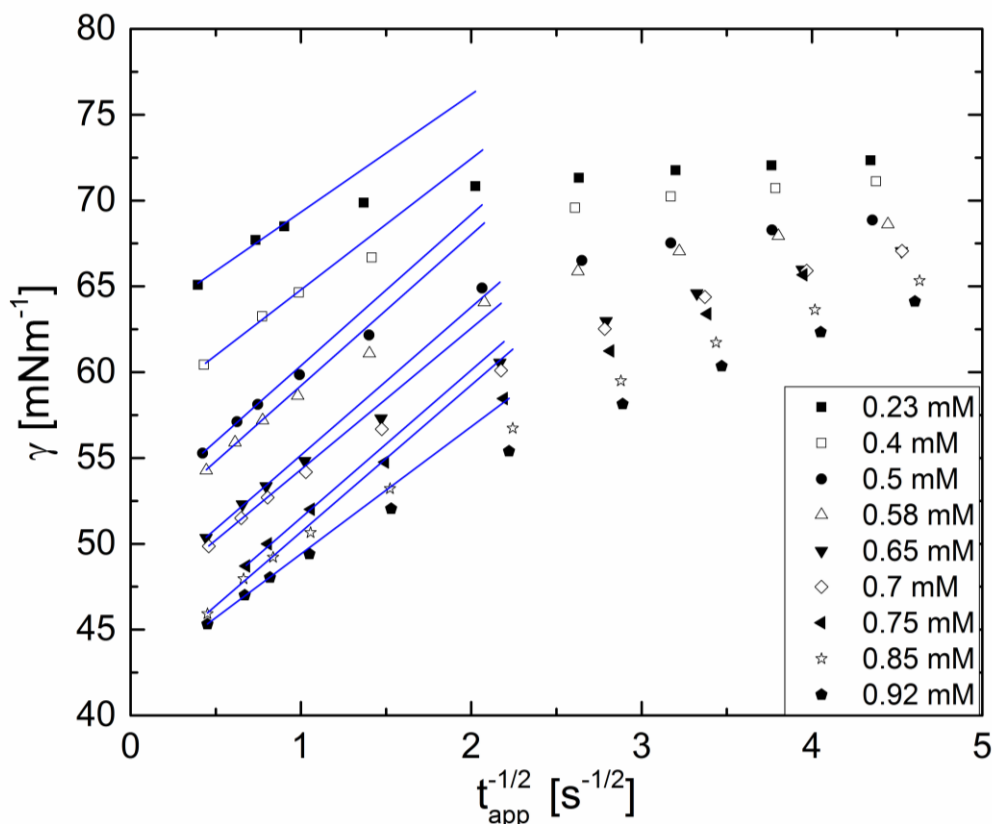


**Figure 14. Dynamic surface tension data for aqueous CTAB solutions (below CMC) is plotted as a function of  $t_{app}^{-1/2}$ .**

DST vs  $t_{app}^{-1/2}$  exhibits a linear relationship for long adsorption times for CTAB.

The asymptotic fits to the long time's datasets shown in Figure 14 yield the value of the  $S_\gamma$  parameter (see discussion of Equation 8,  $g = g_{eq} + S_\gamma / t_{age}^{1/2}$ ). The slope of the lines of Figure 14 for each concentration give a value of  $S_\gamma$  that represents a relation between the surfactant adsorbed into the interface at equilibrium and the effective diffusivity for an interface that is expanding at a constant rate. The value of  $S_\gamma$  is  $8.2 \pm 0.7$  obtained for concentrations range 0.23 - 0.92 mM.

Because  $S_\gamma$  values depend on the apparatus constant  $\lambda$  that depends on the choice of the tensiometer, the absolute value of  $S_\gamma$  values cannot be compared with literature values. However, the concentration-dependent behavior agrees quite well the values obtained for SDS by Christov *et al.* (13).

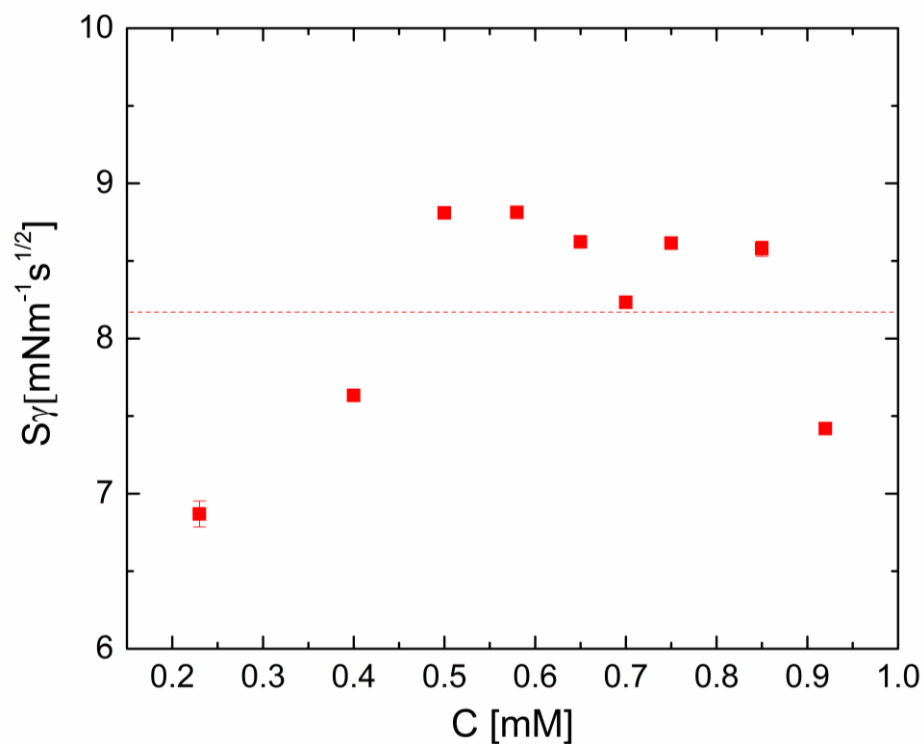


**Figure 15.**  $S_\gamma$  vs concentration for aqueous solutions of CTAB obtained by analyzing dynamic surface tension data.

Using the values of  $S_g$  and plotting  $g = g_{eq} + S_g/t_{age}^{1/2}$  for the entire time range for each concentration shows that the data at short times is not captured by this asymptotic expression (Figure 16), in agreement with the simplifying assumptions and approximations made by Danov *et al.* (22).

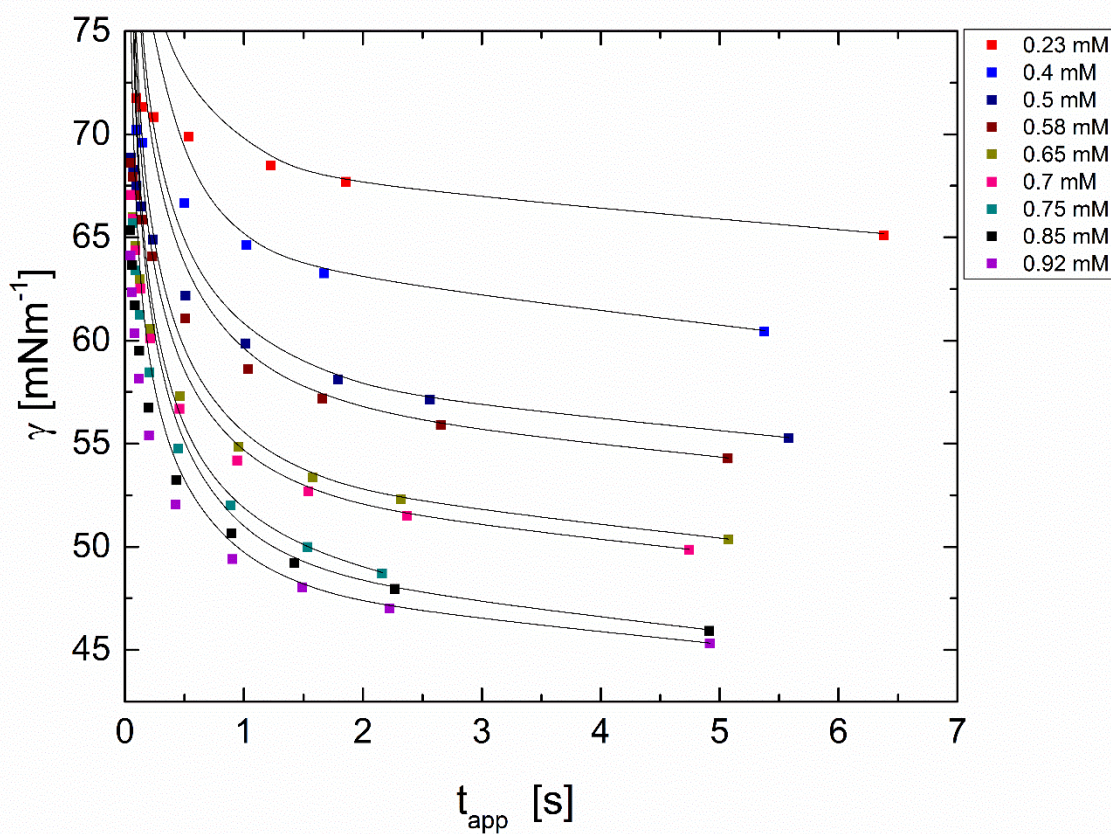


**Figure 16.** Dynamic surface tension data of aqueous CTAB solutions are shown with symbols and the lines represent the behavior captured by the asymptotic result (equation 8).

Figure 17 shows the plot of  $(\gamma - \gamma_{eq,c}) / S_{\gamma,c}$  as a function of apparent surface age ( $t_{app}$ ). in the limit of long apparent surface age, all the curves merge into one, showing that at different concentrations, the dynamic surface tension curve has the same behavior for long times.

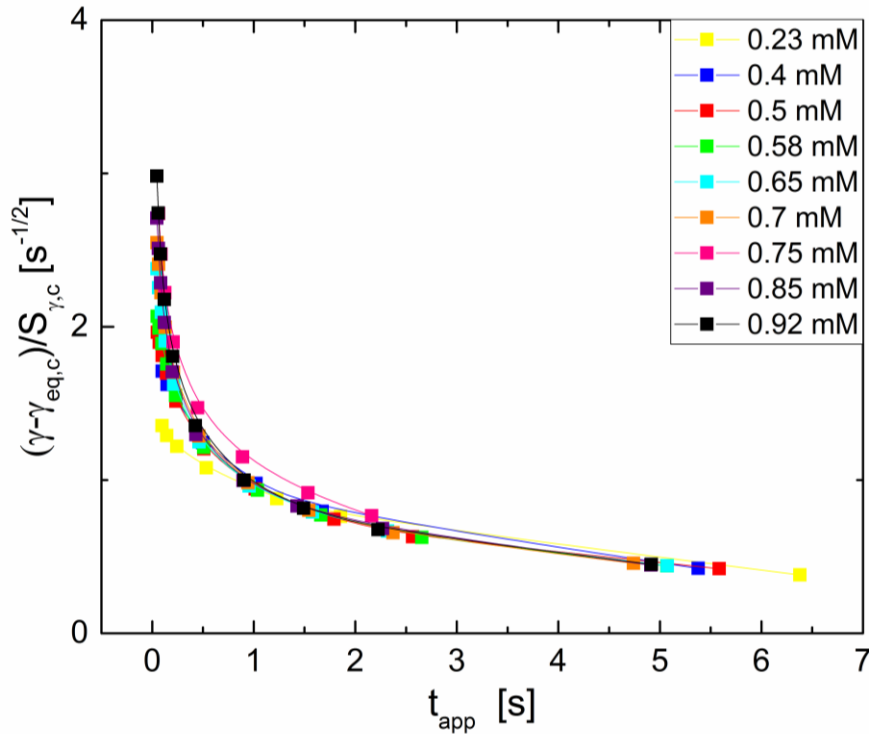


**Figure 17. Plot of  $(\gamma - \gamma_{eq,c}) / S_{\gamma,c}$  vs apparent surface age ( $t_{app}$ ).**

The units for Y-axis are in terms  $s^{-1/2}$  which show that we are calculating the inverse of apparent surface age.

Dynamic surface tension as a function of apparent surface age is compared with literature for three concentrations in Figure 18. The literature data 2 mM concentration data reported by Kawale (51) was acquired using a commercial MBPT-BPA-1S (from SINTERFACE Technologies, Germany), 0.5 mM concentration data, reported by Z. Adamczyk *et al.* (52) was obtained from drop weight

method, and 0.6 mM data, reported by Chi M. Phana *et al.* (53), was obtained from a commercial MBP tensiometer called MPT-C (from Lauda, Germany).

The experimental dynamic surface tension data shows a good agreement with literature data obtained from the commercial MBPT-BPA-1S, and from the drop weight method (see Figure 18). On the other hand, the literature values for a solution with a concentration of 0.6 mM acquired using MBPM MPT-C do not overlap with our experimental data for solution concentration 0.58 mM obtained by our MBP tensiometer (Figure 18). This disagreement arises because of the apparatus constant, that rely on the surface expansion rate of the bubble, differ between the MBP to the expansion of the interface for two MBP is different as suggested by Christov *et al.* (13).

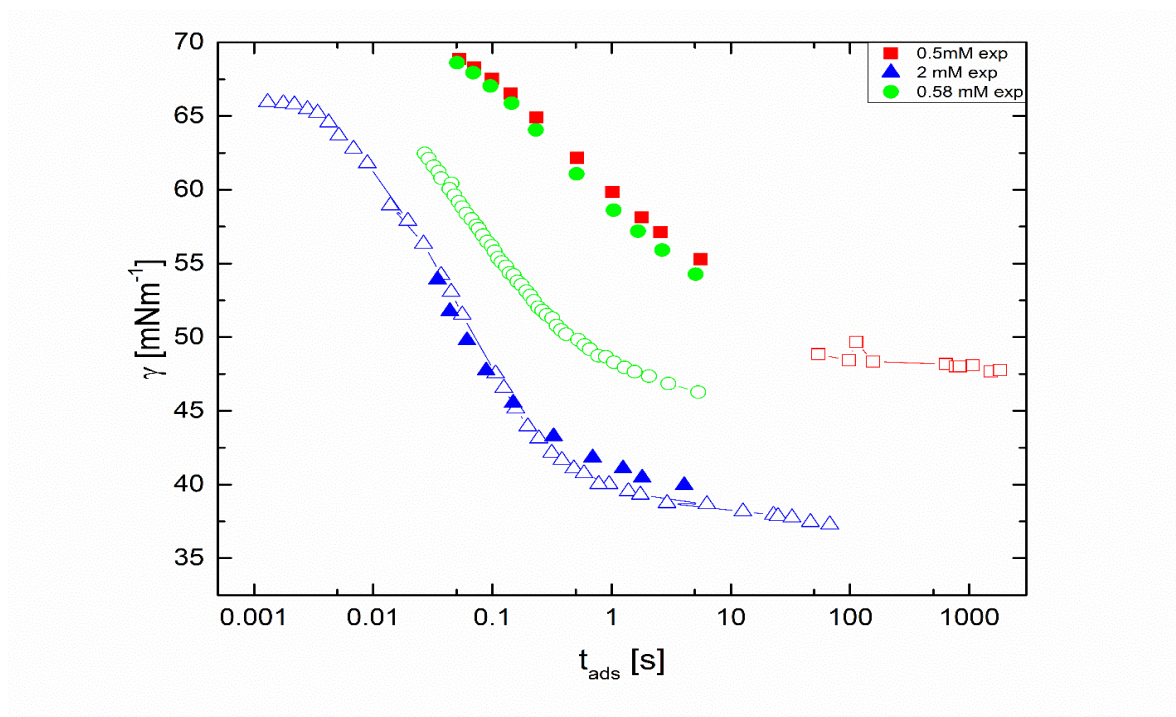


**Figure 18. Dynamic surface tension vs adsorption time of CTAB of different tensiometers.** The empty symbols points represent the experimental data and the full symbols with the lines are the reported from other tensiometers. The 0.6 mM concentration data reported by Chi M. Phana *et al.* (53), the 2 mM concentration data reported by Kawale (51) and 0.5 mM concentration data reported by Z. Adamczyk *et al.* (52).

### 4.1.2 Universal surface age

In order to compare dynamic surface tension data from our maximum bubble tensiometer with other tensiometers with adsorption to an immobile, stationary interface, an apparatus constant is determined and universal surface age is obtained, using the procedure discussed in section 2. The apparatus constant  $\lambda$  is obtained by fitting quasi-equilibrium and dynamic surface tension fitting and then  $\lambda^2$  was calculated for getting universal surface age. Figure 19 demonstrates that  $\lambda$  is nearly constant with concentration ( $\lambda = 2.47 \pm 0.22$ ) in good agreement with the conclusions of Christov *et al.* (13).

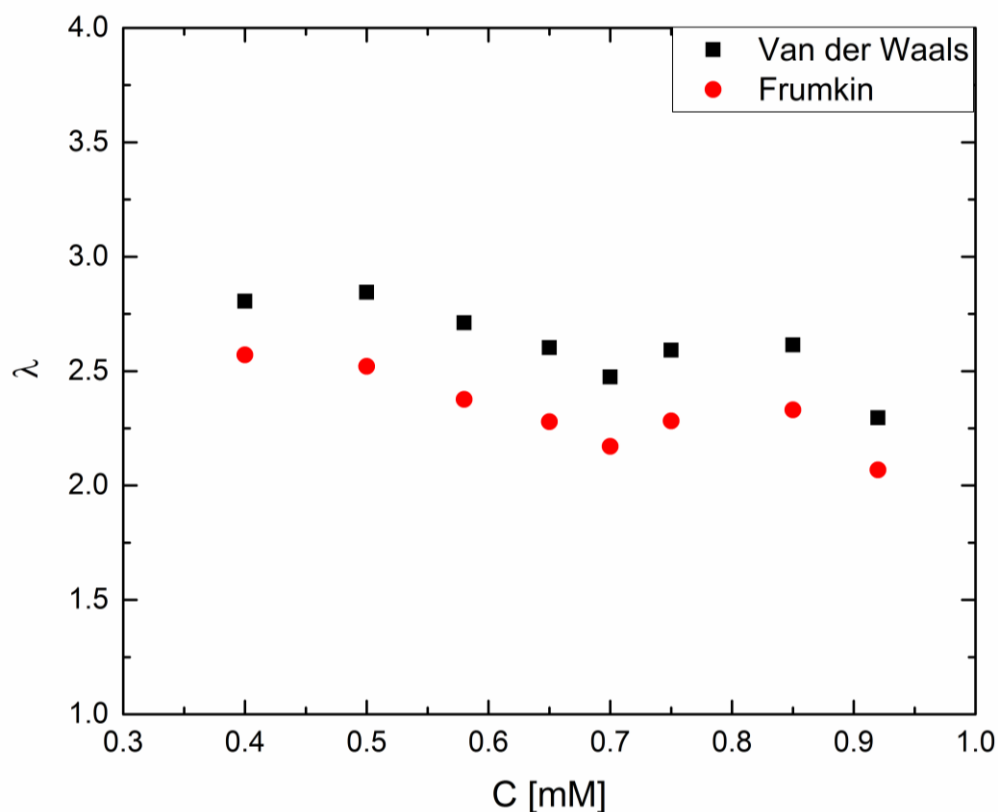


**Figure 19. Apparatus constant versus CTAB concentration.**

The apparatus constant ( $\lambda$ ) of MBPT is evaluated from the fitting of dynamic surface tension.

Figure 20 shows the dynamic surface tension versus universal surface age. The dynamic surface tension data is shifted to the left on the plot, for the surface of the bubble is “younger” than the value obtained from pressure vs time plots. The results reported by Chi M. Phana *et al.* (53) for a 0.6 mM concentration of CTAB could be in terms of the apparent surface age and universal surface age must be calculated in order to compare results.

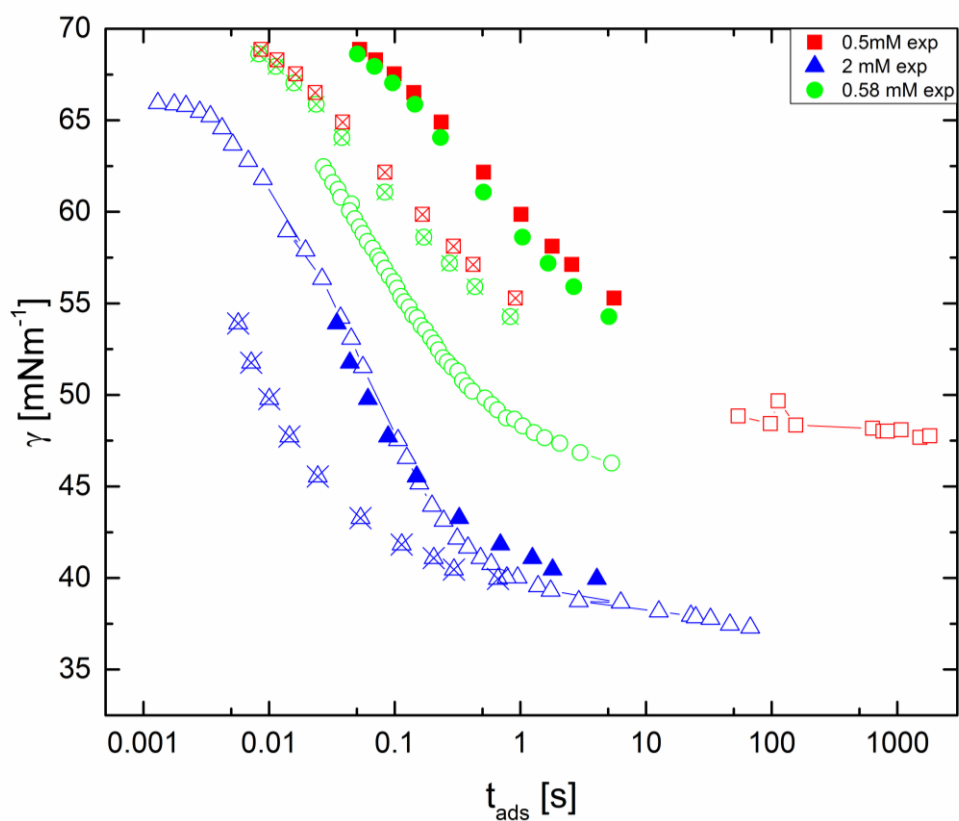


**Figure 20. Variation of dynamic surface tension with universal surface age**

The  $t_{ads}$  represents the adsorption time of the surfactant. In the case of MBP is the surface age which is named as apparent surface age if this has no be modified with the apparatus constant, otherwise, this time corresponds to the universal surface age.

Using the apparatus constant values obtained allows a calculation of universal surface age. The dynamic surface tension variation with universal surface age is shown in Figure 21 can be used in

the future for comparing dynamic surface tension data acquired from other techniques. The minimum adsorption time obtained by the ODES-lab's maximum bubble pressure tensiometer for CTAB, is then around 8ms. The results shown in Figure 21 indicate that the adsorption time at higher concentration is relatively short, and the initial regime of surface tension drop is not captured by the measurements. Nevertheless, the measurements access short time data for adsorption times at least two orders of magnitude lower than those accessible with pendant drop tensiometry or Du Nuoy ring or Wilhelmy plate methods.

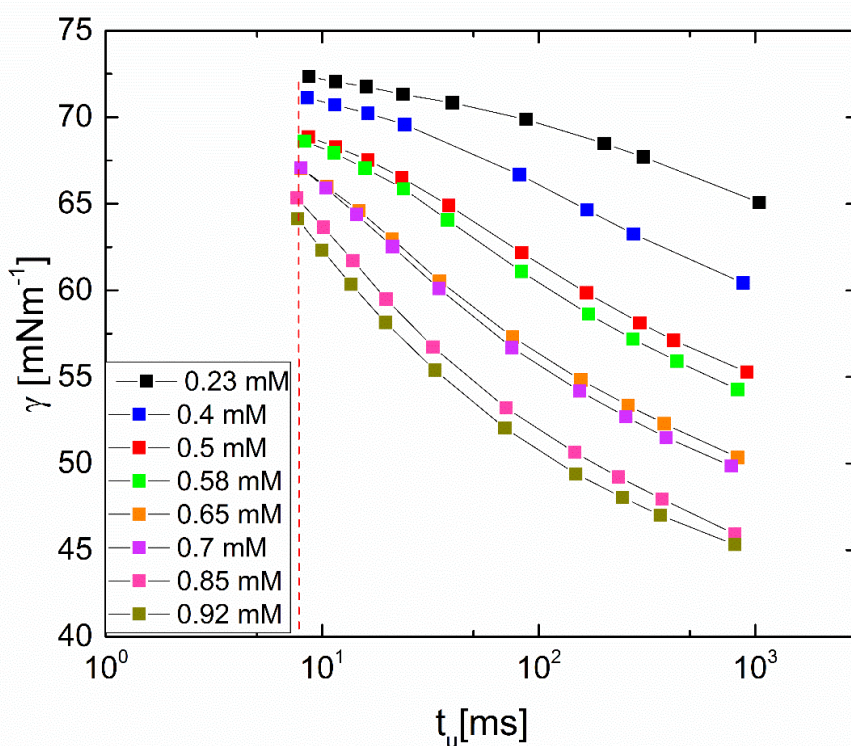


**Figure 21. The dynamic surface tension of CTAB from MBPM with universal surface age for concentration ranging from 0.23 mM to 0.92 mM.**

### 4.1.3 Quasi-equilibrium surface tension

The critical micelle concentration (CMC) and adsorption parameters like surface potential and surface concentration can be determined from the equilibrium surface tension. In order to analyze

equilibrium surface tension data, it is necessary to obtain dynamic surface tension for a wide range of concentration and obtain  $\gamma$  values at steady state/long times. Also, dynamic surface tension data for a wider range of solution concentration gives a better understanding of the surface properties, and the adsorption process. The surface tension values computed using maximum bubble pressure tensiometer as a function of surface age for different CTAB concentration are plotted in Figure 22. The shape of dynamic surface tension curves changes dramatically at concentrations higher than 2 mM implying the existence of two regimes with distinct concentration-dependent behavior. Though surfactants exist only as monomers in the lower concentration regime, at high concentration surfactant molecules spontaneously self-assemble to form agglomerated structures called micelles. The concentration above which surfactant self-assemble and form micelles is known as Critical Micelle Concentration (CMC)(54), and its value can be determined by measuring concentration-dependent variation in surface tension. For CTAB solutions with concentrations below CMC, it is observed that the equilibrium surface tension is reached at higher adsorption times, instead for concentrations above the CMC, lower adsorption times are necessary to reach equilibrium.

Furthermore, as it is shown in Figure 22 in the first regime, the equilibrium surface tension is a strong function of the concentration. For example, for a concentration,  $c = 0.23 \text{ mM}$  the quasi-equilibrium concentration would be around  $g_{eq} \gg 65 \text{ mNm}^{-1}$  and for  $c = 0.5 \text{ mM}$  the value drops to  $g_{eq} \gg 55 \text{ mNm}^{-1}$ . In the second concentration regime (for  $c > 2 \text{ mM}$ ), a tenfold increase in concentration results in a slight decrease of  $Dg = 2.4 \text{ mNm}^{-1}$  in the value of quasi-equilibrium surface tension, approaching the value of around  $g_{eq} \gg 36 \text{ mNm}^{-1}$ . Reported values of this

equilibrium surface tension  $\gamma_{eq} \gg 35 \text{ mNm}^{-1}$  were acquired with a pendant drop tensiometer (55).

The difference between the values could be due to the fact that the longest time achieved in the MBP tensiometer is not enough for the system to reach the equilibrium surface tension. Longer adsorption times require low flow rates, and the limit, in this case, is set by the limited accuracy of the pumping mechanism. The limit for the fast adsorption times is set by hydrodynamic effects that dominate as flow rate is increased leading to a bubbling-to-jetting transition. Though the data at the shortest time was acquired using the same flow rate in Figure 22, different surface age value (red dashed line) is realized for each concentration, and this implies that either the rate of expansion of the interface seems to be concentration-dependent or peak pressure values are reached even before the bubble radius is minimum.

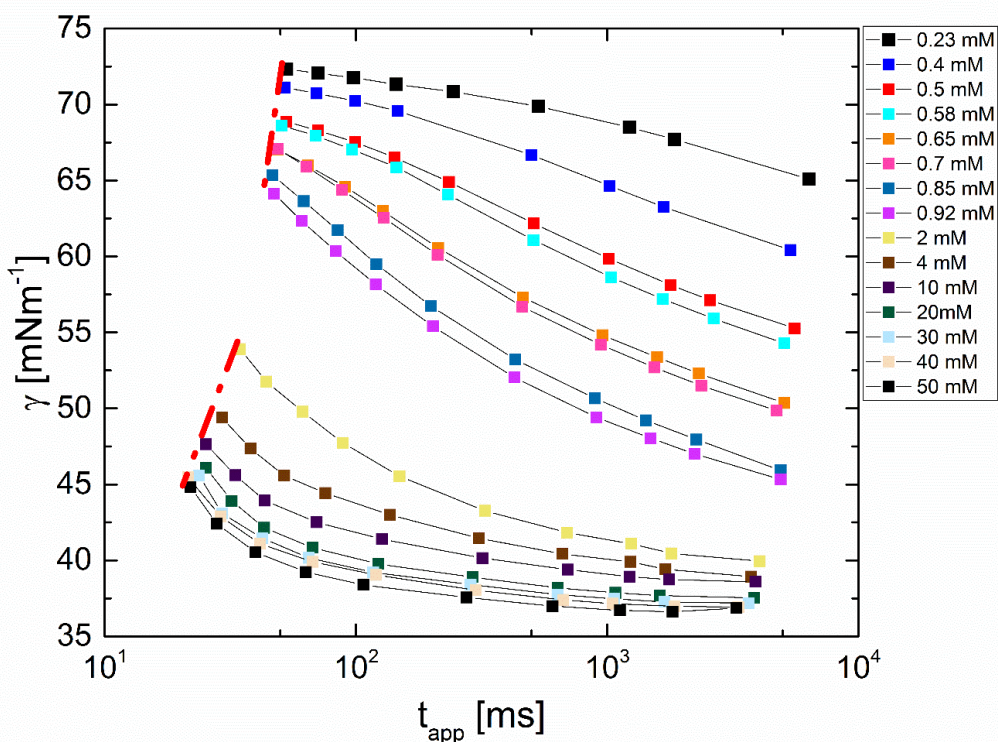


**Figure 22.** The plot of dynamic surface tension vs apparent surface age for solutions of CTAB with concentrations from 0.23mM – 50mM .

The time evolution of the dynamic surface tension data depends on the mechanisms underlying mass transfer of the surfactant molecules to the interface. For concentrations below CMC, the change of surface tension with respect to time is controlled by three flux contributions: convection, diffusion, and migration. Convection term arises due to flows caused by bubble growth and expansion of the interface, diffusive flux depends on the mobility of the surfactant within the solution, and the migration flux is controlled by charge on surfactant as well as interfacial concentration, which determines the electrostatic potential at the interface as well as the thickness of electrical double layer. On the other hand, for concentrations above CMC, the change in surface tension with respect to time will be affected not only by the three previous terms but also by the kinetics of micellization-demicellization process and the diffusion of the micelles towards the subsurface layer. It is typically assumed that micelles are not adsorbed to the interface and only monomers (single surfactant molecules) can be adsorbed (35, 56). A detailed analysis of micellar solutions was not attempted in this study. The quasi-equilibrium surface tension values obtained for CTAB from the measured values acquired at the longest adsorption times are shown in Figure 23. Two concentration-dependent regimes are clearly visible and the transition seems to occur at  $c = 1.1$ . The transition is associated with concentration beyond which micelles appear in the bulk and this critical micelle concentration value is quite close  $CMC = 1 \text{ mM}$  to the value reported in the literature (including product information provided by Sigma Aldrich,).

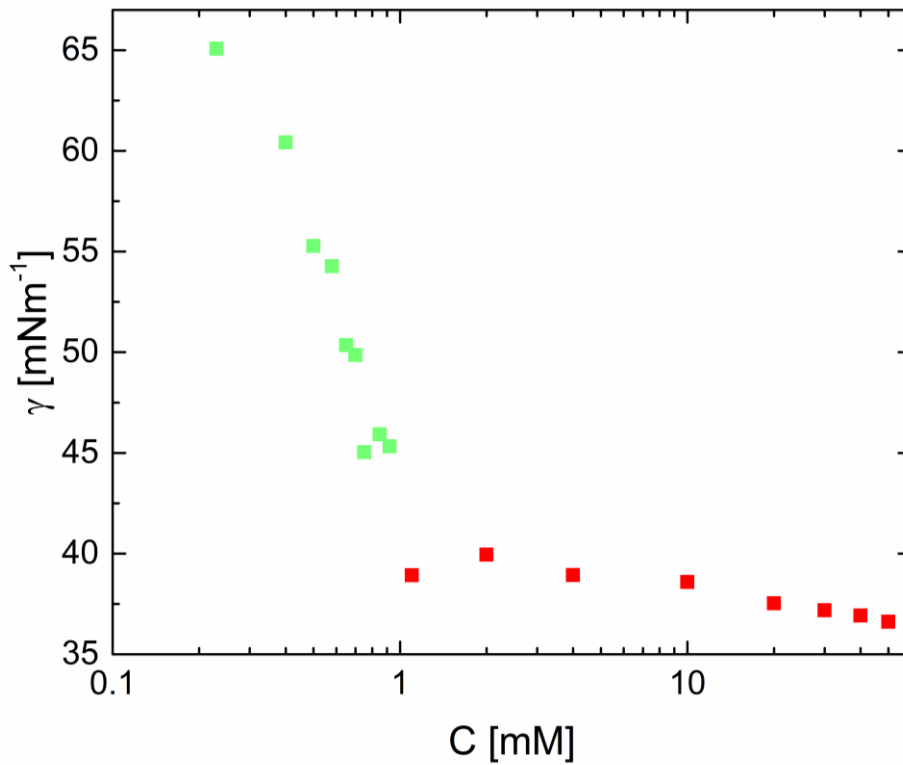


**Figure 23. Quasi-equilibrium surface tension as a function of bulk surfactant concentration for CTAB.**

The change of slope marks the onset of surfactant aggregation in the bulk solution.

Using the Gibbs equation (Equation 30) we can estimate the maximum surface concentration below micelle concentration, where  $n = 2$  for ionic solutions (47). The value calculated from the data of Figure 23 is  $G_{1,<CMC_{max}} = 3.087 \cdot 10^{-6} \text{ mol/m}^2$ . This value is quite similar to the value

$G_{1,<CMC_{max}} = 3.1 \cdot 10^{-6} \text{ mol/m}^2$  reported by Szymczyk and Janczuk (47), where the maximum surface concentration is.

$$\Gamma_{\max} = -\frac{1}{nRT} \frac{d\gamma}{d \ln C} \quad (30)$$

#### 4.1.4 Adsorption Isotherms and surface tension data

The calculation of adsorption parameters from the quasi-equilibrium surface tension data is discussed next, and the analysis, as discussed in section 2, relies on an equation of state that takes accounts for counterion binding and electrical double layer. Quasi-equilibrium surface tension values for concentrations below CMC is used for computing surface pressure,  $\pi = \gamma_0 - \gamma$  that represents the difference between the surface tension of surface with and without adsorbed surfactant. Figure 24 shows surface pressure (symbols) as a function of surfactant concentration. Also included in Figure 24 are fits obtained using Frumkin and van der Waals isotherms (equation 14 and 15). Frumkin Isotherm models the surfactant adsorption processes as localized adsorption, assuming a heterogeneous interface and taking into account the interaction between adsorbed molecules. This model represents the general form of Langmuir isotherm. On another hand, van der Waals isotherm models a non-localized adsorption and accounts for interaction between molecules in the adsorption layer. It is clear that both models fit the surface pressure data quite well, and the parameter obtained from the fits are listed in Table III. The positive sign of  $b$  implies attraction between surface molecules, and the magnitude of  $K_1$  and  $K_2$  is related to the adsorption free energy of the interface.

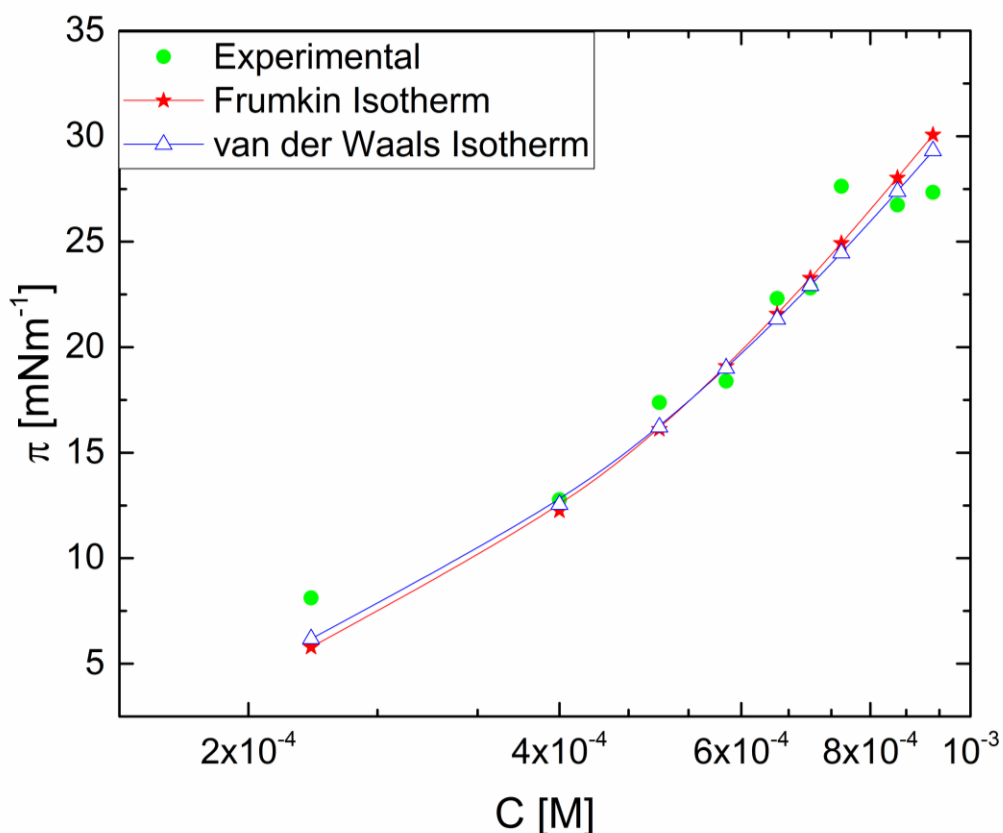


**Figure 24.** The variation in surface pressure with concentration for aqueous CTAB solutions is shown together with Frumkin and van der Waals isotherm.

The  $K_1$  value obtained by the fits (Table III) is slightly lower than the value  $K_1 = 4.9 \cdot 10^3 \text{ mM}^{-1}$  (37) reported in the literature. The value  $G_{\ddot{y}} = 6.26 \cdot 10^{-6} \text{ mol/m}^2$  obtained by using Frumkin isotherm is higher than the alternative value calculated from the slope of  $d\gamma/d \ln C$  because this slope does not reflect a closed packed layer (35). In the evaluation of this parameter, the binding of counterion and the electrical double layer has been considered. The  $\Gamma_{\infty}$  value for van der Waals is greater than the one obtained using Frumkin isotherm (see Table III), which means that the area per molecule ( $1/\Gamma_{\infty}$ ) evaluated with Frumkin is greater, probably due to the fact that Frumkin

isotherm described localized adsorption process, while van der Waals describe non-localized adsorption (57). The value of area per molecule ( $1/\Gamma_{\infty}$ ) for van der Waal is  $21 \text{ \AA}^2$  which is smaller to the area of the surfactant molecule in ref (57) while for Frumkin the area per molecule obtained is closer  $26.5 \text{ \AA}^2$ .

**Table III. Parameters of van der Waals and Frumkin isotherms.**

	$\frac{2\beta\Gamma_{\infty}}{kT}$	$K_1 [mM^{-1}]$	$K_2 [mM^{-2}]$	$\Gamma_{\infty} \left[ \frac{mol}{m^2} \right]$
van der Waals	0.23	$1.54 \times 10^3$	4.51	$8.88 \times 10^{-6}$
Frumkin	0.03	$1.65 \times 10^3$	5.69	$6.26 \times 10^{-6}$

Additionally, surface potential as a function of bulk concentration (shown in Figure 25) is obtained by fitting the quasi-equilibrium surface tension data with the equation of state (equation 19) that considers the contributions of the charged interface as well as counterion binding. The surface potential generated by the adsorbed molecules in the interface will affect the mass transfer of another charged amphiphiles in the case where there is not isolated system (one surfactant and water) or in the case of thin film the electrostatic forces will play an important role in the drainage of the thin film how mentioned above.

Figure 25 show how surface potential changes with CTAB concentration. The decrease of surface potential could be due to progressive neutralization of the interface due to counterion binding. The absolute values of the surface potential are comparable to the results of Nakahara *et al.* (58) who show an increase of surface potential with concentration for the CTAB monolayer.

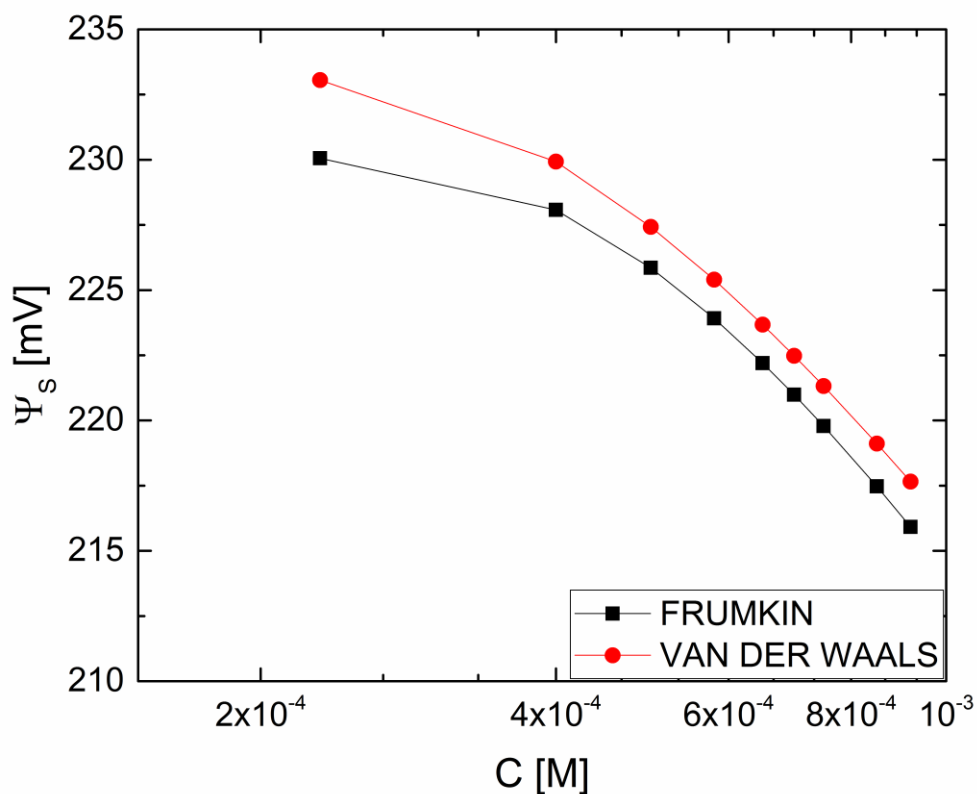


**Figure 25.** The plot of surface potential as a function of CTAB bulk concentration, using Frumkin and van der Waals isotherm models.

Additionally, the model allows evaluation of occupancy in the Stern layer (Figure 26) that shows how counterions bind at the interface and neutralize it. Such neutralization could lead to the observed decrease in charge density, and as a decrease in charge density changes the electrostatic potential driving the transport of ions in an electrolyte solution, resulting in an increased adsorption at the interface. It is evident that even to low concentration, counterion binding is present. A value of  $\Gamma_2 / \Gamma_1 = 0.85-0.95$  was obtained for the range of 0.23-0.92 mM. In literature counterion binding to micelles has been investigated for CTAB solutions only above CMC for understanding the shape of micelles (59). However, for non-micellar solutions formed at a concentration below CMC,

counterion binding has not received the requisite attention. The counterion binding ( $\text{Na}^+$ ) for SDS solution shows a sharp increase with bulk concentration (25) as is visible from trends visualized in Figure 26.

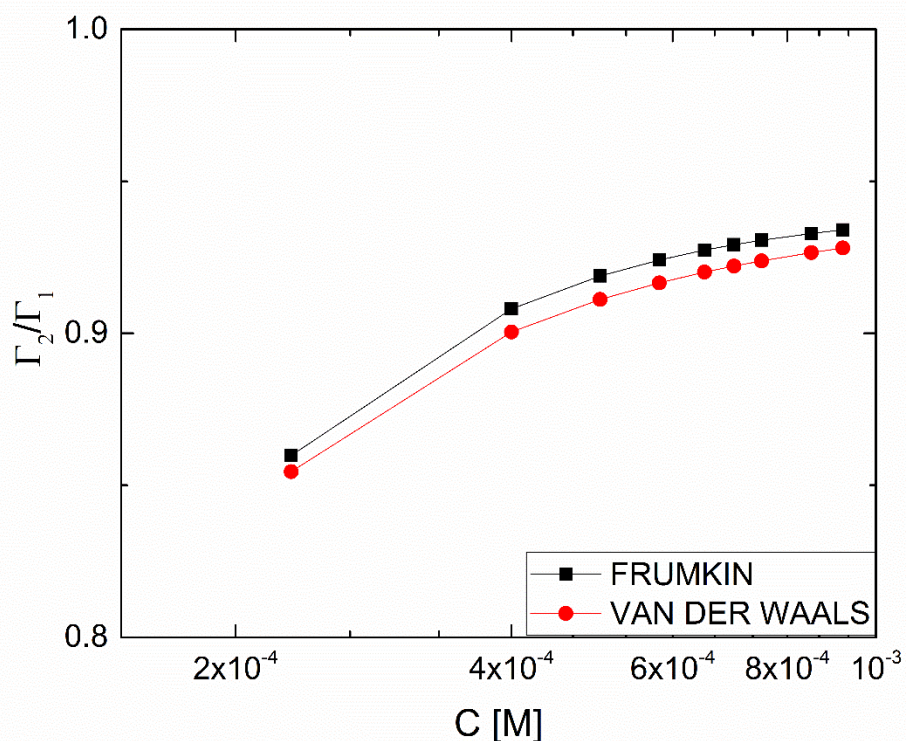


**Figure 26. Occupancy of the Stern layer  $\left(\frac{\Gamma_2}{\Gamma_1}\right)$  as a function of CTAB concentration in the bulk, evaluated using Frumkin and van der Waals isotherms.**

The occupancy in the Stern Layer goes from 0.85 to 0.93 for both isotherm models. As the concentration increase the occupancy in the Stern layer increase.

Dimensionless adsorption as a function of bulk solution concentration is shown in Figure 27. Values obtained using Frumkin isotherm are higher than the values obtained using the van der Waals isotherm. The dimensionless adsorption shows how the increase in bulk concentration solution results in an increase the surface concentration. The relative values and slope of the

dimensionless adsorption data depend on the specific surfactant used and are sensitive to the structure and intermolecular interaction forces, that vary with charge and affinity of the surfactants.

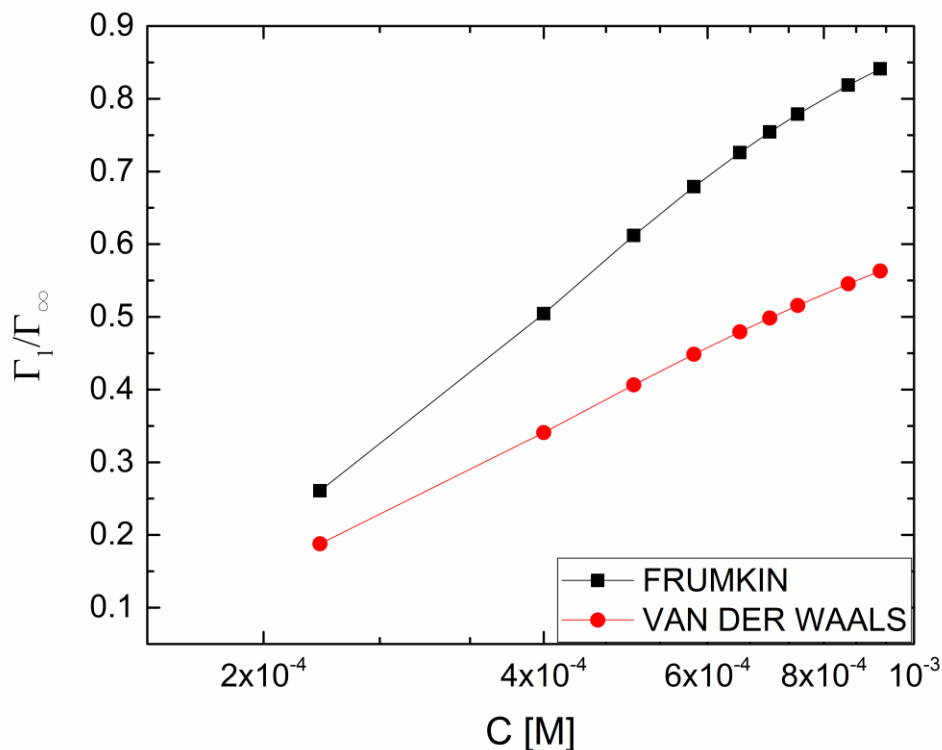


**Figure 27. Plots of dimensionless adsorption of surfactant ion ( $\Gamma_1/\Gamma_\infty$ ) vs concentration of CTAB. Surface concentration and the maximum surface concentration were obtained from the best fitting of experimental data (Figure 24).**

#### 4.1.4.1 Gibbs elasticity

The rheology (flow behavior in response to applied stress) of the interfaces gives a better understanding of how the interfaces respond to perturbations, and the rheological behavior depends on the interaction of surfactant molecules at the interface (correlated with Gibbs elasticity discussed here), surfactant mobility, and the capacity of surfactant to populate the interface. There is a fair bit of disagreement in the literature about the true definition and interpretation of Gibbs

elasticity. Authors as Lucassen-Reynders *et al.* (60) define it as the differential change in surface tension per change of surface area, while Liggieri and Miller (61) define it as the increase in surface pressure with the increase of surface concentration. However, both approaches agree that the slope of surface tension with surface concentration  $-\frac{d\gamma}{d \ln \Gamma}$  is a thermodynamic parameter that determines the elastic response of the interface. However, additional mass transfer effects can influence the measured response (62), and more recent work in the field has emphasized that interfacial elasticity should be defined a priori as a material response independent of mass transfer kinetics. In this contribution, Figure 28 shows how Gibbs elasticity (evaluated using the approach from Liggieri and Miller (61)) changes with concentration.

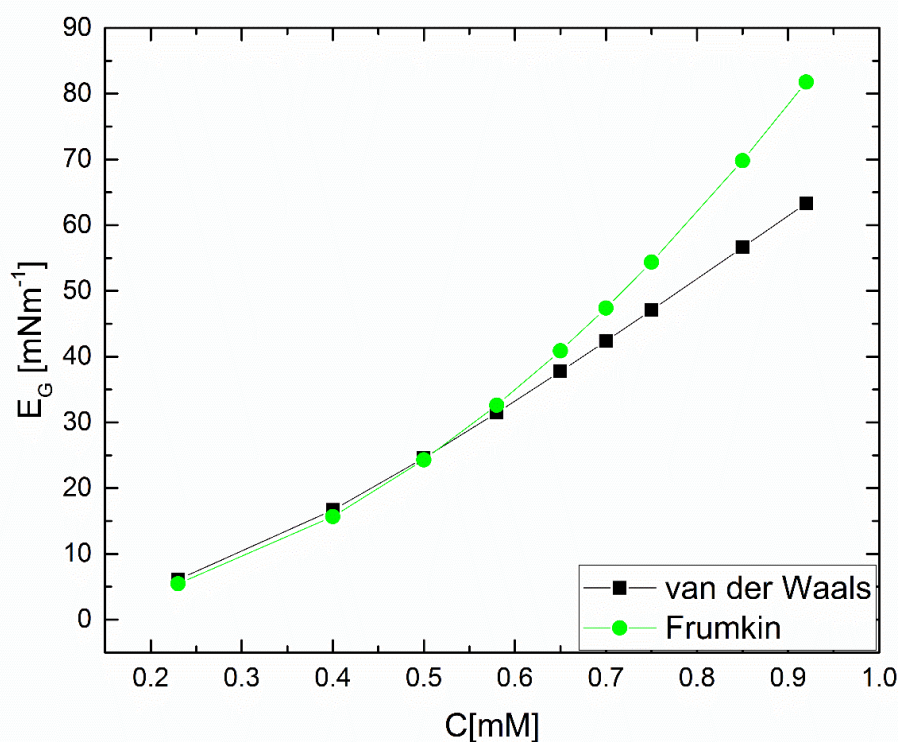


**Figure 28. Gibbs elasticity as a function of CTAB concentration in bulk solution.**

The surface elasticity measure that characterizes the elastic property related how the ability to restore overcome gradients in the surface tension created on expanding a surface (60). Limiting elasticity, or maxima elasticity (also called Gibbs elasticity) of the surface, is defined as the change in surface tension over surface concentration, without the influence of mass transfer from bulk to interface or vice versa. Hence Gibbs elasticity can be calculated using the equilibrium isotherms, and the higher values of this limiting elasticity imply a higher capacity to recover from an interfacial perturbation.

As surface concentration increases, the surface's stiffness increases until a point that the surface behaves as solid and there is no tangential fluidity. In dilute concentrations, Marangoni effect is more significant and often needed to be incorporated to tangential stress balance; at higher concentrations, both Gibbs elasticity and lack of fluidity result in the so-called rigid interfaces. The values of Gibbs elasticity obtained using the fitting of the isotherms are shown in figure 29; here the empty symbols represent the taken experimental data from Stubenrauch *et al.* (63). The data represented by empty symbols shows Gibbs elasticity measurements that take into account the mass transfer of surfactant from the bulk to the interface during the perturbation. It is clear that the limiting elasticity should be shifted to left-hand side of the graph because it should be higher than the Gibbs elasticity (change of surface tension per surface area).

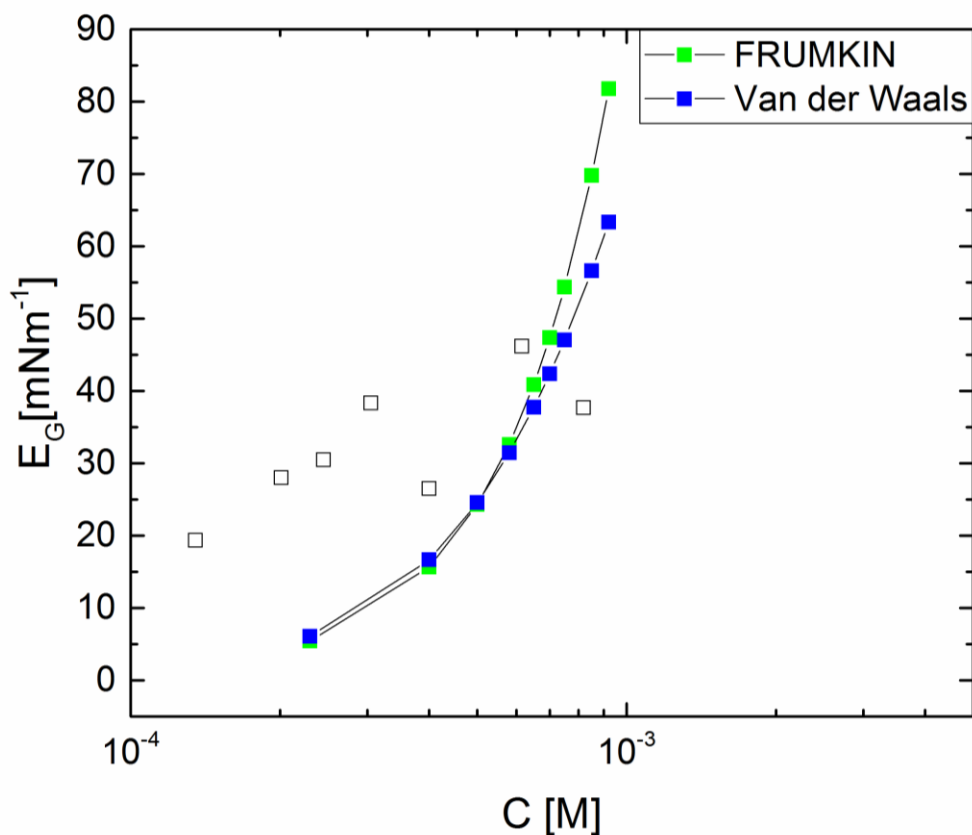


**Figure 29. Gibbs elasticity as a function of CTAB concentration in bulk solution. The empty symbols in the figure represent data taken by Stubenrauch (63).**

As the bulk solution concentration increase, the Gibbs elasticity increases.

#### 4.1.5 CTAB summary

The results and discussion have focused solely on the characterization of dynamic adsorption in aqueous CTAB solutions. Measurements of dynamic surface tension were obtained using maximum bubble pressure. The DST data was then analyzed using the selected mass transfer model, to establish an apparatus constant and to show that the long time asymptotic results of the adsorption process can be described using a diffusion model (that accounts for the charge effects). Quasi-equilibrium surface tension data were obtained and analyzed using the Frumkin and van der Waals equilibrium isotherms. More specifically, dynamic surface tension fits yield  $S_\gamma$  and quasi-

equilibrium surface tension data allows computation of equilibrium surface concentration  $\Gamma_{1,eq}$  that in turn allow the evaluation of the apparatus constant ( $l = 2.46$ ) for our MBPT was determined. This apparatus constant allows the calculation of the universal surface age (adsorption time) for dynamic surface tension values, and the experimental results show that surface tension values can be measured for the relatively short adsorption time ( $\sim 10$  ms). The properties of the adsorbed surfactants were obtained by further analyzing the quasi-equilibrium surface tension datasets to obtain parameter including surface pressure ( $\gamma_o - \gamma$ ),  $\beta$  which refers to the interaction between hydrophilic tails of the adsorbed molecules, equilibrium surface concentrations of counterion ( $\Gamma_{2,eq}$ ) and surfactant ( $\Gamma_{1,eq}$ ) for different concentrations, the adsorption constant of surfactant ( $K_1$ ) and counterion ( $K_2$ ) that is related to the free energy of adsorption, the surface potential ( $\phi_s$ ), and the maximum surfactant surface concentration ( $\Gamma_\infty$ ). These parameters were determined by taking into account of counterion binding, the electrical field generated by the surface charge density, and by assuming a surfactant adsorption follows the localized, Frumkin or non-localized van der Waals isotherms respectively. The measurement and analysis protocols seem to be pretty robust, compare well with literature, and are therefore applied next to a detailed investigation of the dynamic adsorption of four bile salts.

## 4.2 Bile Salts

Bile salts are the product of the synthesis of cholesterol in the liver (8). First the cholesterol is catalyzed by the enzyme  $7\alpha$ -hydroxylase (classical pathway) to produce the two primary bile acids (the chenocholic acid and the cholic acid), then dehydroxylation (removal of OH) of these bile acids by intestinal bacteria results in the second set of bile acids (Deoxycholic acid and lithocholic acid). These bile salts (sodium or potassium salts) can be conjugated with glycine or taurine (8). The specifics of their molecular structure affect micellization process as well as their dynamics of adsorption. In contrast to CTAB or SDS, the bile salts have a fairly rigid, flat structure, and hydrophobic and hydrophilic regions are not simply recognizable as hydrophilic head and hydrophobic tail.

Bile salts have been investigated extensively for their role in physiological processes and their value in designing new pharmaceutical formulations. The physical chemistry of micellization and interfacial adsorption has also received some attention, and the following properties have been investigated before: micelle properties (critical micelle concentration (CMC), aggregation number and counterion binding to micelles) (27, 64, 65), interfacial properties (surface rheology, adsorption, desorption, surface activity) (2, 30), diffusion coefficients using light scattering (40), thermodynamic of interfacial adsorption and micellization (32). However, there is the extremely limited amount of data of dynamic surface tension of bile salts in the literature (30, 66). Also, the adsorption parameters that take counterion binding and electrical double layer into account in the fashion described earlier in this thesis have not been reported. In this section, an extensive set of dynamic surface tension data is presented for four bile salts. The dynamic adsorption and quasi-equilibrium surface tension data of these bile salts are analyzed in great detail to obtain parameters like effective diffusivity, surface concentration, surface potential, Stern layer occupancy, etc.

### 4.2.1 Dynamic Surface Tension

During lipid digestion, partially digested food is mixed with bile and pancreatic fluids(2). This mixture contains a large number of amphiphilic molecules including food-products as well the products of the human body. Different surface active molecules compete as they get adsorbed to oil-water interfaces formed during food consumption. Therefore, quantitative understanding of adsorption kinetics and thermodynamics is crucial for better understanding food digestion and digestive health, the design of processed food as well for developing better cures and nutrition programs. In this section, the focus is on bile salts that clean fat interfaces and allow the enzymes (pancreatic lipases) to act on fats by changing interfacial structure due to their interaction with the hydrophilic part of amphipathic polar lipids in the fat surface (2).

The dynamic surface tension measurements for the four bile salts were carried out using maximum bubble pressure tensiometry, and the data is presented in the next-subsection. As the time dependent values of surface tension are discussed, they will be contrasted to the behavior observed for typical surfactants (including CTAB measurements included in this thesis). Dynamic surface tension curve of many surfactants shows into three different kinetics regimes: in the first regime called the induction regime is characterized by a slow decrease in the value surface tension. Indeed, the value of surface tension of the surfactant solution is nearly indistinguishable from the value for pure solvent, indicating the amount of adsorbed surfactant is low. In the second regime, a fast and rather abrupt decrease of surface tension is typically detected, and the surface coverage is >50 % is established quickly. Finally, the last kinetic regime is reached when a meso-equilibrium or quasi-equilibrium surface tension value is reached and the slow change in surface tension is attributed to a rearrangement of adsorbed surfactant molecules (67).

### 4.2.1.1 Sodium Glycodeoxycholate

The dynamic surface tension curves for different bulk concentrations of Glycodeoxycholate are shown in Figure 30b and data for CTAB solutions is included as Figure 30a for comparison. At low concentrations, induction regime is observed in the dynamic surface tension data that indicates the existence of a kinetic barrier to adsorption. This can be contrasted with the dynamic surface tension data for aqueous CTAB solutions that for all concentrations show only the second regime of fast, abrupt decrease in the surface tension until arriving at a quasi-equilibrium (left-hand side Figure 30). In the datasets shown for bile salt, dynamic surface tension curves show a nearly concentration-independent value between 4-10 mM. However, further increase in concentration results in a progressive increase in surface tension. Unlike CTAB solutions that show two distinct concentration-dependent regimes, below and above a critical micelle concentration, for the bile salt, the equilibrium surface tension seems to vary continuously. The behavior is consistent with other studies that attribute it to micellization by step-wise aggregation for Sodium Glycodeoxycholate (64).

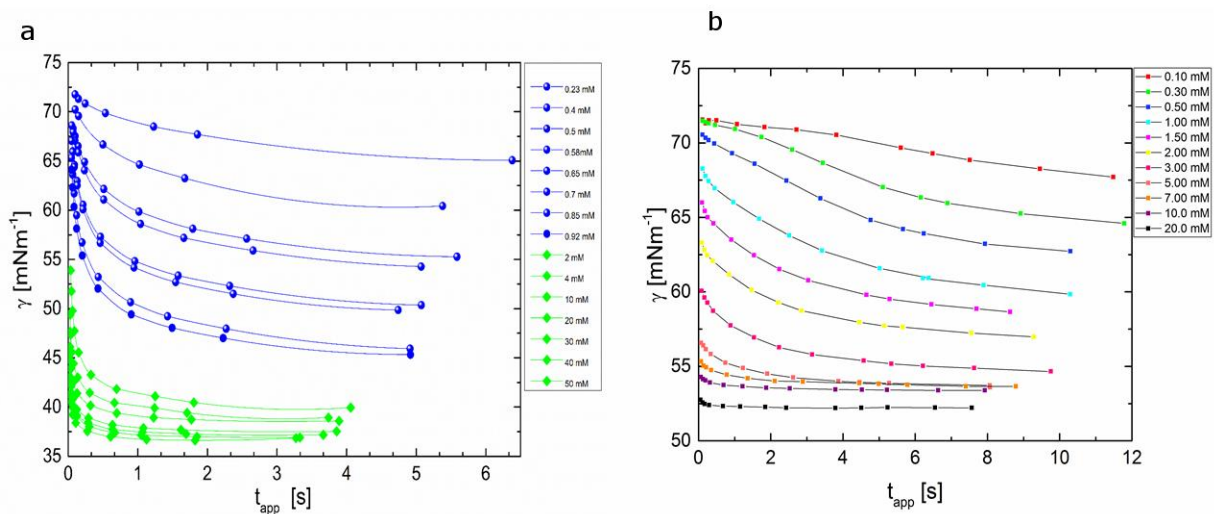


**Figure 30. The plot of dynamic surface tension as a function of apparent surface age and concentration for CTAB (a) and Sodium Glycodeoxycholate (b).**

In the left-hand-side of the figure, the dynamic surface tension for CTAB at solution concentration from 0.23mM to 50mM is plotted (a). In the right-hand side, dynamic surface tension NaGDC at concentrations from 0.1mM to 20mM.

In Figure 30, the DST values are plotted against the apparent surface age obtained from the MBP tensiometer. As the apparatus constant is supposed to be independent of the type of surfactant, surfactant and surfactant bulk concentration, universal surface age was calculated for the different bile salts. Figure 31 shows the dynamic surface tension versus universal surface age ( $t_u = t_{\text{app}} / \lambda^2$ ) for glycodeoxycholate. Adsorption times of around 9.5 ms are achieved. The maximum drop of surface tension is around 20mM.

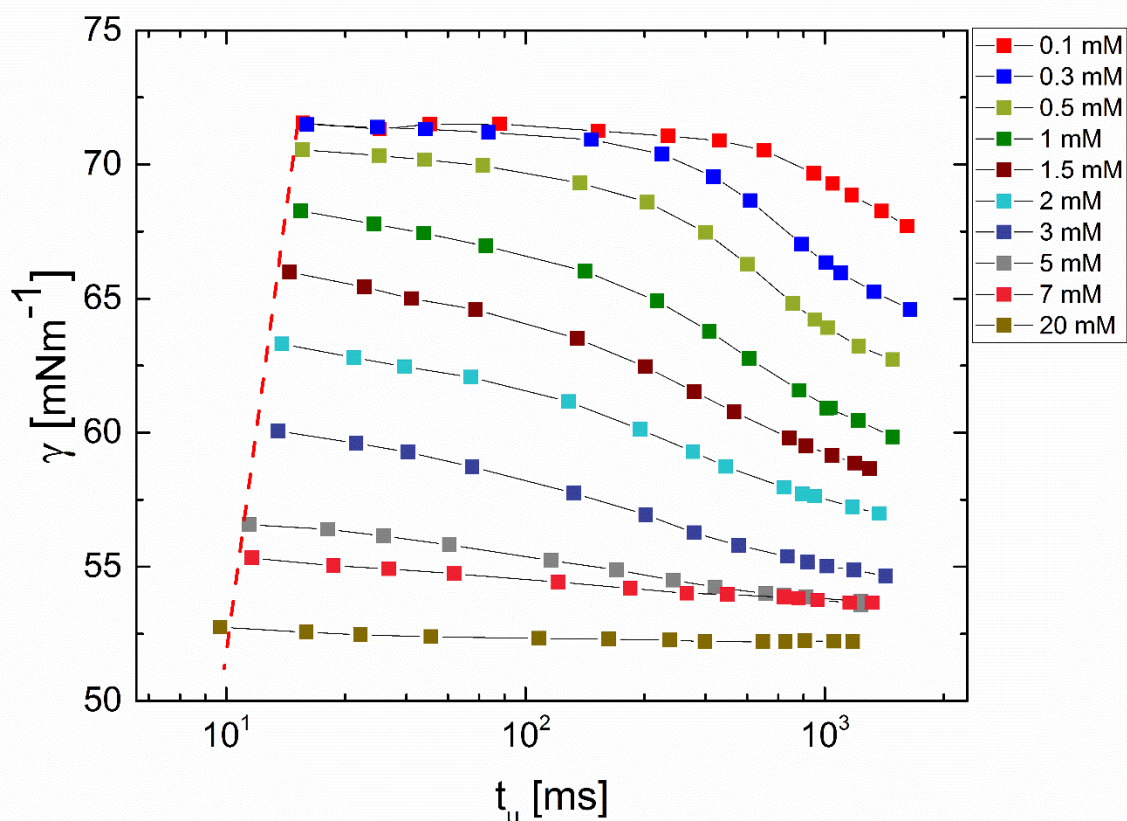


**Figure 31.** The plot of dynamic surface tension vs universal surface age for Sodium Glycodeoxycholate solutions with a range of concentration from 0.1 - 20 mM.

The maxima surface pressure is  $20 \text{ mNm}^{-1}$ . The shortest measured time of adsorption is 24 ms for a solution concentration 20 mM.

Experimental data obtained in this study is contrasted with the dynamic surface tension data reported by Valderrama *et al.* (2) in Figure 30. Though a reasonable agreement is observed at low concentrations, the higher concentration data show substantial differences. The results reported by Valderrama *et al.*(2) were acquired using pendant drop tensiometry and a commercially-available MBP tensiometer represent the only other study of dynamic adsorption of sodium glycodeoxycholate solutions, and datasets for only a handful of concentrations were reported in their study.

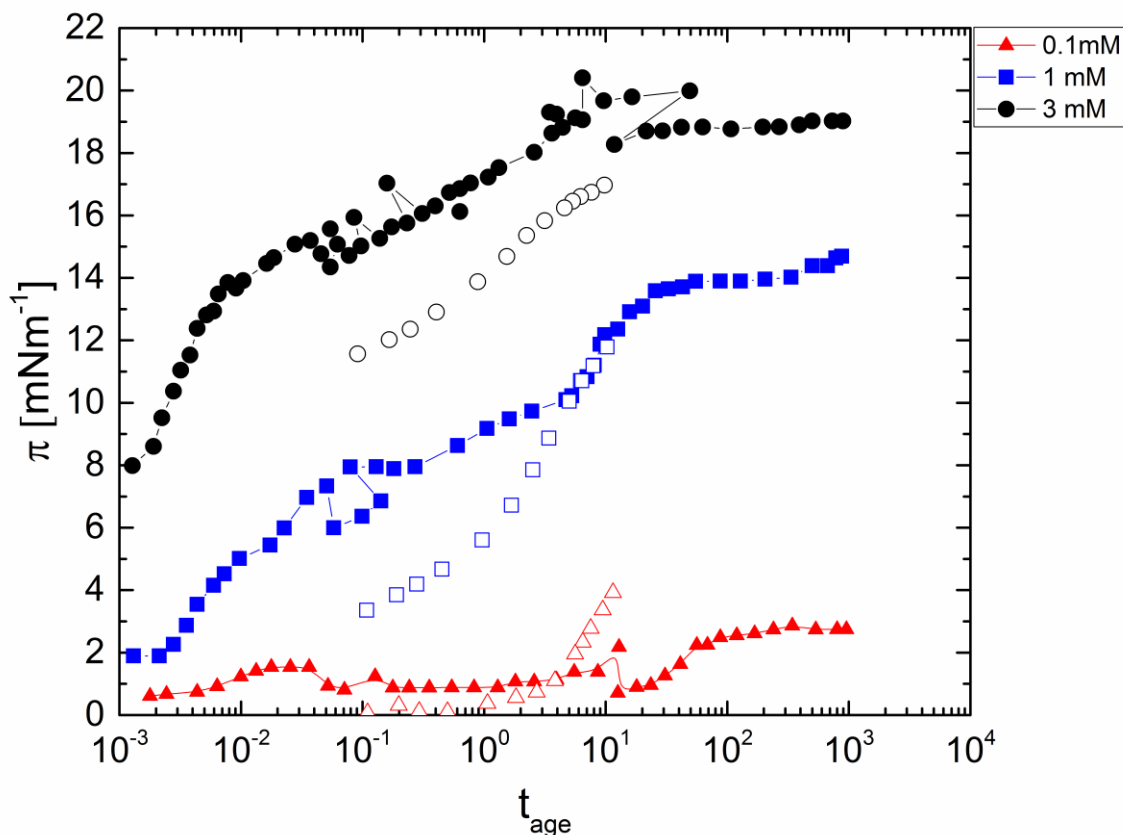


**Figure 32.** The plot of dynamic surface tension vs apparent surface age of Sodium Glycodeoxycholate from reported data by Valderrama *et al.* (2) and experimental data obtained in this report.

The attached points are the data reported by Valderrama *et al.*(2) and the points are our experimental data.

#### 4.2.1.2 Sodium Cholate

The surface tension values for sodium cholate (NaC) computed using maximum bubble pressure as a function of universal surface age are plotted in Figure 33. Even for 40 mM NaC solutions, the surface tension value is only 55 mNm<sup>-1</sup>. The progressive decrease in surface tension with concentration is more rapid for  $c < 7$  mM. Like sodium glycodeoxycholate, sodium cholate shows the concentration-dependent values of surface tension above apparent CMC.

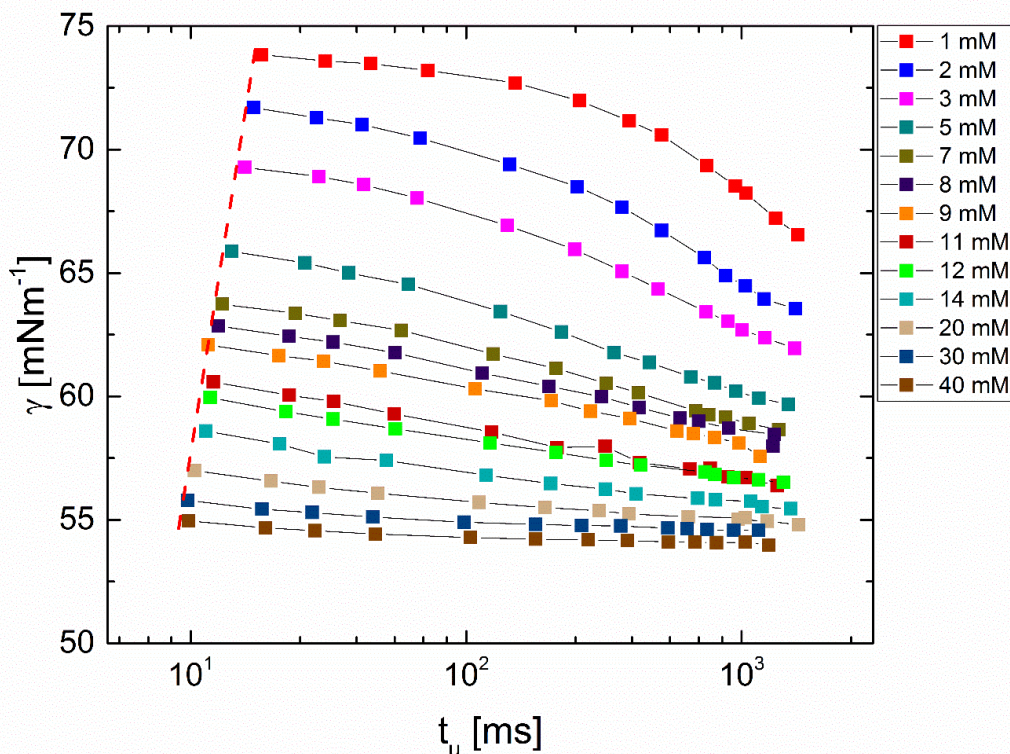


**Figure 33.** The plot of dynamic surface tension vs universal surface age for Sodium Cholate solutions in a range of solution concentrations from 1 - 40 mM.

The maxima surface pressure is  $20 \text{ mNm}^{-1}$ . The shortest time of adsorption measured is 9.83 ms that is the one gotten for a solution concentration of  $40 \text{ mM}$ . The dashed line represents the dilatation rate for the same flow for different surfactant concentrations.

#### 4.2.1.3 Sodium Deoxycholate

According to the results in Figure 34, in the case of sodium deoxycholate, the surfactant molecules take longer to reach the interface than CTAB or NaC, but at low concentrations, they are more effective than the other bile salts in reducing the equilibrium value of surface tension. The concentration-dependent surface tension values seem to show less variation above 5 mM. Again, the surface tension values measured are  $\gamma > 55 \text{ mNm}^{-1}$ . NaGDC shows more affinity for the

interface than NaDC because of reach equilibrium surface tension values faster. The slope of the red line for NaDC seems to be even shallower than that observed for CTAB and NaC solutions

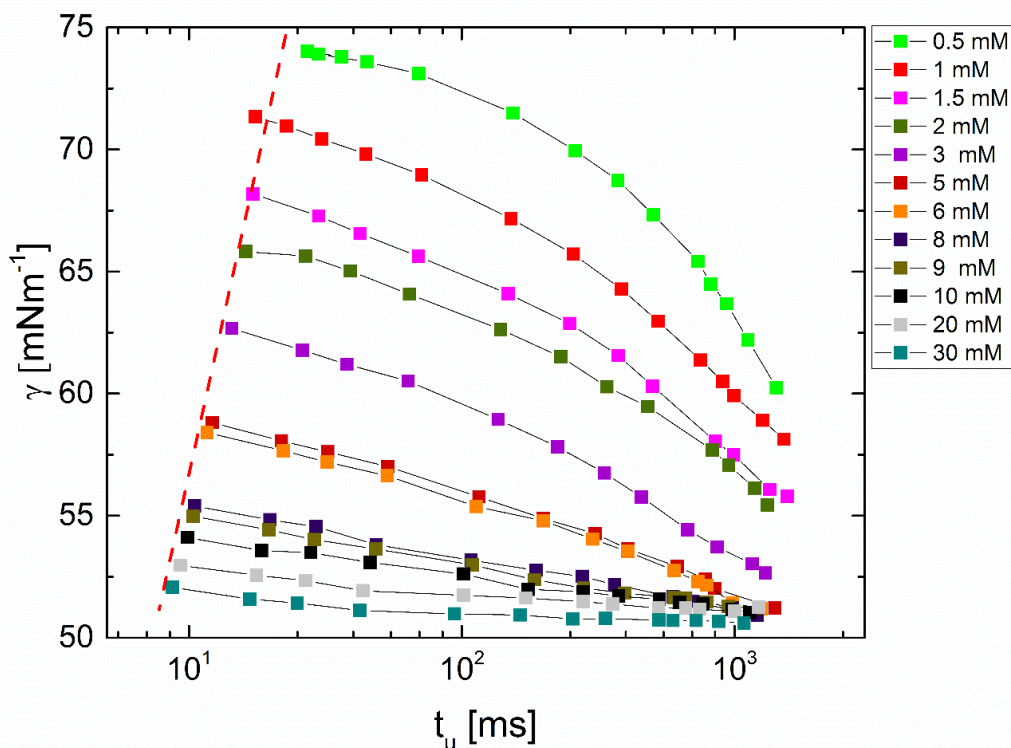


**Figure 34.** The plot of dynamic surface tension vs universal surface age for Sodium Deoxycholate solutions with a range of concentration of 0.5 - 30 mM.

The maxima surface pressure is  $23\text{mNm}^{-1}$ . The shortest measured time of adsorption is 8.7 ms for a solution concentration 30mM.

#### 4.2.1.4 Sodium Taurocholate

Equilibrium surface tension values have been obtained for Sodium Taurocholate by many authors (32, 68, 69), as it plays an important role in solubilization of cholesterol in the intestine and together with other bile salts, can be applied in the development of new drugs. However, the dynamic surface tension of taurocholate has been reported only in one paper and for few

concentrations (2). The evolution of dynamic surface tension vs universal surface age is plotted in Figure 35 is in striking contrast to the other surfactants. The surface tension of sodium taurocholate achieves the equilibrium surface tension much faster than another bile salts or CTAB, implying both a higher surface activity and higher mobility. Nevertheless, the effectiveness for reducing surface tension is as that high as CTAB or other surfactants as SDS. Since NaTC is a conjugated bile salt, it seems conjugation increase the affinity for the interface as also happen with NaGDC. The conjugated acids also have other characteristics that are biologically relevant, for example, the amidation with glycerin and taurine gives them greater acidity, which prevents these conjugated bile acids from passing through membranes in the process of elimination of cholesterol, besides that they are not hydrolyzed by enzymes like Pancreatic carboxypeptidases (70). These conjugated bile acids are preferably absorbed by the ileum, and among them, taurocholate acid is preferably adsorbed, the absorption of these acids is important for the digestion of lipids. This absorption affinity of the taurocholate acid for the ileum could be related to the same affinity that NaTC has with the interfaces (water-air or oil-water), but a deeper study would be needed.

The minimum evaluated adsorption time measured in this case is 11 ms. The dashed line shows that the surface expansion rate does not change with concentration for this surfactant.

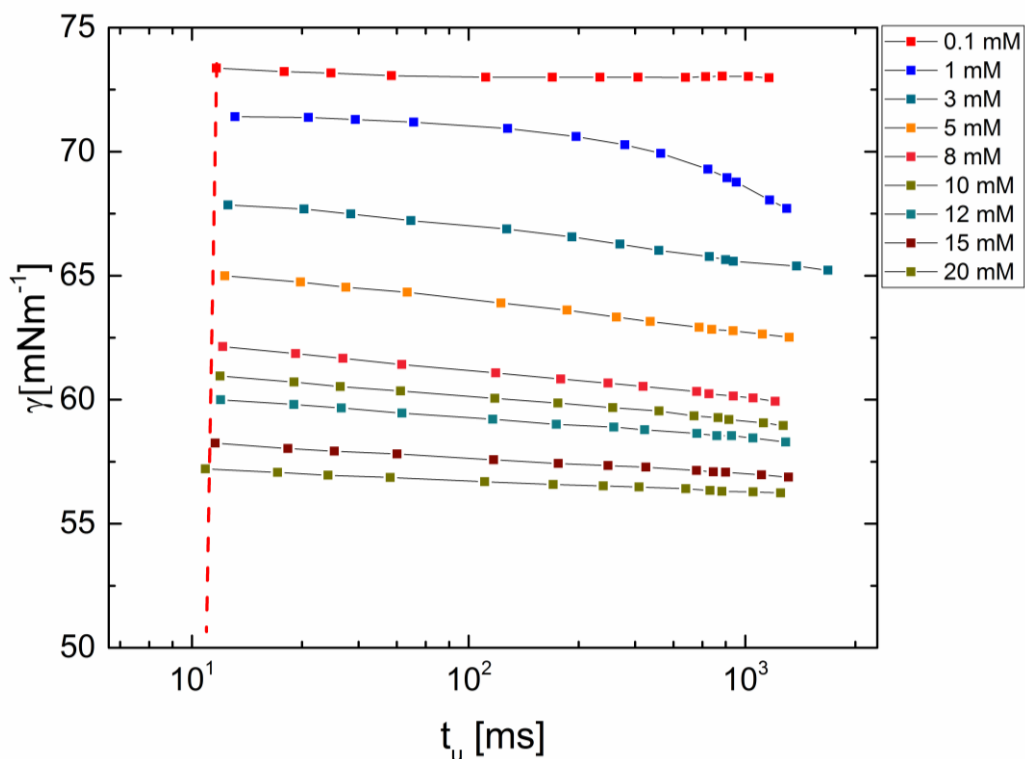


**Figure 35.** The plot of dynamic surface tension vs universal surface age for sodium taurocholate solutions with a range of concentration from 0.1 mM to 20 mM .

The maxima surface pressure amounts to  $17 \text{ mNm}^{-1}$ . The shortest measured time of adsorption is 11 ms for a solution concentration 20 mM.

The dataset for NaTC shows that the value of surface tension continues to decrease considerably even when  $c > \text{CMC}$  (see Table IV). According to literature(64), the micelles formed by NaTC are small in size and relatively unstable, and as the rate of demicellization is high, surfactant molecules are added to the interface at relatively short times. The presented in Figure 35 is compared the measurements by Valderrama *et al.*(2) are shown in Figure 36. The datasets overlap at low concentrations only.

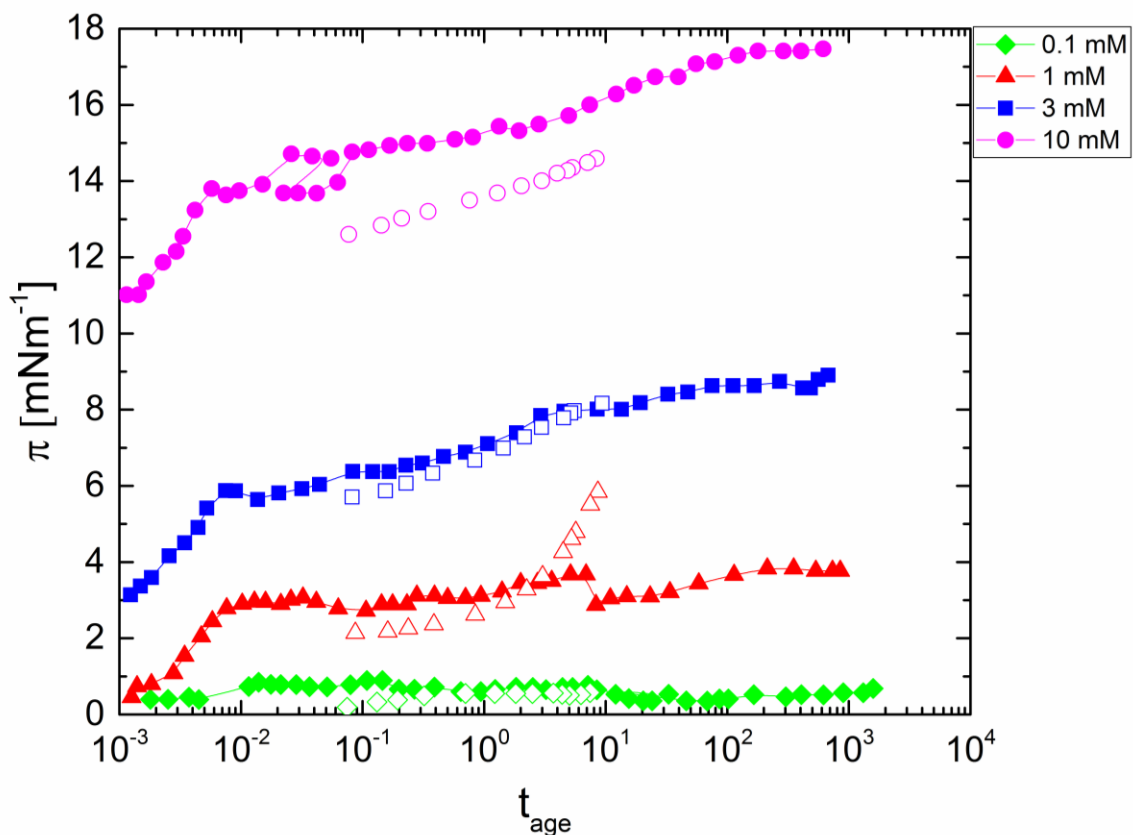


**Figure 36.** The dynamic surface tension of sodium taurocholate, data is closed symbols show values reported by Valderrama *et al.*(2) and the open symbols show valued of MBP measurements obtained in this study.

#### 4.2.2 Equilibrium surface tension

Figure 37 shows the plots of the quasi-equilibrium surface tension for four bile salts and CTAB.

The effectiveness of surfactants in modifying surface tension decreases as follows: CTAB>NaDC>NaGDC>NaC>NaTC. In the case of bile salts, the maximum drop of surface tension is obtained for sodium deoxycholate. The effectiveness could be linked to the shape of the surfactants molecules. For bile salts, the equilibrium surface tension curve is smooth, that contrasts

with the sharp change in slope for CTAB observed at CMC. The datasets appear to be consistent with reports of stepwise aggregation in bile salts.(64).

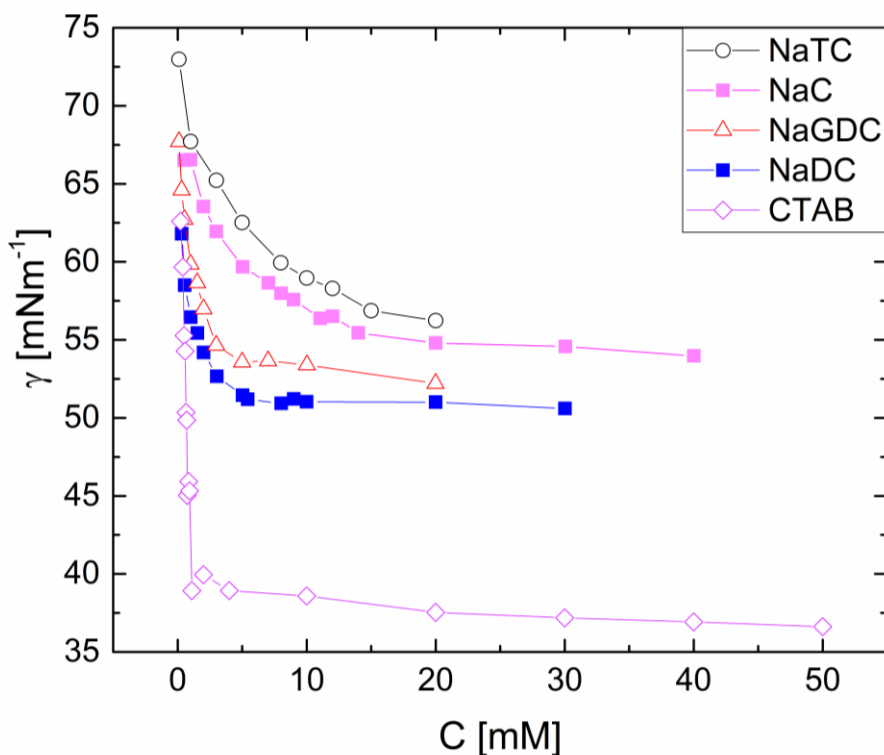


**Figure 37. Equilibrium surface tension of Sodium taurocholate, Sodium Chololate, Sodium Glycodeoxycholate, Sodium Deoxycholate, and CTAB.**

The quasi-equilibrium data sets are replotted in Figure 38 using a semilog plot for the change of slope is observed more clearly than in Figure 37. The value CMC follows the order: NaTC>NaC>NaDC>NaGDC>CTAB. In the case of the Cholic and Deoxycholic salts, results follow the trends expected from the relative hydrophobicity of the molecules. Cholic salts are more hydrophobic than Deoxycholic salts. Though the self-assembly of bile salts surfactant is driven by the reduction of the hydrophobic surfaces exposed to water as stated by Maldonado (2), hydrogen bonding also affects the micellization process for bile salts. In the case of the conjugates of bile salts, it is seen that their effect in the micellization process is minor

compared with the molecule structure (see Table IV), although they should follow the same behavior (higher hydrophobicity higher CMC), results are not clear in the case of Sodium Taurocholate which should have lower CMC than a no conjugate molecule, because this conjugate make bile salts less hydrophobic.

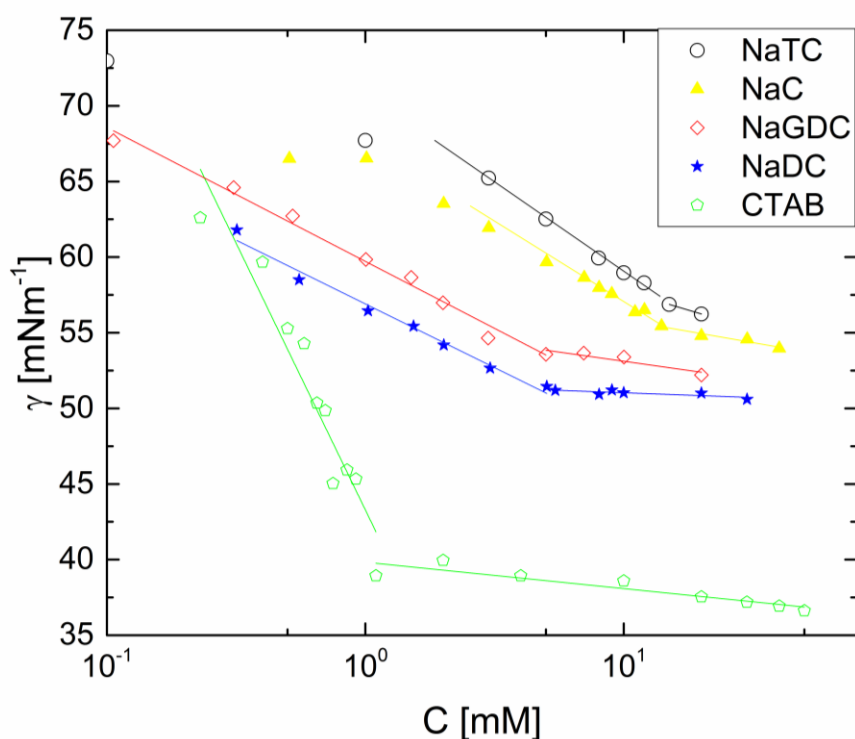


**Figure 38 Equilibrium Surface Tension Sodium Cholate (NaC), Sodium Deoxycholate, Sodium Glycodeoxycholate, Sodium taurocholate and CTAB**

The difficulty in determining the CMC for taurocholate (see Figure 38) is due the aggregates are too small for being clearly detected by surface tension measurements (69). The value of CMC obtained by the surface tension measurements for an aqueous solution of NaTC is around 12mM (68, 69). The curve of equilibrium surface tension for sodium cholate has been reported by Natalini *et al.* (65) which agree with the critical micelle concentration of 12.8 mM (see Table IV) but the

minimum equilibrium surface tension is 50 mN/m and in Figure 25 the minimum equilibrium surface tension reached is 53 mN/m .

**Table IV. Maximum surface concentration from the Gibbs equation and CMC values for bile salts and CTAB.**

**Maximum surface concentration evaluated with the slope of equilibrium surface tension. (a) Sigma-Aldrich, (b) (71), (c) (68).**

	Our Results		Literature values
	$\Gamma_{\max} \left[ \frac{\text{mol}}{\text{m}^2} \right]$	$cmc [mM]$	$cmc [mM]$
NaC	$8.67 \times 10^{-7}$	12.8	9-15 a
NaDC	$7.38 \times 10^{-7}$	4.71	2-6 a
NaGDC	$7.78 \times 10^{-7}$	4.43	2.12 b
NaTC	$1.03 \times 10^{-6}$	15.40	8.12 c
CTAB	$3.09 \times 10^{-6}$	1.12	0.92-1.0 b

The values of maximum surface concentration evaluated from Gibbs equation on Table IV has the trend NaDC<NaGDC< NaC<NaTC<CTAB, so CTAB has the smallest area per molecule. This sequence differs from the one obtained by Jana (72) using du Nouy Ring. However, the value of maximum surface concentration reported for CTAB from Jana (72) differs from Szymczyk (47); the data by the latter agrees with our results. The conjugated bile salts seem to occupy less surface area than the simpler analogues, although they reach interfaces faster in the dynamic surface tension measurements.

Critical micelle concentration for bile salts has been evaluated by different authors (47, 64, 72, 73) using surface tension measurements for example Najjar *et al.*(73) results show that for NaC the  $cmc = 8.61mM$  and for NaDC the  $cmc = 3.23mM$  , this solutions were prepared in  $pH = 6.5$  a phosphate buffer solution; O'Connor (64) measurements show that for NaC the  $CMC=10.2 mM$  and for NaDC the  $cmc = 1.26mM$ , in a solution buffer at  $pH = 7$  with a phosphate buffer

solution, while for an aqueous solution of NaTC at  $pH = 4.09$  the  $cmc = 33 \text{ mM}$ . The wide difference between reported values could be due to sensitivity to  $pH$  or presence of impurities that can affect the aggregation as well as adsorption processes. Additional effects arise due to the fact that the self-assembly of surfactant molecules in the case of bile salts is not driven only by the hydrophobic effect but also its driven by hydrogen bonding that is affected by the  $pH$  of the solution (2).

Dynamic surface tension data for all four bile salts were analyzed using the procedure described earlier in theory section and implement for CTAB solutions. Table V shows the values of parameters obtained by utilizing Frumkin isotherm in the fit. Comparing results of the maximum surface concentration between reported values and the ones obtained in this study shows a good agreement of the order of magnitude of the results. The slight difference between reported ones and the calculated values of the maximum surface concentration could be due to the difference in assumptions made in the respective analysis. For example, Chang and Franses (35) do not take into account the electrical double layer for NaC and NaDC results and assume a kinetic relation for the adsorption process. Szymczyk and Jańczuk (47) used only the slope of the equilibrium surface tension for evaluating the maximum surface concentration. The approach used here accounts for the electrical double layer, counterion binding and also involves a detailed analysis of the dynamic surface tension datasets.

**Table V. The adsorption parameters obtained using Frumkin isotherm and quasi-equilibrium surface tension data for aqueous dispersions of CTAB and for bile salts.**

Parameters were evaluated from fits to equilibrium surface tension with the equation of state for bile salts and CTAB and by using Frumkin isotherm. Literature values are included for comparison. The values for NaDC and NaC (a) are taken from Chang and Franses (35) and the value for CTAB (b) is from Szymczyk and Jańczuk (47).

	Frumkin				Literature Values
	$\beta \left[ \frac{kgm^4}{s^2mol} \right]$	$K_1 [mM^{-1}]$	$K_2 [mM^{-2}]$	$\Gamma_\infty \left[ \frac{mol}{m^2} \right]$	$\Gamma_\infty \left[ \frac{mol}{m^2} \right]$
NaDC	$3.7 \times 10^{-16}$	$1.32 \times 10^3$	0.13	$1.8 \times 10^{-6}$	$2.20 \times 10^{-6}$ a
NaGDC	$2.8 \times 10^{-16}$	$9.73 \times 10^2$	0.09	$1.5 \times 10^{-6}$	--
NaC	$7.0 \times 10^{-17}$	$3.18 \times 10^2$	0.57	$1.5 \times 10^{-6}$	$1.80 \times 10^{-6}$ a
NaTC	$2.1 \times 10^{-16}$	$1.41 \times 10^3$	$2.7 \times 10^{-15}$	$2.4 \times 10^{-6}$	--
CTAB	$1.0 \times 10^{-17}$	$1.65 \times 10^3$	5.69	$6.3 \times 10^{-6}$	$3.10 \times 10^{-6}$ b

The area per molecule reported for NaDC is  $93 \text{ \AA}^2$  for the air-water interface, measured by Wilhelmy technique (29), is close to the value obtained here ( $92.25 \text{ \AA}^2$  per molecule) using the Frumkin isotherm. For NaC the area per molecule estimated from MBP data is  $110 \text{ \AA}^2$  is close to the values reported by Jana (72). The occupancy of the Stern layer vs surfactant concentration is plotted in Figure 39. The occupancy in the Stern layer shows how much counter ion is binding. Almost all of the bile salts seems to do not have counter ion on the Stern layer except Sodium Chololate, which presents an increase in counter ion concentration on the Stern layer with the increase of the bulk concentration. The occupancy reached by NaC at a concentration of  $12 \text{ mM}$  is 0.5. It seems that sodium deoxycholate and sodium glycodeoxycholate present the same behavior in the occupancy of the counter ion on the Stern layer. In contrast, sodium taurocholate does not present counterion binding that all, which agrees with the result obtained on Table V, where the  $K_2$  value is almost zero. This last constant is related to the energy of adsorption of the counter ion.

The dynamic adsorption studies provide critical insights into the physicochemical parameters that determine surface tension, surface elasticity, self-assembly and rheology of the amphiphilic molecules. The contrast between the four bile salts, for example, needs to be further investigated to draw clinical and medically-relevant conclusions about their respective role in digestion, drug-delivery, and diseases like gall stones. Formation of gallstones, for example, is sometimes related to the selective solubilization of phospholipids by bile micelles, which leaves cell membranes or vesicles richer in cholesterol (microcrystals) to form gallstones (70) .

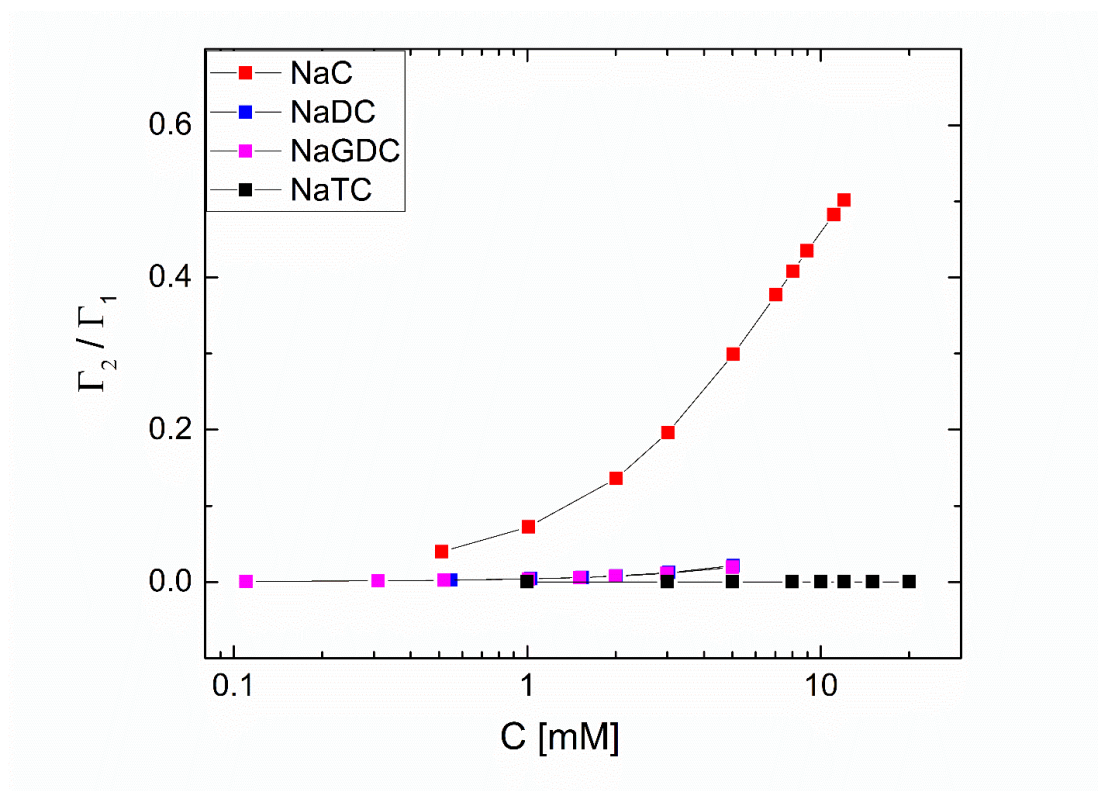


**Figure 39. Occupancy of the Stern layer of counterion ( $G_2/G_1$ ) vs concentration of surfactant in the bulk solution.**

The data was obtained from the fitting of equilibrium surface tension, using Frumkin isotherm as a model of adsorption.

The dimensionless adsorption shows how the maximum surface concentration changes with an increase in concentration. In Figure 40, dimensionless adsorption of the studied bile salts has been plotted vs the bulk solution concentration. Sodium deoxycholate values are close to 1 in the whole range of plotted concentrations. The curves in Figure 40 mimic the behavior seen in Figure 37, follow from higher to lower: NaDC>NaGDC>NaC> NaTC. Even though sodium taurocholate (see Figure 35) reached its equilibrium surface tension values faster than the other bile salts, the overall interfacial concentration of surfactant and ability to reduce surface tension are distinctly lower than other bile salts and CTAB.

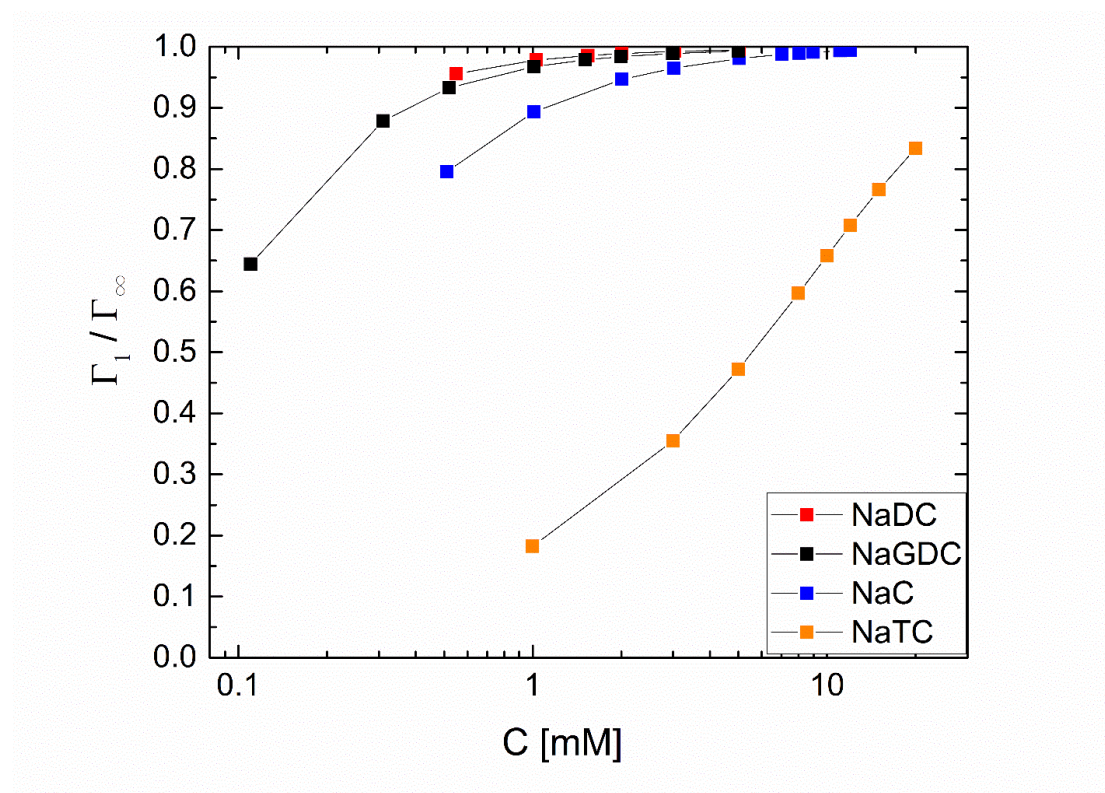


**Figure 40. Dimensionless adsorption ( $\Gamma_1/\Gamma_\infty$ ) for Bile salts vs concentration in the bulk solution.**

The data was obtained from the fitting of equilibrium surface tension, using Frumkin isotherm as a model of adsorption.

Finally, the surface potential of bile salts vs surfactant solution concentration is shown in Figure 41. The surface potential for NaC, NaDC, and NaGC have values of around 100 mV for the evaluated concentration range and follow similar dependence of surface potential with concentration. On the other hand, NaTC values are much higher. It is not obvious as to why the values are so different for NaTC, and independent measurements of zeta potential (57) could help in deciphering the origin of such high charge. The surface potential generated by the adsorption of the bile salts generates a barrier to the mass transport of other amphiphiles present in the solution, thus influencing lipid digestion and drug solubilization.

The dynamic adsorption of bile salts analyzed in this study represents an important and crucial step in establishing the difference between kinetic and hydrodynamic effects that affect the interfacial properties and self-assembly of these physiologically significant compounds. In spite of a large number of studies on the equilibrium surface tension of bile salts, relatively little was known about the dynamic adsorption of these bile salts. The data and the analysis are presented here with a certain hope that the experimental and analysis framework outlined here will find further use in the characterization of bile salts, bile salt derivatives and other biologically relevant amphiphilic molecules that display faster adsorption kinetics than can be resolved by pendant drop tensiometry or Wilhelmy plate techniques.

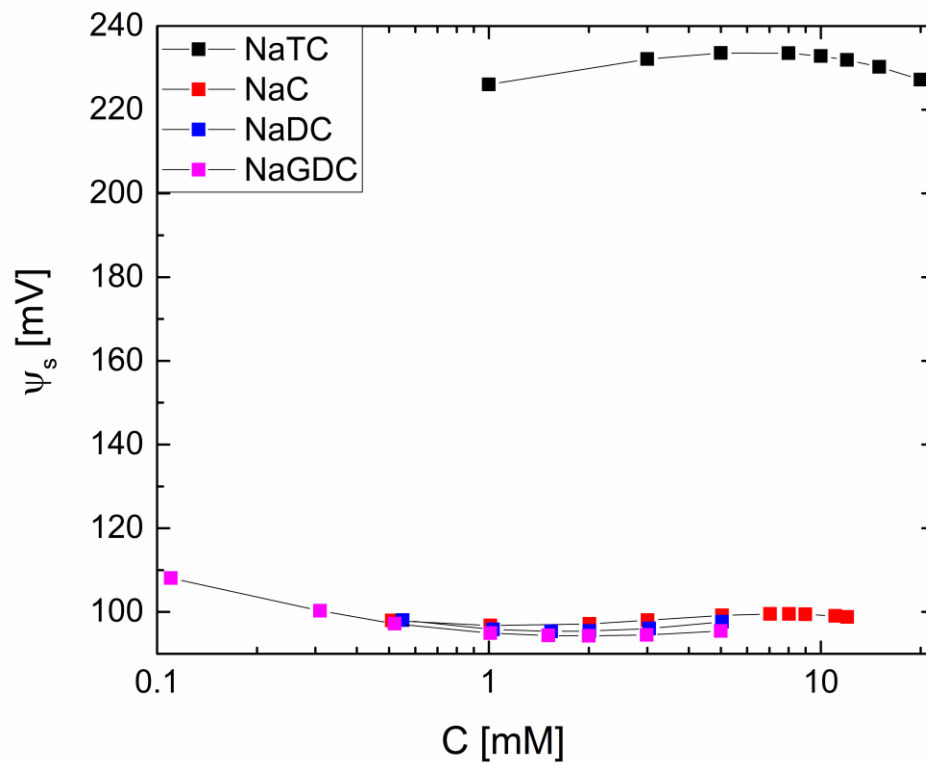


**Figure 41. The surface potential of bile salts as a function of concentration.**

The data was obtained from the fitting of equilibrium surface tension, using Frumkin isotherm as a model of adsorption.

## 5 CONCLUSIONS

### 5.1 Summary

An extensive set of measurements of dynamic surface tension were carried out using maximum bubble pressure tensiometry and the dynamic adsorption was analyzed for five ionic surfactants: cetyltrimethylammonium bromide (CTAB) and four bile salts. The interfacial adsorption of CTAB and bile salts is a relatively fast process, and surface tension variation occurs over short timescales (<50 ms) inaccessible in measurements with Du nouy ring, Wilhelmy plate, and pendant drop methods, but accessible with MBP tensiometer. The time evolution of surface tension is analyzed using a full transient model for mass transfer of ionic surfactants that accounts for non-stationary interface, charge, and diffusion, and the quasi-equilibrium surface tension data are analyzed by using Frumkin and van der Waals isotherms. Surface concentration, surface potential, Gibbs elasticity, critical micelle concentration are obtained for CTAB and four bile salts. The values obtained using Frumkin isotherm for maximum surface concentration seems to have an agreement with literature than those obtained with van der Waals isotherm.

In addition, the CTAB data are analyzed to determine an apparatus constant value ( $2.46 \pm 0.06$ ) that allows the computation of dynamic surface tension variation with the universal surface age. The calculation of apparatus constant and universal age is necessary for correcting for the influence of non-stationary interface. The value of apparatus constant indicates that the bubble surface is younger than nominal surface age obtained from MBP method by almost a factor of six. The adsorption time of 8 ms was accessible using the apparatus built in the laboratory, and the bubbling-to-jetting transition limits the shortest times reachable for the MBP tensiometry.

The dynamic adsorption data for bile surfactants shows a more rapid adsorption to the interface, and the quasi-equilibrium datasets indicate that even though bile micelles are highly surface active, the effectiveness as surfactants for reducing surface tension values is quite limited. The DST data for low concentration of bile salt NaGDC shows the existence of a kinetic barrier for the transport of surfactant to the interface. Sodium Cholate and its conjugate have higher affinity to the interface than Sodium Deoxycholate and its conjugated bile salt.

## **5.2 Recommendations for future work**

Here is a short list of tasks that can be accomplished by a future student or researcher:

Determine the value of apparatus constant by finding the rate of expansion of the interface by recording the growth of the bubble in the capillary submerged in an aqueous solution for different solution concentration. Then, compare results with those obtained Figure 19.

Determine dilatation visco-elasticity of the interface for these surfactant solutions by producing perturbation over a certain frequency and quantifying the response to pressure pulses.

Determining surface potential data for bile salts in order to corroborate data with the fitted models.

Analyzing the transition of the bubbling to jetting, using flow rates higher in order to corroborate theories from Fainerman, and check if shorter time scales can be accessed using say a different nozzle size or modified analysis protocols.

## 6 REFERENCE LIST

1. Schramm LL. Fundamentals and Applications in the Petroleum Industry. 1992.
2. Maldonado-Valderrama J, Wilde P, Macierzanka A, Mackie A. The role of bile salts in digestion. *Advances in Colloid and Interface Science*. 2011;165(1):36-46.
3. Nikolov A, Wasan D. Ordered micelle structuring in thin films formed from anionic surfactant solutions: I. Experimental. *Journal of colloid and interface science*. 1989;133(1):1-12.
4. Clarke JD. Cetyltrimethyl ammonium bromide (CTAB) DNA miniprep for plant DNA isolation. *Cold Spring Harbor Protocols*. 2009;2009(3):pdb. prot5177.
5. Cárdenas M, Schillén K, Nylander T, Jansson J, Lindman B. DNA Compaction by cationic surfactant in solution and at polystyrene particle solution interfaces: a dynamic light scattering study. *Physical Chemistry Chemical Physics*. 2004;6(7):1603-7.
6. Sau TK, Murphy CJ. Self-assembly patterns formed upon solvent evaporation of aqueous cetyltrimethylammonium bromide-coated gold nanoparticles of various shapes. *Langmuir*. 2005;21(7):2923-9.
7. Hubert F, Testard F, Spalla O. Cetyltrimethylammonium bromide silver bromide complex as the capping agent of gold nanorods. *Langmuir*. 2008;24(17):9219-22.
8. Elnaggar YS. Multifaceted applications of bile salts in pharmacy: an emphasis on nanomedicine. *International journal of nanomedicine*. 2015;10:3955.
9. Bellesi FA, Ruiz-Henestrosa VMP, Pílosof AM. Behavior of protein interfacial films upon bile salts addition. *Food Hydrocolloids*. 2014;36:115-22.
10. Malysa K, Miller R, Lunkenheimer K. Relationship between foam stability and surface elasticity forces: Fatty acid solutions. *Colloids and surfaces*. 1991;53(1):47-62.
11. Wasan D, Nikolov A, Huang D, Edwards D. Foam stability: effects of oil and film stratification. ACS Publications; 1988.
12. Sharma V, Haward SJ, Serdy J, Keshavarz B, Soderlund A, Threlfall-Holmes P, et al. The rheology of aqueous solutions of ethyl hydroxy-ethyl cellulose (EHEC) and its hydrophobically modified analogue (hmEHEC): extensional flow response in capillary break-up, jetting (ROJER) and in a cross-slot extensional rheometer. *Soft matter*. 2015;11(16):3251-70.
13. Christov NC, Danov KD, Kralchevsky PA, Ananthapadmanabhan KP, Lips A. Maximum bubble pressure method: Universal surface age and transport mechanisms in surfactant solutions. *Langmuir*. 2006;22(18):7528-42.
14. Kovalchuk V, Dukhin S. Dynamic effects in maximum bubble pressure experiments. *Colloids and Surfaces A: Physicochemical and Engineering Aspects*. 2001;192(1):131-55.

15. Drelich J, Fang C, White C. Measurement of interfacial tension in fluid-fluid systems. *Encyclopedia of surface and colloid science*. 2002;3:3158-63.
16. Miller R, Joos P, Fainerman VB. Dynamic surface and interfacial tensions of surfactant and polymer solutions. *Advances in Colloid and Interface Science*. 1994;49:249-302.
17. Fainerman V, Miller R. Maximum bubble pressure tensiometry—an analysis of experimental constraints. *Advances in colloid and interface science*. 2004;108:287-301.
18. Fainerman V, Miller R, Joos P. The measurement of dynamic surface tension by the maximum bubble pressure method. *Colloid and Polymer Science*. 1994;272(6):731-9.
19. Ward A, Tordai L. Time - dependence of boundary tensions of solutions I. The role of diffusion in time - effects. *The Journal of Chemical Physics*. 1946;14(7):453-61.
20. Borwankar R, Wasan D. The kinetics of adsorption of surface active agents at gas-liquid surfaces. *Chemical Engineering Science*. 1983;38(10):1637-49.
21. Datwani SS, Stebe KJ. The dynamic adsorption of charged amphiphiles: The evolution of the surface concentration, surface potential, and surface tension. *Journal of colloid and interface science*. 1999;219(2):282-97.
22. Danov KD, Kralchevsky PA, Ananthapadmanabhan KP, Lips A. Influence of electrolytes on the dynamic surface tension of ionic surfactant solutions: Expanding and immobile interfaces. *Journal of colloid and interface science*. 2006;303(1):56-68.
23. MacLeod C, Radke C. Charge effects in the transient adsorption of ionic surfactants at fluid interfaces. *Langmuir*. 1994;10(10):3555-66.
24. Diamant H, Andelman D. Kinetics of Surfactant Adsorption at Fluid– Fluid Interfaces. *The Journal of Physical Chemistry*. 1996;100(32):13732-42.
25. Kralchevsky P, Danov K, Broze G, Mehreteab A. Thermodynamics of ionic surfactant adsorption with account for the counterion binding: effect of salts of various valency. *Langmuir*. 1999;15(7):2351-65.
26. Madenci D, Egelhaaf S. Self-assembly in aqueous bile salt solutions. *Current Opinion in Colloid & Interface Science*. 2010;15(1):109-15.
27. Matsuoka K, Moroi Y. Micelle formation of sodium deoxycholate and sodium ursodeoxycholate (Part 1). *Biochimica et Biophysica Acta (BBA)-Molecular and Cell Biology of Lipids*. 2002;1580(2):189-99.
28. Carey MC, Small DM. Micellar properties of dihydroxy and trihydroxy bile salts: effects of counterion and temperature. *Journal of colloid and interface science*. 1969;31(3):382-96.

29. Tiss A, Ransac S, Lengsfeld H, Hadvàry P, Cagna A, Verger R. Surface behaviour of bile salts and tetrahydrolipstatin at air/water and oil/water interfaces. *Chemistry and physics of lipids*. 2001;111(1):73-85.
30. Maldonado-Valderrama J, Muros-Cobos J, Holgado-Terriza J, Cabrerizo-Vílchez M. Bile salts at the air–water interface: adsorption and desorption. *Colloids and Surfaces B: Biointerfaces*. 2014;120:176-83.
31. Bleys G, Joos P. Adsorption kinetics of bolaform surfactants at the air/water interface. *Journal of physical chemistry*. 1985;89(6):1027-32.
32. Mukherjee B, Dar AA, Bhat PA, Moulik SP, Das AR. Micellization and adsorption behaviour of bile salt systems. *RSC Advances*. 2016;6(3):1769-81.
33. Eastoe J, Dalton J. Dynamic surface tension and adsorption mechanisms of surfactants at the air–water interface. *Advances in colloid and interface science*. 2000;85(2):103-44.
34. Deen WM. *Analysis of Transport Phenomena, Topics in Chemical Engineering*: Oxford University Press, New York; 1998.
35. Chang C-H, Franses EI. Adsorption dynamics of surfactants at the air/water interface: a critical review of mathematical models, data, and mechanisms. *Colloids and Surfaces A: Physicochemical and Engineering Aspects*. 1995;100:1-45.
- 7 36. Kolev V, Danov K, Kralchevsky P, Broze G, Mehreteab A. Comparison of the van der Waals and Frumkin adsorption isotherms for sodium dodecyl sulfate at various salt concentrations. *Langmuir*. 2002;18(23):9106-9.
37. Taylor CD, Valkovska DS, Bain CD. A simple and rapid method for the determination of the surface equations of state and adsorption isotherms for efficient surfactants. *Physical Chemistry Chemical Physics*. 2003;5(21):4885-91.
38. Birdi K. *Handbook of surface and colloid chemistry*: CRC Press; 2015.
39. Casandra A, Lin Y-C, Liggieri L, Ravera F, Tsay R-Y, Lin S-Y. Adsorption kinetics of the ionic surfactant decanoic acid. *International Journal of Heat and Mass Transfer*. 2016;102:36-44.
40. Oh S, McDonnell M, Holzbach R, Jamieson A. Diffusion coefficients of single bile salt and bile salt-mixed lipid micelles in aqueous solution measured by quasielastic laser light scattering. *Biochimica et Biophysica Acta (BBA)-Lipids and Lipid Metabolism*. 1977;488(1):25-35.
41. Mittal KL. *Solution chemistry of surfactants*: Springer Science & Business Media; 2012.
42. Movchan T, Soboleva I, Plotnikova E, Shchekin A, Rusanov A. Dynamic light scattering study of cetyltrimethylammonium bromide aqueous solutions. *Colloid Journal*. 2012;74(2):239-47.

43. Vitagliano V, Sartorio R, Ortona O, Paduano L, D'Errico G, Capuano F, et al. A diffusion study on the ternary system, sodium cholate–sodium deoxycholate–water. *Journal of Molecular Liquids*. 2010;156(1):70-5.
44. Hao L, Lu R, Leaist DG, Poulin PR. Aggregation number of aqueous sodium cholate micelles from mutual diffusion measurements. *Journal of solution chemistry*. 1997;26(2):113-25.
45. Mangiapia G, D'Errico G, Capuano F, Ortona O, Heenan RK, Paduano L, et al. On the interpretation of transport properties of sodium cholate and sodium deoxycholate in binary and ternary aqueous mixtures. *Physical Chemistry Chemical Physics*. 2011;13(35):15906-17.
46. Valkovska DS, Shearman GC, Bain CD, Darton RC, Eastoe J. Adsorption of ionic surfactants at an expanding air– water interface. *Langmuir*. 2004;20(11):4436-45.
47. Szymczyk K, Jańczuk B. The adsorption at solution–air interface and volumetric properties of mixtures of cationic and nonionic surfactants. *Colloids and Surfaces A: Physicochemical and Engineering Aspects*. 2007;293(1):39-50.
48. Sarkar A, Ye A, Singh H. On the role of bile salts in the digestion of emulsified lipids. *Food Hydrocolloids*. 2016;60:77-84.
49. Manojlović JŽ. The Krafft temperature of surfactant solutions. *Thermal Science*. 2012;16(suppl. 2):631-40.
50. Makievski A, Fainerman V, Joos P. Dynamic surface tension of micellar Triton X-100 solutions by the maximum-bubble-pressure method. *Journal of colloid and interface science*. 1994;166(1):6-13.
51. Kawale D. Influence of dynamic surface tension on foams: Application in gas well deliquification: MSc. Thesis. Delft University of Technology of Applied Sciences Department of Multi-Scale Physics; 2012.
52. Adamczyk Z, Para G, Warszyński P. Influence of ionic strength on surface tension of cetyltrimethylammonium bromide. *Langmuir*. 1999;15(24):8383-7.
53. Phan CM, Le TN, Yusa S-i. A new and consistent model for dynamic adsorption of CTAB at air/water interface. *Colloids and Surfaces A: Physicochemical and Engineering Aspects*. 2012;406:24-30.
54. Domínguez A, Fernández A, González N, Iglesias E, Montenegro L. Determination of critical micelle concentration of some surfactants by three techniques. *J Chem Educ*. 1997;74(10):1227.
55. Yacilla MT, Herrington KL, Brasher LL, Kaler EW, Chiruvolu S, Zasadzinski JA. Phase behavior of aqueous mixtures of cetyltrimethylammonium bromide (CTAB) and sodium octyl sulfate (SOS). *The Journal of Physical Chemistry*. 1996;100(14):5874-9.

56. Danov K, Kralchevsky P, Denkov N, Ananthapadmanabhan K, Lips A. Mass transport in micellar surfactant solutions: 2. Theoretical modeling of adsorption at a quiescent interface. *Advances in colloid and interface science*. 2006;119(1):17-33.
57. Kralchevsky PA, Danov KD, Denkov ND. Chemical physics of colloid systems and interfaces. *Handbook of Surface and Colloid Chemistry*. 1997;2.
58. Nakahara H, Shibata O, Rusdi M, Moroi Y. Examination of surface adsorption of soluble surfactants by surface potential measurement at the air/solution interface. *The Journal of Physical Chemistry C*. 2008;112(16):6398-403.
59. Lindblom G, Lindman B, Mandell L. Effect of micellar shape and solubilization on counter-ion binding studied by  $^{81}\text{Br}$  NMR. *Journal of Colloid and Interface Science*. 1973;42(2):400-9.
60. Lucassen-Reynders E, Cagna A, Lucassen J. Gibbs elasticity, surface dilational modulus and diffusional relaxation in nonionic surfactant monolayers. *Colloids and Surfaces A: Physicochemical and Engineering Aspects*. 2001;186(1):63-72.
61. Liggieri L, Miller R. Relaxation of surfactants adsorption layers at liquid interfaces. *Current Opinion in Colloid & Interface Science*. 2010;15(4):256-63.
62. Bianco H, Marmur A. Gibbs elasticity of a soap bubble. *Journal of colloid and interface science*. 1993;158(2):295-302.
63. Stubenrauch C, Fainerman V, Aksenenko E, Miller R. Adsorption behavior and dilational rheology of the cationic alkyl trimethylammonium bromides at the water/air interface. *The Journal of Physical Chemistry B*. 2005;109(4):1505-9.
64. O'Connor CJ, Ch'ng BT, Wallace RG. Studies in bile salt solutions: 1. Surface tension evidence for a stepwise aggregation model. *Journal of Colloid and Interface Science*. 1983;95(2):410-9.
65. Natalini B, Sardella R, Gioiello A, Ianni F, Di Michele A, Marinozzi M. Determination of bile salt critical micellization concentration on the road to drug discovery. *Journal of pharmaceutical and biomedical analysis*. 2014;87:62-81.
66. Joos P, Bleys G. Desorption from slightly soluble monolayer. *Colloid & Polymer Science*. 1983;261(12):1038-42.
67. Tripp BC, Magda JJ, Andrade JD. Adsorption of globular proteins at the air/water interface as measured via dynamic surface tension: concentration dependence, mass-transfer considerations, and adsorption kinetics. *Journal of colloid and interface science*. 1995;173(1):16-27.
68. Meyerhoffer SM, McGown LB. Critical micelle concentration behavior of sodium taurocholate in water. *Langmuir*. 1990;6(1):187-91.

69. Kratochvil J, Hsu W, Jacobs M, Aminabhavi T, Mukunoki Y. Concentration-dependent aggregation patterns of conjugated bile salts in aqueous sodium chloride solutions. *Colloid & Polymer Science*. 1983;261(9):781-5.
70. Hofmann AF, Hagey LR. Key discoveries in bile acid chemistry and biology and their clinical applications: history of the last eight decades. *Journal of lipid research*. 2014;55(8):1553-95.
71. Reis S, Moutinho CG, Matos C, de Castro B, Gameiro P, Lima JL. Noninvasive methods to determine the critical micelle concentration of some bile acid salts. *Analytical biochemistry*. 2004;334(1):117-26.
72. Jana PK, Moulik SP. Interaction of bile salts with hexadecyltrimethylammonium bromide and sodium dodecyl sulfate. *The Journal of Physical Chemistry*. 1991;95(23):9525-32.
73. Najjar MH, Chat OA, Dar AA, Rather GM. Mixed micellization and mixed monolayer formation of sodium cholate and sodium deoxycholate in presence of hydrophobic salts under physiological conditions. *Journal of Surfactants and Detergents*. 2013;16(6):967-73.

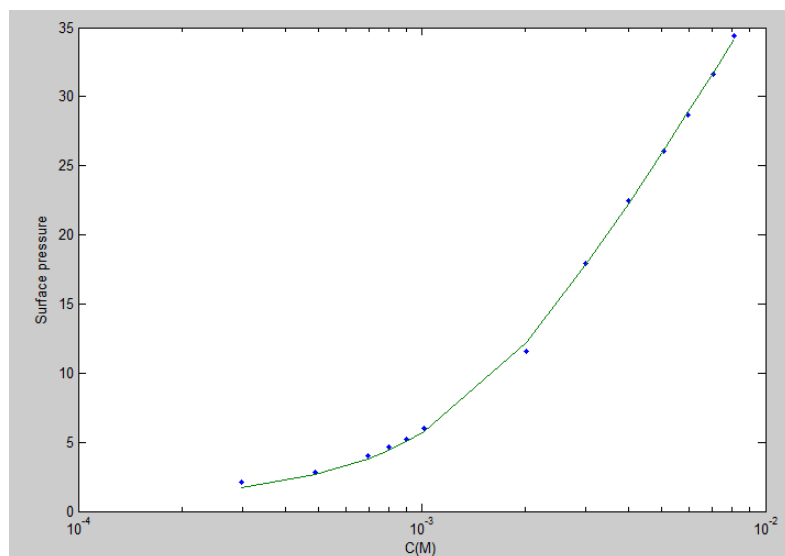
## 8 APPENDICES

### 8.1 Appendix A

For reproducing the data obtained by Kralchevsky and et al (25), it has been followed the steps proposed by them and these have been the results got:

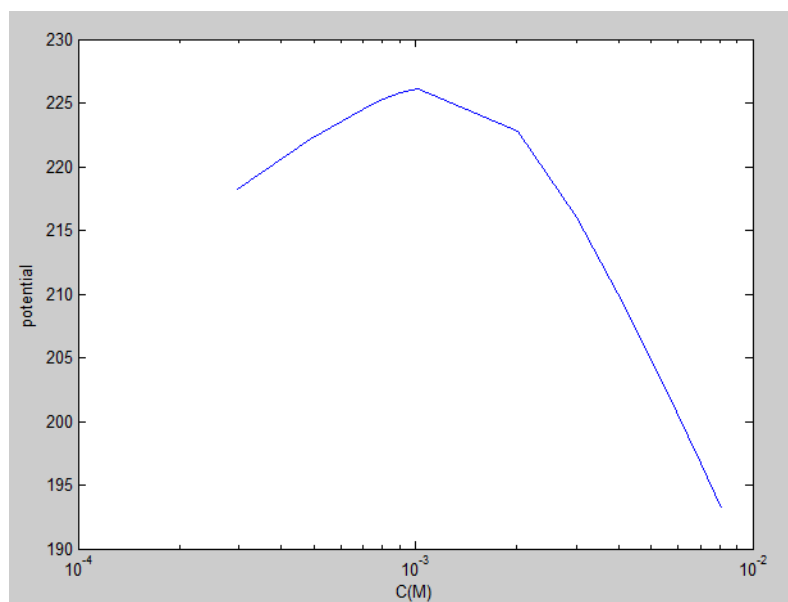
If we compare the values calculated and reported, the disagreement in the values is due to the experimental data that has been taken directly from the graph that they show in their paper. Also, the tolerance could affect the results markedly.

	$\beta \left[ \frac{kgm^4}{s^2mol} \right]$	$K_1 [mM^{-1}]$	$K_2 [mM^{-2}]$	$\Gamma_{\infty} \left[ \frac{mol}{m^2} \right]$
Calculated	4.409E-16	979.358	0.279	3.55E-6
Literature Value	3.72E-16	156	0.128	4.42E-6



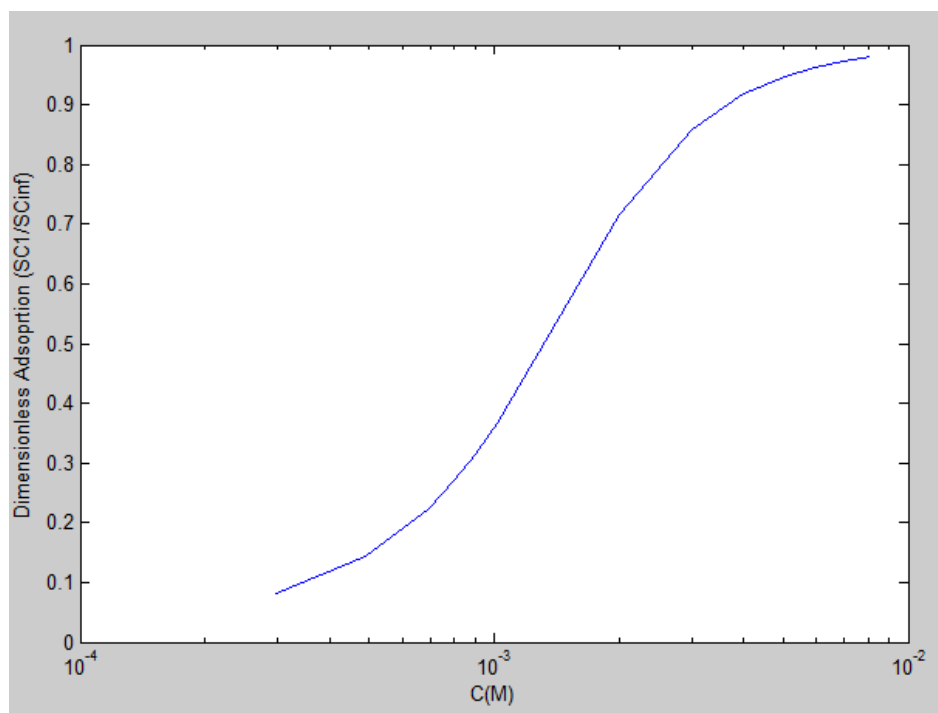
**Figure 42. Surface pressure vs Concentration**

The potential vs time graph is higher than the reported (180-190), this could be done because the simulation was made putting a solver into another so the error could be propagated.



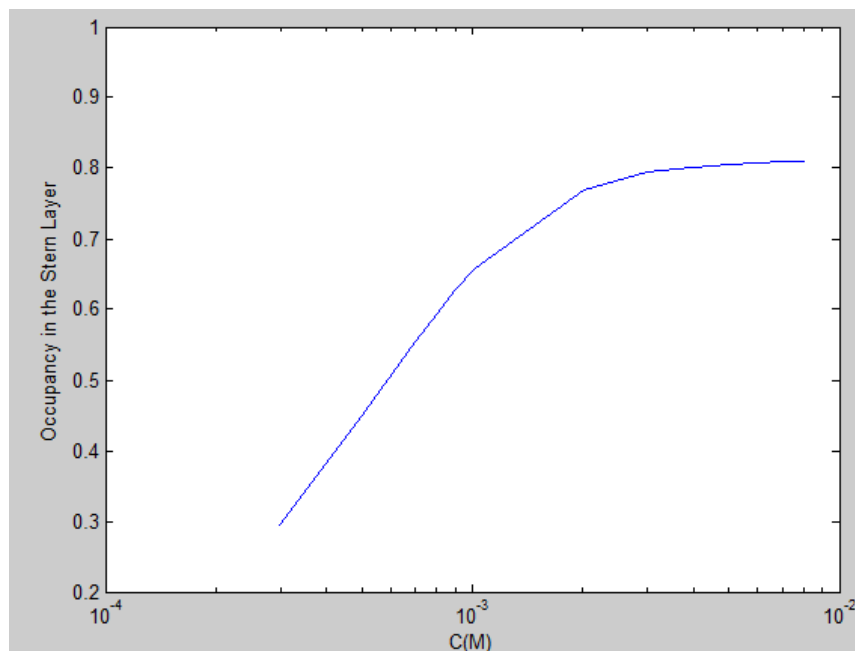
**Figure 43. Potential vs Concentration**

The dimensionless adsorption agrees with the reported.



**Figure 44. Dimensionless Adsorption**

And the occupancy in the stern layer agrees with the reported, even though there is a small offset in the y-axis of 0.1 higher than the reported.

**Figure 45. Occupancy in the Stern Layer**

## 9 VITA

### Camila Uribe Ortiz

---

#### EDUCATIONAL BACKGROUND

---

**Master of Science: Chemical Engineering**

*University of Illinois at Chicago – Chicago, Illinois, 2017*

**Bachelor of Science: Chemical Engineering**

*Universidad Nacional de Colombia – Bogotá, Colombia, 2014*

#### RESEARCH AND WORK EXPERIENCE

---

**Teaching assistant**

January 2016 -- May 2016

*University of Illinois at Chicago – Chicago, Illinois*

Evaluated submitted work from students of Chemical Process Control, and provided office hours for Chemical Process Control course for helping and advising students with their homework and exams.

**Quality Control Engineer**

April 2015 -- August 2015

*Instituto departamental de Salud de Norte de Santander – Cúcuta, Colombia*

Analyzed foods such as salt, milk, and alcoholic beverages; determined their characteristics such as fat percentage, acidity, water percentage, and realized chemical analysis.

**Internship in Research and Development**

August 2012 – January 2013

*Lipasa S.A – Cundinamarca, Colombia*

Reformulated emulsions, coordinated and implemented activities for installation and commissioning on a reactor of 16 liters capacity and supported activities for obtaining sorbitan monolaurate at the laboratory.

#### LEADERSHIP ACTIVITIES

---

**External Relation Assistant**

July 2010– June 2011

*National Students Conference of Chemical Engineering and Processes – Bogota, Colombia*

Recruited corporate sponsors for chemical engineering conference and organized logistics for conference events.

#### SKILLS

---

**Aspen Hysys/Plus, Matlab, Cyclepad, MBPT, Autocad Plant 3D, Excel, Bilingual (English and Spanish).**